Cranfield UNIVERSITY

School Of Engineering

MSc by Research

THESIS

Academic year: 2011-2012

Eva HOLZHAUER

Assessment of the Power Available in a Fixed Offshore Oscillating Water Column Plant

Supervisors: Dr J. Amaral Teixeira / Dr F. Trarieux

December 2012

Abstract

The early effects of the global warming can be observed and people around the world are beginning to realize the seriousness of the situation. Reducing the CO_2 emissions produced by fossil energy seems to be one of the main worldwide technological challenges at the time of writing. Hence, since the oil crisis in the 70s, a growing interest in renewable energies has been noticed. In Europe, the European Commission fixed a target: to produce 20% of the EU energy from renewable sources by 2020. Similar initiatives, in varying degrees, are being considered around the globe.

Among all the renewable energy technologies currently on the market, the ocean energy industry is still at an early stage, despite investigations that have been carried out on both tidal and wave energy devices over the past 40 years. The subject of this thesis focuses on one of the wave energy devices: the Oscillating Water Column.
The information found in the literature about this type of plants is mainly about onshore and floating offshore OWCs. Very little information about fixed offshore OWC is available. Besides, the availability of large numbers of fixed offshore structures installed in the world oceans suggests that many of these could possibly host an OWC plant. Hence, the present study investigated a fixed offshore OWC.

The aim of this thesis is to assess the power available in a fixed offshore OWC plant. To illustrate the procedure of power assessment, the fictional scenario of a platform located in the Santa Maria sea region, off the coast of Californian, is introduced. This work intends to develop a methodology to study the feasibility of such installation and estimate the power extractable through various complementary approaches. From a theoretical approach based on the wave climate of Santa Maria to wave tank experiments with various geometries and shapes of chamber (cylinder and bent duct buoy in frontward and backward position), the viability of a fixed offshore OWC plant is demonstrated for the chosen location. Results highlight the performance of the Backward Bent Duct Buoy (BBDB) for the Santa Maria characteristic sea conditions. With the intention of completing the study with a Computational Fluid Dynamics (CFD) analysis, numerical investigations about the implementation of an alternative method to generate regular waves demonstrates better results of wave propagation than the common wave generation method based on Linear Wave Theory previously used at Cranfield University. In the conclusion, the work achievements and recommendations for future CFD investigations to reproduce the wave tank experiments are discussed.

Acknowledgements

I would like to thank my supervisors Dr Joao Amaral Teixeira for his constant helpfulness and Dr Florent Trarieux, for giving me the opportunity to work on this project.

I wish to thank Olivia Thilleul who gave me first the opportunity to discover the challenging word of marine energy and finally recommended me for this MSc.

I am also grateful to the PhD student Judith Farman, and Shahab Natanzi, with whom I worked for a part of the project.

There is no word to thank enough my parents and sister who have always given me support all over the years whatever the distance.

This year in Cranfield wouldn't have been the same without Luca, Carlotta, Donna, Eva, Krish, Rajib, Ben, Anne-Lise who helped me to keep a smile upon my face.

And of course "thanks a lot" to my longtime friends: Agnès, Eliza, Sabine, Lucie, Aurélie, Diane and Lucile who might be far away but crossed the Channel anyway to come enjoying the *Light*, a snow storm in London, orange balloons in the tube, a rainy Queen's Jubilee, the Paralympics and my little house.

Table of contents

List of Figures

List of Tables

Nomenclature

A	wave amplitude
$A_{orifice}$ or A_0	orifice section
B	damping coefficient
C	hydrostatic restoring coefficient
C_d	coefficient of discharge
C_s	speed of sound is the air
Dw	mean wave direction
F(t)	total force acting on the water column
$F_a(t)$	added mass force
$F_{FK}(t)$	Froude-Krylov force
$F_{\delta Pair}(t)$	vertical force due to the varying air pressure inside the chamber
Hs	significant wave height
H	wave height
M	mass of the column of water
M	torque
P	pressure
P	wave power per unit of crest length
P_{atm}	atmospheric pressure
P_{ave}	annual average wave power
Q	flow rate
R	chamber radius
Ta	average wave period
T	wave period
W	occurrence of a sea state

a_i	amplitude
d	water depth
g	gravitational acceleration
h_{a0}	air draft
k	wave number
u	horizontal component of the orbital velocity
v	vertical component of the orbital velocity
x_0	amplitude of the movement of the wave maker
z	internal water elevation in the chamber

ΔP	pressure drop
$\varepsilon_{capture}$	capture efficiency
ϕ_i	wave phase
λ	wavelength

$\eta_{generator}$	generator efficiency
$\eta_{overall}$	overall efficiency
$\eta_{turbine}$	turbine efficiency
ρ	water density
ρ_{air}	air density
ω	rotational speed
ω_i	angular frequency
γ	heat capacity ratio

Acronyms

BBDB	Backward Bent Duct Buoy
BEM	Boundary Element Methods
CCL	CFX Command Language
CEL	CFX Expression Language
CFD	Computational Fluid Dynamics
DECC	Department of Energy and Climate Change
DTI	Department of Trade and Industry
EIA	(US) Energy Information Administration
EPRI	Electric Power Research Institute
EREC	European Renewable Energy Council
EU	European Union
EU-OEA	European Ocean Energy Association
FBDB	Frontward Bent Duct Buoy
IEA	International Energy Agency
JONSWAP	Joint North Sea Wave Project
LIMPET	Land Installed Marine Pneumatic Energy Transformer
LWT	Linear Wave theory
MATLAB	Matrix Laboratory
MRC	Multi Resonant Chamber
NDBC	National Data Buoy Center
NOAA	National Oceanic and Atmospheric Administration
NRDC	Natural Resource Defence Council
OECD	Organization for Economic Cooperation and Development
OWC	Oscillating Water Column
RANSE	Reynolds Average Navier-Stokes Equations
VOF	Volume Of Fluid
WEC	Wave Energy Converter
WMT	Wave Maker Theory

Chapter 1

INTRODUCTION

1. 1. Background - World Energy Resources

While climate changes and increasing dependence on oil and fossil fuels highlight the current worrying situation, the promotion for renewable energies has grown quasi steadily since the oil crisis in the 70s, to cope with global warming and reduce climate CO_2 emissions produced by fossil fuels.

In Europe, the European Commission fixed a new target to tackle the situation. The goal is to produce 20% of the EU energy from renewable sources by 2020 [1], and all around the globe, the will spreads to meet the challenge. For instance in 2011, Germany produced 10.7% of its electricity by renewable sources while the United Kingdom produced 4.2%.

Meanwhile, at the 2012 Earth Summit in Rio de Janeiro, a new Natural Resource Defence Council (NRDC) report communicated the latest predictions about electricity produced by renewable energy by 2020. In the current context, “the G20 countries are expected to produce less than 4% of their electricity from renewable sources by 2015 and less than 6% by 2020” [2]. In 2011, the amount was 2.6%. However, the NRCD new goal “is to conceive a plan that will boost total world electricity production via renewable resources to 15% by 2020”.

Among all the renewable energy technologies currently on the market, the ocean energy involves the generation of energy from the tides, the waves, the currents, the salinity gradient and the thermal gradient of the sea or the ocean. Even though investigations on both tidal and wave energy devices have been carried out over the past 40 years, the industry is still at an early stage. The main reason of this reserve is financial. Indeed, the installation of such structure represents a significant cost; it needs the development of high technology to harness and distribute the offshore power. However, this effort might worth it, as in Europe, if the ocean energy exploitation was facilitated, an installed capacity of 3.6 GW by 2020

(equivalent to 0.3% of the projected EU-27 electricity demand), and close to 188 GW by 2050 [3] would be expected.

This significant challenge shows a great interest in a more sustainable future and predicts an investment in the development of ocean energy facilities during the next 40 years.
In fact, the amount of the global gross wave power resources is estimated to be 3.7 TW, However this resource decreases by 20% if the area with very low energy (P≤5 kW/m) and the area impacted by sea ice are excluded [4].

World case – The world energy consumption is currently around 16000 TWh/yr [5] while the global annual wave energy resource is assessed to be 80000 TWh/yr and the practical worldwide market potential for wave energy is estimated to be 2000 – 4000 TWh/yr [6], [7].

In its Annual Energy Outlook, EIA predicts the world renewable energy generation by source until 2035 not considering hydropower which accounts for 83% of total renewable electricity generation in 2010 (Figure 1) [8].

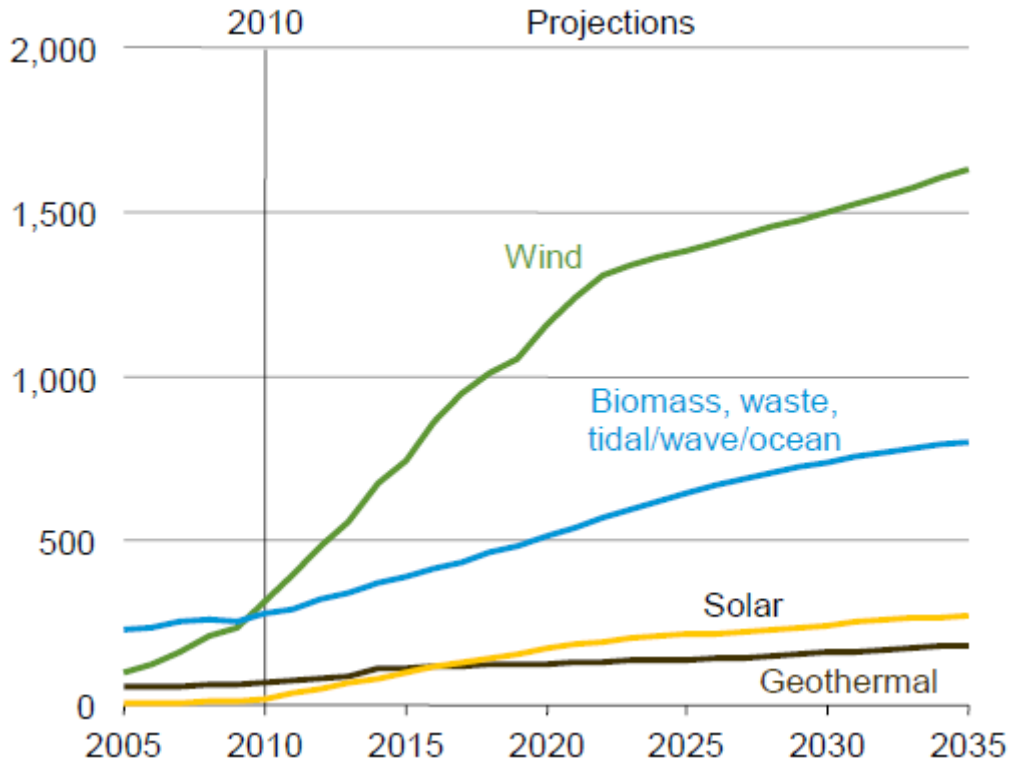

Figure 1 - World renewable electricity generation by source, excluding hydropower, 2005-2035 (TWh) [8]

First, wind generation is predicted to have the largest increment in non hydro power. In fact, between 2000 and 2010, wind-powered generating capacity grew swiftly from 18 GW of

installed capacity to 179 GW. However, after 2020, the rate of wind generation is expected to slow frankly because most of the governments will achieve their wind goals. Besides, wind must have to compete on the basis of economics with fossil fuels [8].

A significant growth should occur in the sector of biomass, waste, wave and tidal energy, nevertheless in 2035 the amount of wave power will still be far from the practical potential available; therefore the trend is expected to keep on rising thereafter.

UK case – More specifically, the interest for renewables in the UK can be brought out by the records of electricity generation over the past 3 years (Table 1) [9]. Indeed, increasings of 69% and 21%, respectively for electricity provided by wind turbines and other renewables, have been recorded between 2009 and 2011. Meanwhile the contribution of fossil fuels (coal, gas and oil) seems to stagnate or even decline.

Primary and secondary production (GWh/yr)	**2009**	**2010**	**2011**
Gas	166 499	175 655	146 814
Coal	103 038	107 694	108 583
Nuclear	69 098	62 140	68 980
Oil	5 995	4 805	3 665
Other	3 200	2 482	2 444
Hydro	5 241	3 644	5 686
Wind	9 324	10 216	15 750
Other renewables	10 694	11 987	12 973
Total production (GWh/yr)	**373 089**	**378 622**	**364 897**

Table 1 - Primary and secondary production of electricity in the UK [9]

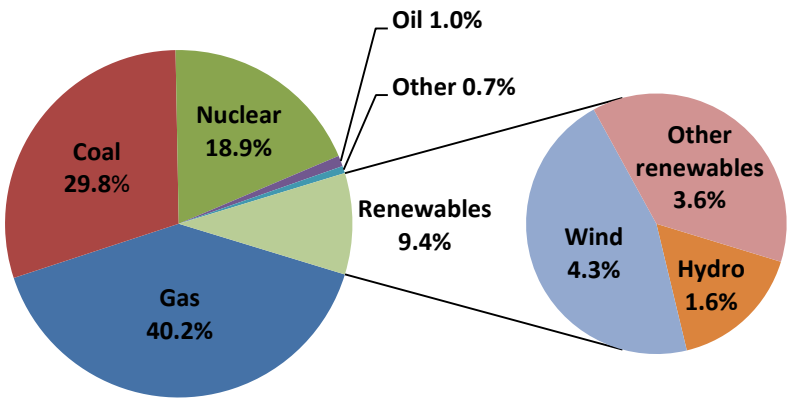

Figure 2 - Primary and secondary production (%) in the UK in 2011 according to [9]

In 2011, the total production of electricity in UK was 365 TWh: 71% came from fossil fuels, 18.9% from nuclear power, 9.4% from renewables and 0.7% from others (Figure 2). With 4.3% of the UK electricity production, wind power is the leading renewable resource and this trend should keep on growing as the offshore wind turbines market is booming.

Among the other 3.6% of renewable resources, only a small amount comes from ocean resources. However as presented in Figure 3, a great potential of wave power is surrounding the UK. The mean wave energy flux along the west coast of Europe was obtained with the oceanic model ANEMOC [10]. This model reveals that the Scottish North-Western coast and the Irish Western coast have high potential with wave energy flux up to 70 kW/m.
At the same time, equivalent or smaller amounts of energy are available in the North Sea depending on the distance from the coast. In fact, the wave power decreases when approaching the continental coasts because of dissipation effects due to friction with the seabed and depth breaking in shallow waters.

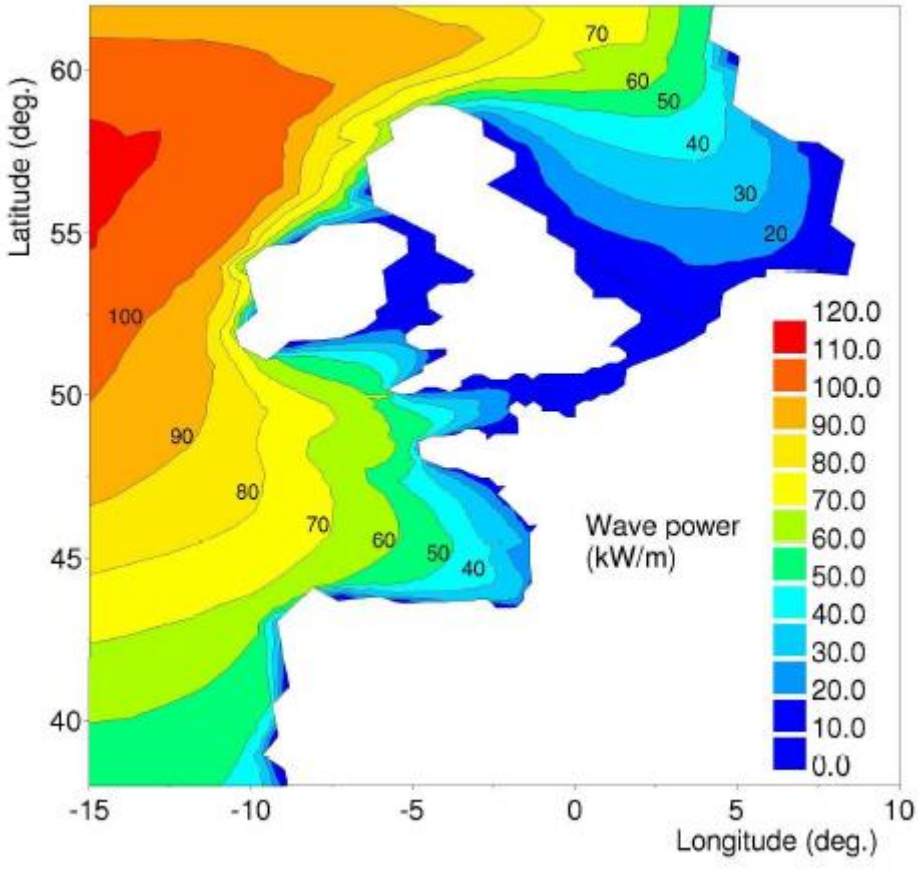

Figure 3 - Mean wave energy flux along the west coast of Europe [10]

More specifically, a recent study of Carbon Trust [6], exhibited in Table 2, estimates the total wave energy resource in the UK at around 230 TWh/yr, which is mainly concentrated in the deeper offshore parts of the UK environs.

Two locations in UK waters were retained as least cost areas, making a compromise between more energetic offshore climates and less mooring cost, at around 100km from the shore. They are located at the edge of the Rockall Trough to the West of Scotland and at the edge of the UK waters in the Southwest with an available theoretical offshore resource around 146 TWh/yr.

Technically, meaning that the installation of huge arrays of devices will be required, it would be possible to extract 95 TWh/yr. However by taking into account the environment restrictions such as shipping, fishing, cables and pipelines the amount of power extractable would be reduced to 70 TWh/yr. Of this around 42 TWh/yr would be available at or below three times the cost of the energy of the cheapest site.

At the same time, the important difference between the theoretical near shore resource (133 TWh/yr) and the technical resource (10 TWh/yr) can be explained by the fact that the variability of seabed and technical conditions in shallow water reduced the number of suitable sites. Hence, the important efforts made recently focuses on offshore technologies to allow maximum energy extraction.

	Offshore		**Near shore**	
	Annual energy [TWh/yr]	**Mean power [GW]**	**Annual energy [TWh/yr]**	**Mean power [GW]**
Total	230	26	230	26
Theoretical	146	18	133	15
Technical	95	11	10	1
Practical	70	8	5.7	0.6

Table 2 - UK Wave Energy Resource in 2011 [6]

According to the statistics released by the Department of Energy and Climate Change (DECC), up to 50 TWh/yr could be produced from wave power; this represents 12.4% of UK electricity generation [9]. In the future, marine energy could provide up to 20% of UK electricity demand; a realistic scenario expected a production of 13.2GW extracted thanks to wave and tidal technologies in 2050 (~11%) [6].

US case – Meanwhile in the USA, a total of 4105.8 TWh was produced in 2011 (Table 3); this is 11.3 times the amount of electricity produced by the UK for the same period [9,11]. The electricity production repartition in the US, presented in Figure 4, draws attention to a high dependency on fossil fuels (67.9%), especially in coal (42.2%). However, the production of gas is expected to increase in the future. In parallel 12.5% of the electricity comes from renewable resources including mainly 7.8% of hydroelectric power,which is currently the largest producer of renewable energy, and 2.9% of wind power.

Primary and secondary production (TWh/yr)	**2009**	**2010**	**2011**
Gas	931.6	999.0	1 027.9
Coal	1 755.9	1 847.3	1 734.3
Nuclear	798.9	807.0	790.2
Oil	38.9	37.1	28.2
Other	11.9	12.9	11.1
Hydro	268.8	254.7	319.2
Wind	73.9	94.7	119.7
Other renewables	70.4	72.5	75.2
Total production (TWh/yr)	**3950.3**	**4125.2**	**4105.8**

Table 3 - Net Electricity Generation in the US [11]

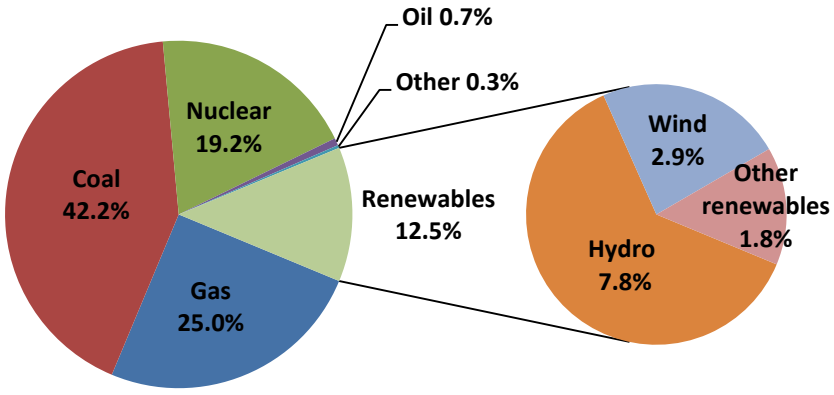

Figure 4 - Primary and secondary electricity production (%) in the US in 2011 according to [11]

The marine renewable market hasn't expanded much in the US. However, in September 2012, for the first, ocean energy has been delivered to the grid. Indeed, tidal and wave power are promising resources. For instance, the total US wave energy flux is about 2300 TWh/yr [12]. If compared to 319 TWh generated by hydroelectric in the US in 2011 [11] which represents little more than a tenth of the offshore wave energy flux into the US, it makes this an attractive source of energy.

The wave energy resource of US coasts is presented in Figure 5 [13]. It highlights a large potential in the Pacific Ocean along the Southern Alaska and the west coast of the US.
The total flux with mean wave power density > 10kW/m is 2100 TWh/yr.

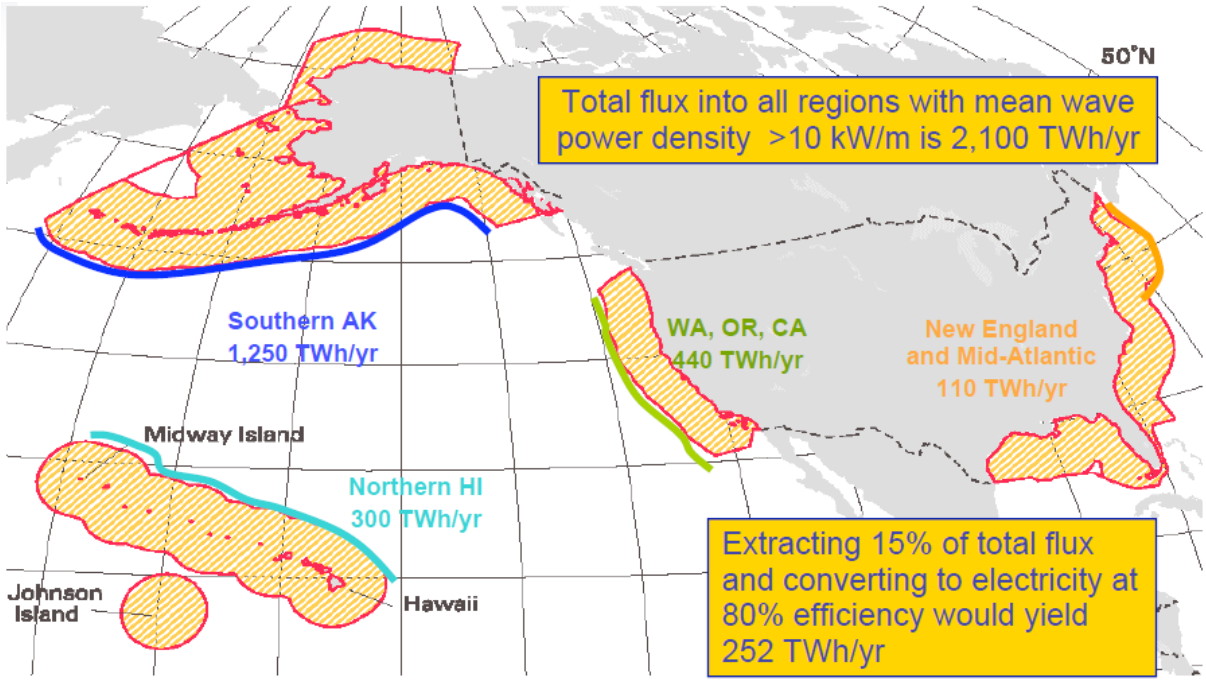

Figure 5 - US offshore wave energy resource [13]

One wave power device among all ocean energy technologies – During the last decades, efforts have been made to develop both tidal and wave energy devices. The subject of this study focuses on one of the most famous of them: the Oscillating Water Column. The purpose of this facility is to harness the wave power available in the ocean to generate an electrical output. It consists of a chamber open to the sea below the water level, equipped with an air chamber and a turbine-generator system linked to the atmosphere; the incident waves cause vertical oscillation of the column of water and the column of air inside the chamber, the generated airflow drives the turbine and the combined generator produces electricity.

1. 2. Rationale of the Work and Objectives

1. 2. 1. Rationale of the Work

Over the past 40 years, OWC have been investigated in different locations. In the literature, many papers studied the case of fixed onshore OWC; the Land Installed Marine Pneumatic Energy Transformer (LIMPET) became a reference in this field. In parallel, an interest was developed for floating offshore OWC to explore more energetic seas. However, there appears to be no record of a fixed offshore prototype.

There are many offshore facilities around the world. First, there are the fixed offshore platforms mainly built during the 70s and 80s which are concentrated in shallow water around 500m of water depth. They are anchored directly onto the seabed, and because of their immobility are designed for very long term use. Secondly there are the floating platforms installed in deeper water, which are generally tethered or moored to the ocean floor and classified in different subcategories. The water depth ranges from 100m to 2500m. Among the fixed offshore platforms some of them are still operating while the others are already decommissioned but not dismantled yet.

In Europe, such structures can be found in the North Sea where oil and gas fields have been harvested since the first extraction of oil in 1851 on the shores of Scotland and of gas in 1910 near Hamburg. The network has expanded in the sea ever since; a map of the oil and gas fields and pipelines is shown in Figure 6. There are two main concentrations of activity located in the northern and southern North Sea. By comparing Figure 3 and Figure 6, it appears that many oil fields, and so-called offshore structures, are located in energetic sea conditions of the northern part of the North Sea with mean wave energy flux ranging from 30 up to 70 KW/m. These installations could represent a large potential to host OWCs.

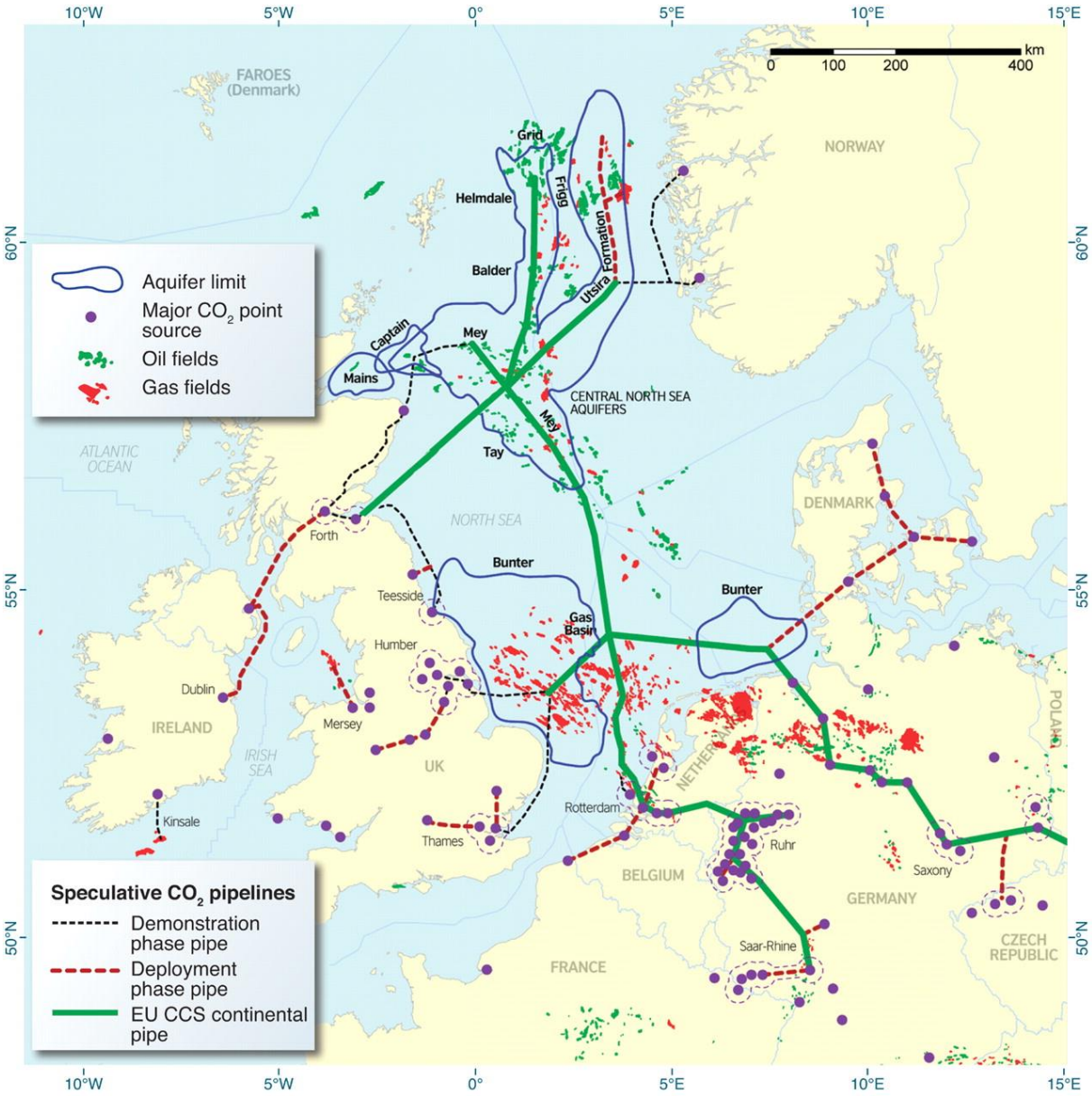

Figure 6 - Map of oil and gas and pipelines in the North Sea [14]

Among all the offshore fields exploited around the world, offshore oil and gas in California provides a significant portion of the US petroleum production. In this area, where most of the fields were discovered between 1890 and 1920; the first offshore drilling began in 1896. The location of the different oil and gas fields off California are presented in Figure 7, where according to Figure 5 a percentage of the 440 TWh/yr US west coast mean wave power flux is concentrated. Thus, like the North Sea offshore structures, the installations located in sea waters off California could offer opportunities to host OWCS.

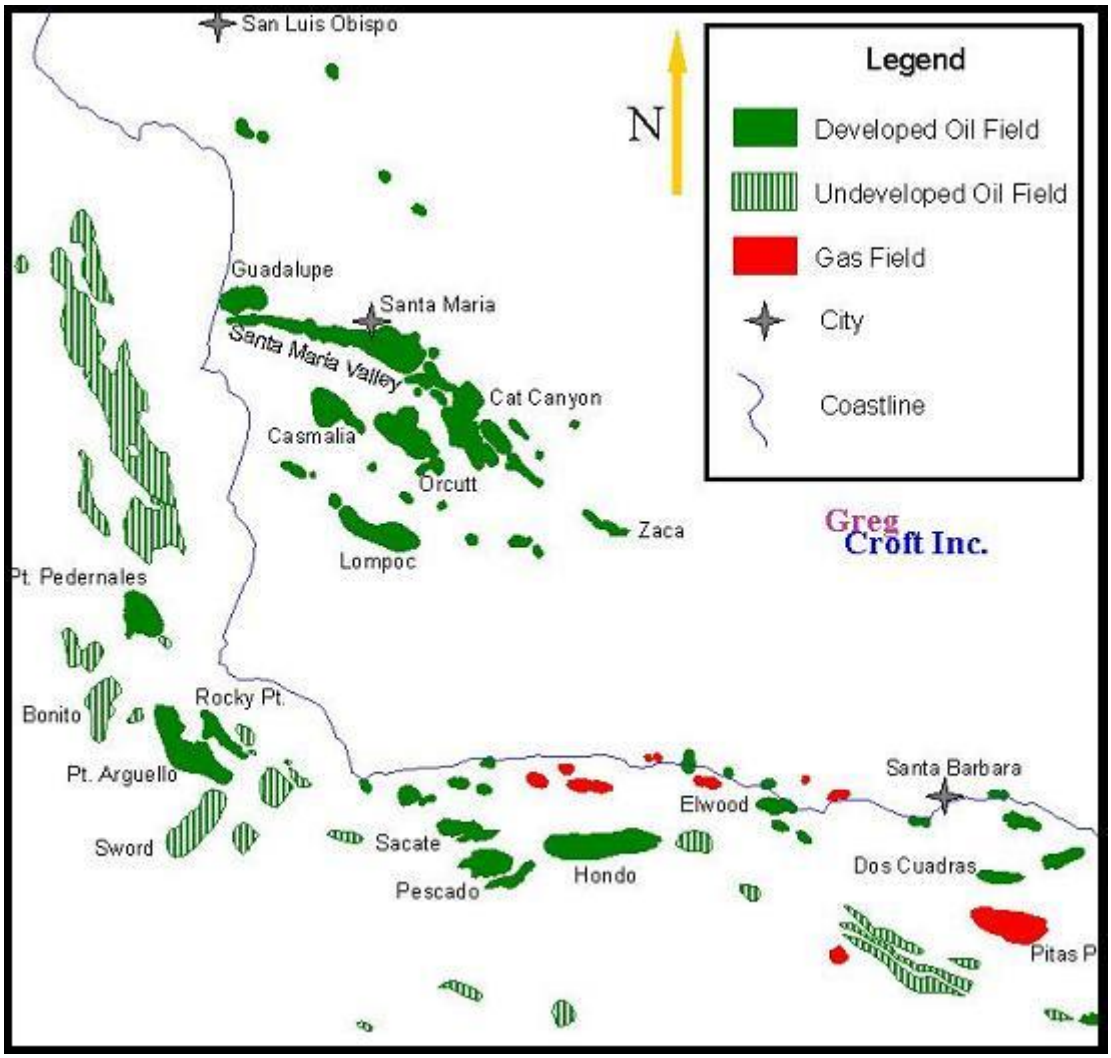

Figure 7 - Oil fields of the Santa Maria Basin and Adjacent Offshore Area, California [15]

Hence, due to the lack of knowledge about the performance of fixed offshore devices, and the potential availability of offshore structures in the energetic climate of the North Sea and California, it is suggested that there is a need to study the integration of OWC devices with these structures.

1. 2. 2. Aims and Objectives

This work is taking part in a broader research project about performance and development of OWC technologies which started in 2007 at Cranfield University and has been sustained, thanks to the works of MSc students [16, 17, 18, 19, 20]. While the previous investigations mainly focused on the improvement of the CFD modelling techniques for OWC, the actual work undertaken tends to have a larger overview and has to be understood as an expansion

of the subject of OWCs investigations. The aim of the thesis is to assess the power available in a fixed offshore OWC plant. Since offshore locations offer more energetic wave climates and there is a lack in the literature about fixed offshore OWC, this work intends to develop a methodology to study the feasibility of such installation and estimate the power extractable with the example of the site of Santa Maria, off California.

For the purpose of the study, different approaches are considered to demonstrate the viability of such unit. The project aims to evaluate the degree of agreement of theoretical expectations, wave tank data, analytical model results and CFD predictions. The idea is to confront them successively as they are complementary to each other. Hence every approach has its own objectives.

From a theoretical approach, it is expected to determine the most occurring wave climate of the location to access to the potential wave power available. Based on the available literature about near shore and offshore floating devices, first predictions are expected to get a clue of the wave power extractable. The procedure is undertaken with the MATLAB tool, to automatize the predictions.

To switch to predictions about fixed unit, an experimental approach based on the wave climate previously identified is carried out. The objective is to check the experimental results against the theoretical approach based on floating devices. Using a wave tank gives also the opportunity to optimize the geometry and test different shapes of chamber. In parallel, an analytical approach is investigated and confronted to the experiments to check its validity.

An additional numerical approach is considered to double check the experimental results. The use of the commercial CFD tool, called CFX, comes also to complete the previous work undertaken at Cranfield University, and suggests the implementation of a new wave generation method for regular waves, based on a physical wave maker, to compare with the commonly used method based on Linear Wave Theory.
Besides, the modelling of sea waves involves the deployment of different CFD features:

- Transient simulation, meaning that the differential partial equations are solved both in time and space
- Two-phase flow, since air and water are simulated simultaneously
- Free surface flow, since the water surface is describe as sharp interface between the two flows
- Moving mesh or deformation, since a method to generate the motion of the flow requires a mesh motion at one boundary to reproduce a physical motion

1. 3. Structure of the Thesis

The present work consists of six chapters. Chapter 1 is an introduction to the topic exploring the wave energy resource around the world and the potential of fixed offshore structures potentially available to host OWC. In this chapter, the main objectives of the thesis are also presented.

Chapter 2 contains a review of the literature. In a first part, a comprehensive summary explores the working principle, the conversion chain and the state-of-the-art in OWC technologies. A second part reviews the different modelling methods to approximate the behaviour of OWCs.

Chapter 3 introduces the power evaluation of a site and a potential fixed offshore OWC implanted there. The methodology to assess the power is presented; a fictional offshore scenario is considered and illustrated by the example of Santa Maria, California.

Chapter 4 presents experimental and analytical approaches undertaken with wave tank tests and an analytical model to complete the theoretical power estimation of Santa Maria. The first objective is to analyse and improve the understanding of the behaviour of fixed offshore OWCs depending of the geometry (cylinder and bent duct buoy) and the orientation (frontward or backward) of the device for a wide range of wave heights and wave periods thanks to wave tank tests. Another goal is to assess the validity of the predictions of power of the analytical OWC model by verifying it against wave tank tests carried out with a vertical cylindrical chamber. Finally, wave tank tests undertaken both with the cylinder and the frontward and backward bent duct buoy configurations are compared to the theoretical assessment made in Chapter 3 from the most occurring sea conditions of Santa Maria site. The post processing of the experimental and analytical data to estimate the power extractable was realized in collaboration with the work of a visiting student in the ocean lab and a PhD student. Quentin Ailloud carried out the wave tank tests and Judith Farman ran the tests with the analytical model.

Chapter 5 applies to numerical investigations with CFD. This chapter intends to compare two wave generation methods in order to run CFD simulations on fixed offshore OWC. In a first part, a review of different methods to generate regular and irregular waves is presenting. It focuses especially on the method of implementation of the Linear Wave Theory generally used by the former students at Cranfield University and the alternative method of a numerical wave maker. The porous absorber method used to damp the wave is also presented in this section.

In a second part, the simulation settings are described presenting the case settings, the boundary conditions, the mesh and the data handling.
In a third part, the results of the comparison between the two wave generation methods and a mesh convergence study are analysed.
And finally, recommendations for CFD investigations on fixed offshore OWC to complete the scenario of Santa Maria are presented.

Chapter 6 outlines the work achievements of the thesis and discussed recommendation for further CFD investigations repeating the wave tank experiments.

Chapter 2

LITERATURE REVIEW

2. 1. OWC Technology

2. 1. 1. OWC Working Principle

An oscillating water column is a partially submerged, hollow structure. It is opened to the sea below the water free surface, enclosing a column of air on top of a column of water. This device converts wave energy into pneumatic energy in the form of alternating air flow, which is created by the vertical oscillations in the water surface. There are two stages of operation: inhalation and exhalation. During the exhalation, the water level in the chamber rises, forcing air out of the chamber and through the turbine (Figure 8). During the inhalation, the retreating wave sucks the air back into the OWC. The air movement past the turbine causes it to rotate which is used to generate electricity.

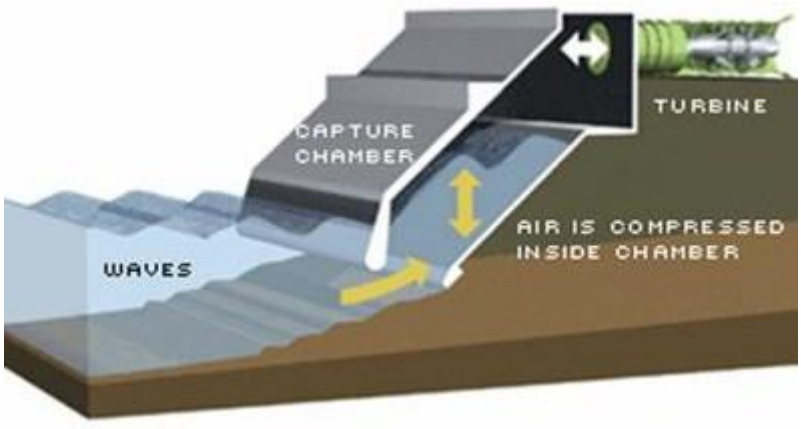

Figure 8 - Working principle of the LIMPET OWC

2. 1. 2. Chain Conversion and Efficiency

The conversion chain (Figure 9) from wave power to electricity is a 3 step process. The incoming wave power converts into pneumatic power in the chamber of the OWC. Then, the

compressed or uncompressed air by passing through the turbine creates mechanical power which is transmitted to the generator to provide electricity.

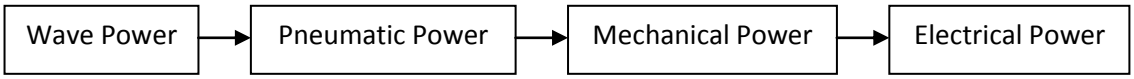

Figure 9 – OWC chain conversion

From this conversion chain can be defined the efficiency of the different OWC parts.
The expression for the overall efficiency (wave-to-wire efficiency) of an OWC, corresponding to the ratio of the power output to the power input, is:

$$\eta_{overall} = \frac{Electrical\ power}{Wave\ power}$$

[2.1]

It can also be defined as:

$$\eta_{overall} = \varepsilon_{capture} \cdot \eta_{turbine} \cdot \eta_{generator}$$

[2.2]

Where $\varepsilon_{capture}$ is the capture efficiency, $\eta_{turbine}$ and $\eta_{generator}$ are the turbine and the generator efficiencies respectively.
The capture efficiency can be defined as the ratio of the pneumatic energy to the incoming wave input energy:

$$\varepsilon_{capture} = \frac{Pneumatic\ power\ in\ the\ OWC\ chamber}{Incoming\ wave\ power}$$

[2.3]

The expression for the turbine efficiency is:

$$\eta_{turbine} = \frac{M.\omega}{Q.\Delta p}$$

[2.4]

Where M is the torque (in Nm^1), ω is the rotational speed of the turbine (in $rad.s^{-1}$), Q is the volumetric flow passing through the turbine and Δp is the pressure difference available to the turbine. In this case, the turbine expands for atmospheric pressure, Δp is the relative pressure inside the chamber.
The pneumatic power available inside the chamber is the product of the volumetric flow passing through the turbine, $Q = \int_A velocity\ dA$, and Δp.
The expression for the generator efficiency is:

$$\eta_{generator} = \frac{Electric\ Power}{M.\omega}$$

[2.5]

Where M is the torque (in Nm) and ω is the rotational speed of the turbine (in $rad.s^{-1}$).

2. 2. The State-of-the-Art in OWC

Over the last four decades, an investment has been made to develop the OWC technology. Different locations were considered: on the shoreline, mounted on a breakwater, near shore and offshore. Nowadays, the working operating systems are mainly shoreline or breakwater units (Table 4). They are actually offering a simpler access for maintenance and power collection.

Device	Nominal Generating Capacity (kW)	Collector width (m)	Location	Type	Company
LIMPET	500	21	Isle of Islay (Scotland)	shoreline	Voith Hydro Wavegen
PICO	400	12	The Azores (Portugal)	shoreline	WavEC
Mutriku	296	72	Basque Country (Spain)	break water	Voith Hydro

Table 4 – Working OWC

Among them, the **Land Installed Marine Pneumatic Energy Transformer** (**LIMPET 500**) *(c),* a Scottish shoreline unit launched in 2000 by Voith Hydro Wavegen, is the first world commercial OWC to be connected to the national grid [21]. It can produce enough electricity for 500 households. Its average wave power density varies from 12 to 15 kW/m. The power modules consist of a Wells turbine, valve and noise attenuator. The modules are very simple and rugged: the blades are fixed onto the rotor, have no pitching mechanism, no gearbox or hydraulics and handles variable bi-directional flow. The turbine has no contact with seawater and, due to the location of the plant maintenance and access are easy. A former version of the current unit is the Limpet (75 kW) which was a project by Queens University of Belfast and sponsored by the Department of Trade and Industry. The OWC was equipped with a 75 kW Wells turbine and flywheel for energy storage. The system was connected to the grid in 1991, but it is no longer working as it was damaged by waves, LIMPET 500 was erected on the same site.

Another operating shoreline plant is the **PICO** *(d),* installed in Portugal [21,22].The plant consists of a hollow reinforced concrete structure, encompassing a pneumatic chamber, above the water free surface, that interfaces with the sea and incident waves by a submerged opening, in its front wall, and is connected to the atmosphere by a fibre duct with

an air turbine (a Wells turbine with symmetric blades). The generated electricity is fed into the local grid. An important factor in designing this kind of plant is the dimensions of the pneumatic chamber, in order to operate in resonance conditions and capture more of the incident wave power. Until now, it has operated for a few hours and had to face various internal problems. During 2011 the priority of the project was to prepare the plant's structure to accommodate a second platform to conduct the testing of turbines. In November the plant was ready for operation but not generating electricity. The WaveC team is currently working on a safety feature and looking for funding to repair the concrete structure.

Meanwhile, **Mutriku** *(g),* the first commercial breakwater energy plant, was inaugurated in 2011 in Spain having begun construction in 2006 [23]. This unit developed by Voith Hydro Wavegen and EVE will generate an output of approximately 300 kW to power 250 households. The OWC plant is integrated into a 440m-long break-water and equipped with 16 chambers all fitted with a Wells Turbine each connected to a generator, with a capacity of 18.5 kW. The design of the Mutriku plant includes a hollow structure. Each chamber has a footprint that is shaped as a trapezium. The structure has a front opening, which is submerged under water, and an opening at the top, connected to a turbine. The turbines do not have a gearbox, hydraulics or pitching blades. The structure encloses a butterfly valve at the entrance to the turbine to isolate the turbine, if necessary. Fresh water injectors clean the blades of the turbine to remove accumulations of salt and other impurities.

Shoreline OWCs (Figure 10) – In the meantime, other shoreline units were investigated. In 1984, JAMSTEC tested a shoreline OWC on the west coast of Japan, in **Sanze** *(a)* [24]. It was equipped with two wells turbines and a 40 kW generator. After it was dismantled, the turbo generator was installed in another OWC device on a breakwater at Sakata port in Japan.

In 1985, Kvaerner-Brug installed a 500kW multi resonant shoreline OWC in **Toftestallen** *(b)* in Norway. The OWC, built in steel, is equipped with a Wells turbine and an electric generator. It operated for four years before it was seriously damaged during a storm, the anchoring gave away and the device sank. After that, the power plant was decommissioned.

Between 1989 and 1991, the first Chinese OWC, equipped with a Wells turbine with the capacity of 3 kW, was installed at **Dawanshan** Island [25]. The average incident wave power density was 4.4 kW/m. It provided electricity to the island community. However, the power station did not operate for very long as the low height of the chamber meant that waves caused significant damage when water entered the turbine. A second experimental OWC

with a capacity of 20 kW began operating in February 1996. The structure was concrete and the device was equipped with a Wells turbine. The annual incident wave power density and the average power output were 4.4 kW/m and 4 kW respectively.

In 2005, the largest OWC was installed in China in **Shanwei** with a capacity of 100 kW [25]. The system is connected directly into the national grid. Its average wave power density is 5 kW/m, its power output varied from 5 to 40 kW and its annual average output is 6 kW. The total efficiency of the power plant station is about 6%.

The project of a **Tunnelled Wave Energy Convertor** (**TWEC**) *(e)* was developed by Wavegen and SEV companies who established a joint venture SeWave for the design and the building of the wave farm project. It is based on the design of LIMPET, which uses a tunnelled wave plant OWC built into the face of a cliff. Model tests, site investigation and design issues were completed in 2005 [26].

(a)

(b)

(c)

(d)

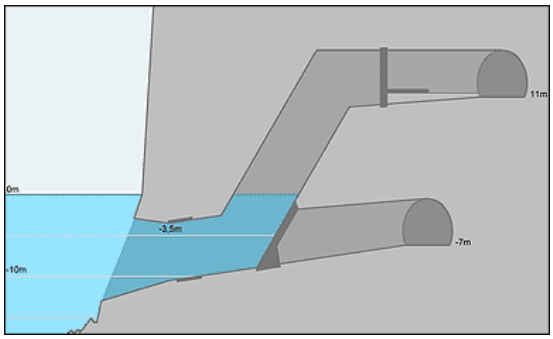

(e)

Figure 10 – Shoreline OWCs: (a) Sanze, (b) Toftestallen, (c) LIMPET, (d) PICO, (e) TWEC

Break-Water OWCs (Figure 11) – In addition to Mutriku, research was carried out on other break-water OWC. Between 1986 and 1988, the OWC integrated into a break-water in **Niigata**-nishi port in Japan, with a capacity of 40 kW, was part of project between collaborating organisations (Matsue National College of Technology, Ministry of Land, Infrastructure, Transport and Tourism amd Saga University). The goal of the facility was to demonstrate the usefulness of the impulse turbine.

In 1989, the break water of **Sakata** harbour is equipped with a 5 chamber OWC *(f)* by the Ministry of Transport of Japan [21]. But after a test program, only 3 of the air chambers were used for energy production. A turbo-generator of 60 kW has been installed and is being used as a power generator unit for demonstration and monitoring purposes. It will be possibly replaced by a larger turbine (130 kW) sometimes in the future.

During the 90's, Takenaka Komentun Co. developed a constant-pressure manifold pump coupled to a 30 kW generator to produce a smooth AC output (200 Volts, 50Hz) mounted on a break-water in **Kujukuri**. It was equipped with 10 cylindrical OWC chambers all connected to the constant-pressure air manifold through one-way valves which allowed only upward water column motion to generate sufficient airflow. The constant-pressure manifold was fitted with a constant-RPM radial air turbine.

In 2008, Ente Vasco de la Energia (EVE) abandoned the project of an OWC equipped with three columns that would have generated 750 kW; enough to power 750 homes. The OWC was supposed to be integrated into a break-water at the mouth of the River **Douro** in Porto.

In January 2009, the Scottish Government granted consent for the **Siadar Wave Energy Project** (**SWEP**) on the Isle of Lewis in the Outer Hebrides [27]. The SWEP will consist of an "active breakwater" equipped with 40 Wells turbine which would harness power from the

Atlantic waves in Siadar Bay to generate up to 4MW of electricity. It will be a near shore structure, about 350m from the shore. The energy produced each year could supply the average annual electricity needs of approximately 1500 homes equal to a fifth of all homes on Lewis and Harris. The team at npower renewables would assist to design the breakwater, while Wavegen would design the turbine. The wave farm was conceived as a demonstration project to showing that wave power technology is commercially feasible. Thus Siadar might be the first multimegawatt project. In the Summer of 2011, Wavegen was forced to start seeking a new developer for the project as RWE withdrew its funding.

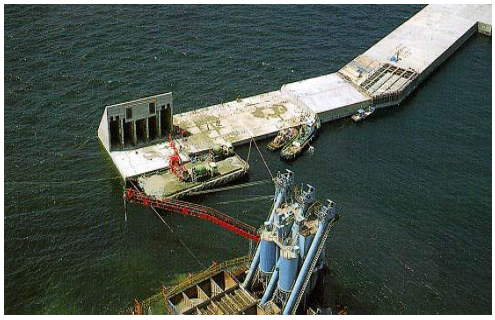

(f)

(g)

Figure 11 – Break-water OWCs: (f) Sakata, (g) Mutriku

Near Shore OWCs (Figure 12) – Between 2005 and 2009 Oceanlinx tested **MK1** *(h),* a full scale near shore prototype which operated many thousands of hours in shallow water [21, 28]. This initially 300 kW wave energy demonstration device is a near-shore OWC installed 200m off Port Kembla breakwater. The device is fixed with legs extending to the seabed and taut mooring lines. The structure was designed by Oceanlinx and JP Kenny Ltd. A novel bi-directional turbine, the Denniss-Auld turbine, was installed in the plant. This single OWC was also equipped with a desalinated water station. The MK1 is currently in the process of being dismantled.

The **Ocean Swell Powered Renewable EnergY** (**OSPREY 1**) *(j),* a near-shore device designed to operate in a water depth of up to 15m and up to 1km offshore, was the first variation of this 2 MW concept, constructed in 1995 to be installed 100m off the coast at Dounreay in the North of Scotland [21]. It comprised a rectangular steel collector chamber with trapezoidal steel ballast tanks fixed either side for gravity anchoring of the device. Mounted on top of the collector chamber was the power module containing the turbine-generators (mounted vertically) and the control equipment. The OSPREY 1 collector chamber is 20m wide and is fabricated using a double skinned, composite construction. However during the installation of the 750 tones structure, a large wave smashed open the ballast tanks and the device had to be abandoned. Wavegen has re-designed this device,

known as the **OSPREY 2000**, as a composite steel and concrete unit. But funding was not forthcoming and the project is not considered likely to proceed.

Oceanlinx has developed specific shallow water OWC, termed **greenWAVE** *(k)* whose ancestor is MK1 [28, 29]. The company is currently preparing the installation of a 5MW greenWave commercial scale array in Australia. This OWC is located in about 10m of water depth, and is mounted on the seabed. While the structure can technically be fabricated from any material, it is generally made from steel or concrete. The method of fixing the structure to the bottom of the ocean is dependent on the geotechnical nature of the seabed. The preferred option, where geotechnical conditions are conducive, is to simply allow the structure to remain in place under its own weight.

(h)

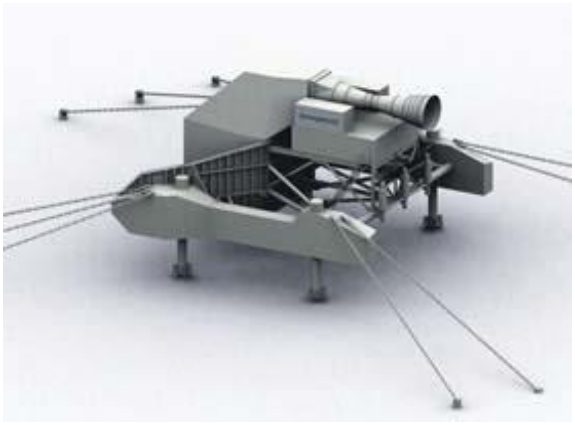

(i)

(j)

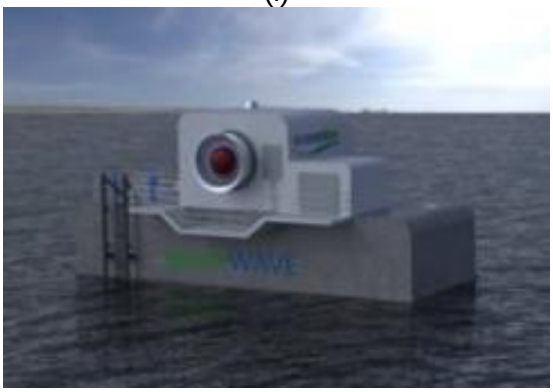

(k)

Figure 12 - Near shore OWCs: (h) MK1, (i) MK1, (j) OSPREY, (k) greenWAVE

Offshore floating OWCs (Figure 13) – In parallel, the study of offshore plants keeps on going, as the amount of energy of developed sea is bigger. Various floating units were investigated. In the late 70's, **Kaimei** *(l)* was the first large scale prototype tested in the Sea of Japan [30, 31]. It was supposed to produce 1.25MW, however the collection efficiency was

reported as 4% [32], but since then some improvements have been made in turbine technology.

Between 1998 and 2002, sea trials were carried out in Japan with the **Mighty Whale** *(n),* a floating moored prototype whose chambers were facing the waves [31]. The power rated was 110 kW but the device showed in general low efficiency. The annual average wave power density at the site where the device was installed was about 4 kW/m, which is considered as quiet sea.

The concepts of **Backward Bent Duct Buoy** (**BBDB**) *(m)* and Frontward Bent Duct Buoy (FBDB) were introduced by Masuda during the 80's [31, 33]. A "pitching resonant state" has even been noticed. Indeed, the phenomenon of resonance can be increased or decreased by varying the length of the horizontal duct, which influenced the pitch motion of the body. In the case of the backward configuration, the opening of the chambers of the floating body is not facing the waves. Compared to the frontward shape, the BBDB has a lower drag design.

Over the years, the design of the **Sea Power Energy Recovery Buoy** (**SPERBOY**) *(o),* a floating buoy OWC, has considerably changed [34, 35]. At the beginning, the device, equipped with 4 tubes, was supposed to extract energy over a wide range of sea states thanks to a number of OWCs of varying length mounted on a floating buoy. Different scaled OWC have been tested. Between 1999 and 2001, a (1:10 scale) was built by a team of the University of Plymouth and deployed in Plymouth Sound, UK. It provided 10 KW in varying wave conditions but was destroyed during a storm due to its mooring. In 2005, Embley Energy completed the Marine Energy Challenge (MEC). At that stage the device was fitted with only one tube. In 2007, a (1:100 scale) mode was tested at the University of Cork. Now they will proceed on the deployment of full-scale prototypes.

Recently, Orecon presented the **Multi Resonant Chamber** (**MRC100**) *(p)* [36]. It is a floating buoy which has vertical mooring attached to a seabed mounted foundation. It was expected to produce 1.5 MW. Unfortunately the project was suspended due to insufficient funding.

Finally during the last three years, Ocean Energy has tested prototypes of its **OE Buoy** *(q)* in the Galway Bay, Ireland [37]. It is a floating device based on a vertical column with a horizontal water intake. When operating in full scale, OE Buoy might generate 1MW.

In 2007 Oceanlinx tested a second third scale prototype, **MK2** *(r),* to improve the design and study the operational behaviour of a floating structure OWC in open sea conditions [28]. The

full scale design is said to be rated at 1.5MW, though no information can be found as to the actual rating of the scaled device.

The last trialled project by Oceanlinx is a pre commercial OWC. It was grid connected between March and May 2010. The Distribution Network Operator (DNO) was Integral Energy. It was designed to be limited in its life and served to validate all design and operating parameters and verify the performance of the blueWave in open sea conditions.
MK3 *(s)* is known as the first Australian grid connected WEC [28]. The full scale design is said to be rated at 2.5 MW, though no information can be found as to the actual rating of the scaled device.

Oceanlinx has developed a specific deep water single oscillating water column device, termed **ogWAVE** *(t)* suitable for deployments in connection with oil and gas platforms or installations in remote areas [28, 29]. This device is a result of the former OWCs MK2 and MK3 and it hasn't been deployed in the sea yet. It is located in water depths above 40m, and is an anchored floating device. The structure can technically be made from any material; it is generally fabricated from steel. The facility can be a simple WEC or a combination of multiple arrays.

Oceanlinx has developed a specific deep water OWC application: the **blueWAVE** *(u)* [28, 29]. This device is a result of the former OWCs MK2 and MK3. This device hasn't been deployed in the sea yet. This structure comprises a cluster of six floating OWCs, joined together via a space-frame. The blueWAVE is located in 40-80m of water depth, and is an anchored floating device. While the structure can technically be made from any material, it is generally fabricated from steel. The method of anchoring the floating structure to the bottom of the ocean is dependent on the geotechnical nature of the seabed. Gravity, drag, and suction anchors are typical candidates for this task. Each blueWAVE is floated to its deployment site, where the task of securing the anchoring system takes place. The distance from shore will depend on the seabed slope, and how rapidly the nominal 40-80m of water depth is achieved. Besides what lies below the waterline, each of the six OWCs also extends several metres above sea level. The above sea level component of the structure is where the airWAVE turbine and electrical control systems are housed. The airWAVE turbine is the only moving part of the technology, and is located well above the waterline.

The Oceanlinx blueWAVE technology differs from greenWAVE in several key areas. Besides being a floating structure in deeper water, its six OWC chambers result in it being bigger than greenWAVE. It is also typically constructed from steel, as opposed to greenWAVE's

concrete. The electrical output of a blueWAVE unit is dependent on the local wave climate. In a good climate, a single blueWAVE device would be rated at 2.5 MW or more. The unit can be dedicated to the production of electricity, desalinated seawater, or both.

MAWEC *(v)* (Multi Wave Absorber Energy Converter) is a floating OWC WEC, developed by Leancon Wave Energy Ltd [38]. It has two arms each angled at 40 degrees to the wave front, both fitted with 30 tubes. To varying extents, depending on the wavelength, air is compressed when the water level is rising and decompressed when it is falling, but tube acts independently. Tests in real sea conditions started up in September 2007. A 1:40 scale prototype, equipped with a turbine, was tested in a wave tank and then at sea. The captured energy of the WEC will be measured by comparing the energy of the waves with the mechanical energy captures by the turbine.

The OWEL Grampus project, started in 2000, combines the OWC principles with a floating horizontal column [39]. The waves travel down a tapering, enclosed box, pushing forward a trapped column of air. The device is designed to have multiple columns mounted side by side. OWEL has already tested a 15m (1:10 scale) prototype and it is currently developing a 750kW device (3:4 scale). The first commercial platform, the 2 MW **OWEL WEC** *(w),* will be available in 2016. It will have three ducts with a total capacity of 2MW, which will provide power for 1200 homes, a 4 MW might follow.

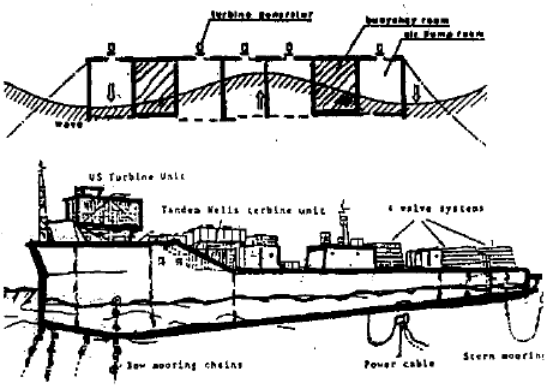

(l)

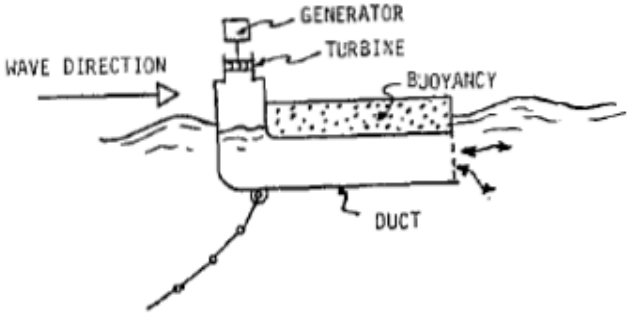

(m)

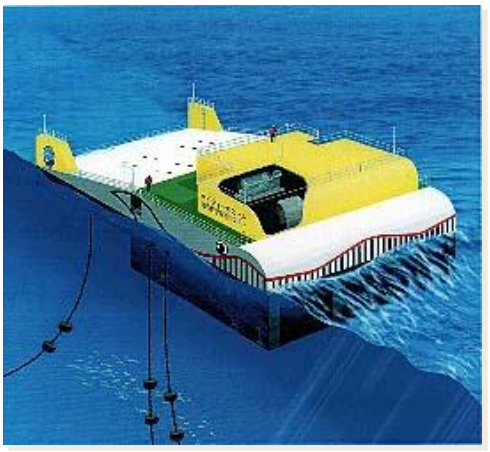

(n)

(o)

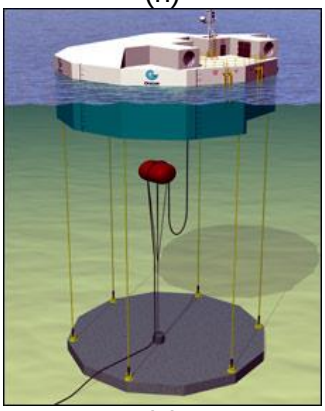

(p)

(q)

(r)

(s)

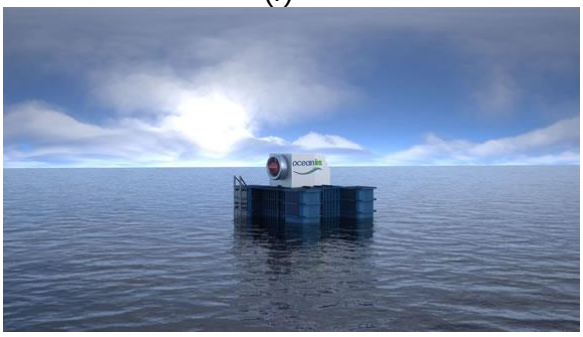

(t)

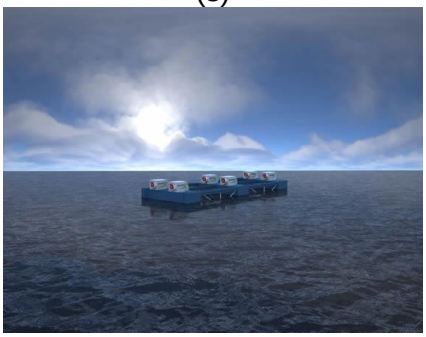

(u)

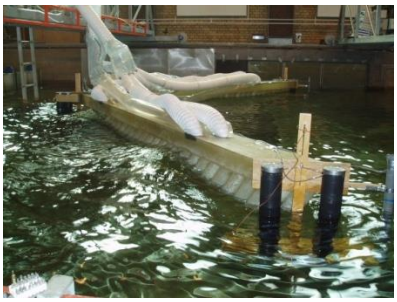

(v)

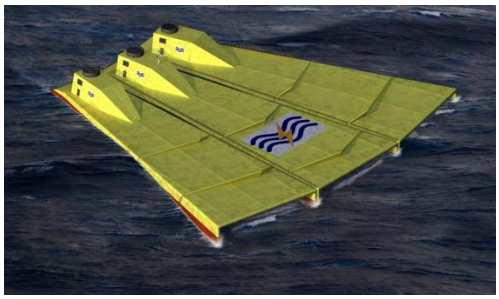

(w)

Figure 13 - Offshore OWCs: (l) Kaimei, (m) BBDB, (n) Mighty Whale, (o) SPERBOY, (p) MRC100, (q) OE Buoy, (r) MK2, (s) MK3, (t) ogWAVE, (u) blueWAVE, (v) MAWEC, (w) OWEL WEC

Offshore fixed OWC – The problem of mooring fatigue does arise in severe and energetic wave climate. Fixed offshore installations have proved their resistance in the past, but no fixed offshore OWC prototype has been deployed until now. There are only a few investigations about fixed offshore units, even though the combination of an OWC and a fixed offshore platform was suggested by McCormick as early as 1974. Indeed, fixed structures are the most durable and cost-effective foundations for waves energy generation as they offer a simpler maintenance of the turbine/generator system than a floating unit. In 1983, a study estimated the best economics match between OWC device and fixed offshore platforms for North Sea site while another considered a fixed OWC integrated into the leg of an immobile offshore platform [40].

As a result, the work of this thesis focuses on the power estimation of an OWC mounted on a fixed offshore installation and the modelling of such a unit. For the moment, the type of offshore installation required is not of concern; it could be a former or a new installation as long as it is fixed to the seabed.

2. 3. Modelling Review

There are various ways of modelling an OWC to predict power capture. These methods can also be used to simulate the system dynamics. The accuracy of these predictions varies depending on the simulation method selected. The models can be grouped into the following topics: (1) those that use impulse response functions, (2) those that are simulated as a mechanical oscillator, and (3) those modelled using BEM or CFD techniques.

2. 3. 1. Impulse Functions and Mechanical Oscillators

Earlier work on OWC in 2D and 3D were investigated by [41]. An analytical problem solved numerically, obtained an expression for the efficiency of wave-energy absorption. Two

models were used to represent the OWC: a float connected to a spring-dashpot system on the top of a column of fluid bounded by two closely-spaced vertical parallel plates (2D) and a narrow tube immersed under waves (3D). The observations showed that plates of equal length might provide a maximum efficiency of 50% (2D) and the capture energy of a crest is greater than the tube diameter (3D).

The mechanical oscillator model considers the resolution of the equation of motion for a mass-damper-spring system. In this model, the internal free surface of the water column is planar as the pressure distribution is deemed homogenous. The mass considered as a rigid body is the mass of the water column between the free surface and the bottom of the OWC. Previous studies, using this model, were carried out for a fixed OWC model [42] with the inclusion of air compressibility. A mechanical oscillator model [43] studied the heave motion of a floating OWC.

2. 3. 2. Boundary Element Methods and Diffraction - Radiation Problem

The BEM are also known as panel methods. In these methods, only the submerged surface (including in some cases the free surface of the water and structure surface) needs to be meshed. This particularity allows quick re-meshing and is less time consuming than methods that solve the Navier-Stokes equations, i.e. CFD. These time-domain modelling methods have been used to predict the diffraction effects around and inside the OWC chamber. The method is based on the specification of flow singularities, sources and sinks of flow, that combined describe a flow velocity field and its associated pressure field given a set of boundary conditions. The technique owes its name to the subdivision of the surface of the body modelled into a number of small surfaces, the panels, over which the discrete singularities act. One of the limitations of the predictions based on boundary element methods is that this approach uses linear diffraction theory and thus cannot account for higher order viscous effects. This is an important shortcoming when the design of the lip of the inlet to the pneumatic chamber is considered.

The interaction of ocean waves with large structures can be described with the potential theory. It means a few assumptions are made about the flow; it is perfect and irrotational, the fluid is incompressible and only small amplitude motions are considered. Thus the flow can be defined by a velocity potential, from which the velocity vector and its components are derived as the gradient of this potential. In this case, the characteristic size of the structure is bigger than the wave height and has the same order than the wavelength [44].

As a result, the incident wave flow is modified by its interaction with the structure; this is called *diffraction*. The phenomena of diffraction must be taken into account when dimensions of the floating body exceed 20% of wavelength of incident regular waves [45]. Besides, if the structure reacts to the wave solicitation by at least one of the 6 DoF (roll, pitch, yaw, heave, surge, sway), a new wave is generated; this is called *radiation*.

In the literature various BEM codes have treated the problem of diffraction-radiation; a review of them is listed below. Two approaches to solve the problem of the oscillating pressure acting on the interior surface of an OWC based on the panel method were presented [46]. In the first one, the velocity potentials are evaluated explicitly while in the second, the problem of diffraction-radiation of a rigid body motion is solved without solving any additional potential. Lee worked on the BEM code WAMIT from MIT, a diffraction-radiation panel code developed for the analysis of the interaction of surface waves with offshore structures. AQUADYN, a BEM code used for floating bodies, developed at Ecole Centrale de Nantes France, was adapted to OWC systems [47]. The results for a bottom-standing OWC were compared to WAMIT predictions and the numerical model was applied to the experimental Pico OWC power plant.

A 3D numerical model of a fixed OWC, used both for regular and irregular waves, was studied [48]. The results revealed asuitability for 3D hydrodynamic design optimisation. An approach considering the resolution of two sub-problems by the BEM method for the inner and the outer behaviours of an OWC chamber was demonstrated [49]. The problem of diffraction and radiation, which requires most of the CPU time, is solved outside the chamber, while the behaviour of the free surface level inside the chamber is modelled considering hydrodynamic and aerodynamical models. The model was applied to the shore based Pico power plant.

2. 3. 3. Computational Fluid Dynamics Investigations

Computational fluid dynamics uses numerical methods to solve Reynolds Average Navier-Stokes Equations (RANSE) problems. These equations can be simplified into Euler equations by removing terms of viscosity. The modelling of two-phase flow is mostly represented by the Volume Of Fluid method (VOF): an advection scheme which describes the shape and location of the free surface. Each cell of the grid is defined by a fraction function comprises between 0 and 1.

As wave propagation is a complex concept, in order to precisely describe the behaviour of the flows inside and outside the chamber, such as the free surface motions, the airflow, or the motions of the water particles, extensive cell refinements would be needed in a CFD model. This characteristic is associated with expensive computational requirements and time consuming solutions. However the accuracy of CFD results would be suitable for the treatment of advanced designs and would be a useful tool for determining the efficiency and power capture of an OWC.

Cranfield University – In recent years, various CFD simulations, investigating the air and water behaviours inside and outside an OWC, have been performed. To model this two-phase flow behaviour, different investigations were carried out at Cranfield University.

In 2007, Fantini began the investigations about the modelling of OWC at Cranfield University [18]. The objective of his work was to assess the abilities of the CFD commercial code ANSYS CFX to model the behaviour of an OWC plant. Different aspects were taken into consideration such as the wave generation, the water column elevation and the aero-hydrodynamic problem.

Given the wave nature, the model ran as transient, using the Linear Wave Theory (LWT) and a two-phase flow inside and outside the chamber. The geometry of OWC was simplified as a quasi-2D model to minimize computational requirement.

The CFD model showed good agreement with LWT to generate waves. After passing from a closed to an opened chamber (equipped with an orifice) which highlighted the drop in extreme values of pressure, he introduced a realistic pressure loss to reproduce the behaviour of a Wells turbine.

The performances of the OWC obtained from the numerical model were compared to an analytical model; the variation between both approaches was theoretically justified by the assumptions made by each model.

The work undertaken by Fantini demonstrated the capabilities of a commercial CFD to model the behaviour of an OWC. Indeed, the model developed managed to capture effectively the interaction of a two-phase free surface flow with the structure both inside and outside the chamber.

In 2008, Brighenti's work extended OWC simulations from 2D to 3D [16]. First, it improved the simulation of the reciprocating airflow across an impulse air turbine fitted downstream and upstream with a bell-mouth. But, it also provided a better water surface fluctuation inside the chamber. In return, computational requirement showed a considerable increase.

Two different intakes (including the bell-mouth) were investigated in order to reduce losses in water to favour a higher water surface displacement.
The pressure inside the chamber and the force exerted by the incident waves were compared to analytical solutions and experimental results, showing again good agreements.

In 2009, the work of Guerrini focused on CFD analysis of OWCs for offshore applications and drew the attention to two key design parameters: resonance and chamber shape [19].
As the previous investigations, simulations to model the wave and their interaction with the structure were run with quasi-2D model and compared to LWT.
The implementation of an energy absorbing volume at the outlet boundary acting like a porous absorber allows to dissipate the wave and to simulate an open sea domain.
To validate the model, a simplified representation of a Mighty Whale prototype has been simulated and compared with sea trials. Numerical results showed good agreement with the tests for wavelengths with the same size than the device only. Indeed, the Mighty Whale is a floating device but the healing motion of the device is not taken into account inside the CFD model.
Numerical simulations carried out with 3 different shapes (bottom intake, forward and backward opening) revealed that the frontward configuration got the biggest performance with a peak of capture efficiency of 32%. Further works is needed to check the capability of the CFD model to identify resonance for OWCs.

In 2010, De Miguel improved the OWC CFD model by implementing random and irregular sea waves, following the JONSWAP spectral energy density distribution, to approach the physics of reel sea waves [17]. A preliminary design study of the turbine diameter demonstrated the capabilities of the CFD model. By combining CFD results and the orifice plate theory, it became possible to determine the optimum turbine diameter for a given geometry and wave climate. Finally, by focusing on OWC control strategies and more specifically the turbine rotational speed control, he drew the attention to a key parameter able to considerably improve the electrical power output.

In 2011, Rigosi extended the work on OWC offshore applications with CFD by introducing the dynamic response of a floating quasi-2D Backward Bent Duct Buoy (BBDB) model in waves [20]. Performances of the floating BBDB were calculated numerically for a range of regular and irregular sea waves and validated against wave tank data and other numerical models. The hull shape was optimized to maximize energy conversion efficiency.
Numerical model demonstrated good predictions of heave motion (heave decay in still water and heave response amplitude in regular wave conditions). It allowed investigating

hydrostatic phenomena by evaluating the position of equilibrium in calm water. It also provided a better understanding of the real operating conditions such as the existence of a damp period depending of the geometry.
Constant air pressure losses for the BBDB ranging 25-30% have been recorded for various sea states.
As a fixed structure constitutes a barrier for wave propagation, the peak of capture efficiency obtained for a fixed BBDB under regular waves wasn't higher than 29%. However, heave motion, generated by a floating BBDB, provided a bigger peak of capture efficiency of 35%. Performances of the BBDB under irregular waves generated by the JONSWAP spectral density distribution are occurring at the same value of λ/L as under regular waves. However, with a lower peak of capture efficiency of 23%, the distribution of capture efficiency is slightly different.
Finally, the addition of an extended duct to the BBDB model showed a significant drop in the capture efficiency due to reducing of pitch and heave motion.

Elsewhere – Others have also been attracted to explore the wave propagation inside CFD codes with is a key parameter of the simulation; an example of investigations is presented here.

An external study with the CFD commercial code ANSYS CFX [50] imagines a 3D numerical viscous tank where the waves are generated with a flat type wave maker in inlet and damped by a beach at the end of the fluid domain to avoid any reflection from the boundary. Dependency of the water depth; time period of oscillations amplitude of oscillations were studied. The accuracy of numerical results was verified against the flap Wave Maker Theory (WMT) and advocated the use of a 1/3 slope ratio. More generally, the study concluded that CFD simulation can replace wave-makers for the generation of regular waves with different wavelengths and amplitudes.

Analysis of water wave modelling was carried out inside the CFD code Fluidity with an open source GNU licence by Imperial College London [51]. Both linear and non-linear hydrodynamics waves were simulated in a 2D Numerical Wave Tank (NWT). For regular waves, the wave field generated was compared with results from the linear WMT.

Chapter 3

POWER EVALUATION

3. 1. Climate Energy Estimation

As many offshore installations are set up off the West coast of the United Stated of America, the fictional scenario of the fixed offshore OWC will take place off California. By choosing a location where offshore structures are already installed, it ensures a favourable wave climate to both OWC unit and offshore installation.

Before estimating the power extractable from a specific device, a preliminary study of the implantation site is suggested. The wave climate data used for this exercise come from the National Oceanic and Atmospheric Administration (NOAA) which gives access to the National Data Buoy Center (NDBC) [52]. For the purpose of this exercise data from Station 46011 – Santa Maria, CA (21 NM Northwest of Point Arguello) were harnessed. Climate for five years was employed 2007, 2008, 2009, 2010 and 2011. The post processing of the wave data was done with routines written by the author in MATLAB.

A wave scatter diagram can be obtained from these data; it shows the wave resource of a location. It is usually omni-directional. For each combination of significant wave height and energy period, the colour indicates its contribution to the total annual energy. The number represents its occurrence. The diagram can be completed with wave power isolines.

For each single year, a MATLAB routine classifies the significant wave height and wave period in bins, generally each meter and second are divided by four. And then it calculates the occurrence of each sea state (formed by one Hs bin and one Ta bin).
The representation of the wave scatter diagram of 2011, presented in Table 5, is slightly different than the one described previously. The probability of occurrence of the different combinations of significant wave height (equivalent to the average wave height, trough to crest, of the one-third largest waves), Hs, and average wave period, Ta, from [0; 1] is indicated by the colour bar. The sea states occurring most appear in warm colours, while the

ones occurring less are dark blue. The number represents the wave power per unit of crest length (kW/m) predicts for each bin [equation 3.2]. A concentration of activity is noticed for waves with Hs from 1.25 to 2m and Ta from 5 to 6s. For instance, the bin [Hs=1.5m, Ta=5.75s] occurred the most during 2011 with 1.55% of occurrences, so its coefficient of distribution is 1.

Significant Wave Height (m) \ Wave period (s) (kW/m)	4.75	5	5.25	5.5	5.75	6	6.25	6.5	6.75	7	7.25	7.5	7.75	8
0.75		1.3		1.4		1.5	1.6	1.6	1.7					
1	2.2	2.3	2.4	2.5	2.6	2.7	2.9	3.0	3.1	3.2	3.3	3.4		
1.25	3.4	3.6	3.8	4.0	4.2	4.3	4.5	4.7	4.9	5.1	5.3	5.4	5.6	
1.5		5.3	5.5	5.8	6.1	6.3	6.6	6.8	7.1	7.4	7.6	7.9	8.2	8.4
1.75		7.2	7.6	7.9	8.3	8.7	9.0	9.4	9.7	10.1	10.5	10.8	11.2	11.5
2			9.9	10.4	10.9	11.4	11.8	12.3	12.8	13.3	13.7	14.2	14.7	15.2
2.25				13.2	13.8	14.4	15.0	15.6	16.2	16.8	17.4	18.0	18.6	19.2
2.5						17.8	18.6	19.3	20.1	20.8	21.6	22.3	23.1	23.8
2.75							22.6	23.5	24.4	25.3	26.2	27.1		
3								28.0	29.1					

Table 5 - Santa Maria wave scatter diagram (2011)

Figure 14 is another representation of Table 5, presenting the occurrence of each bin with a distribution from 0 to 1. The colour bar is the same than Table 5.

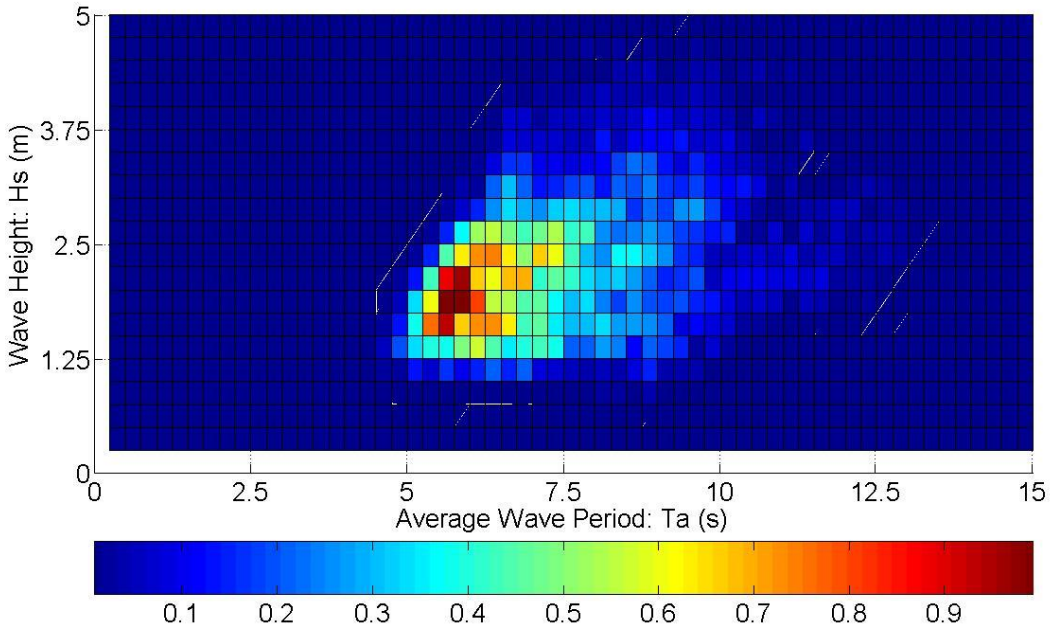

Figure 14 – Sea states occurrence (2011)

Then, the average of the most occurring sea state of Santa Maria was calculated over the past five years: it has a significant wave height of 2m and an average wave period of 6s. This

is in agreement with the mean significant wave height records near Santa Maria between 1997 and 2006, the red cross on the map, around 2-2.5m according to Figure 15; the data originate from the ECMWF WAM model archive and are calibrated and corrected by Fugro OCEANOR against a global buoy and Topex satellite altimeter database.

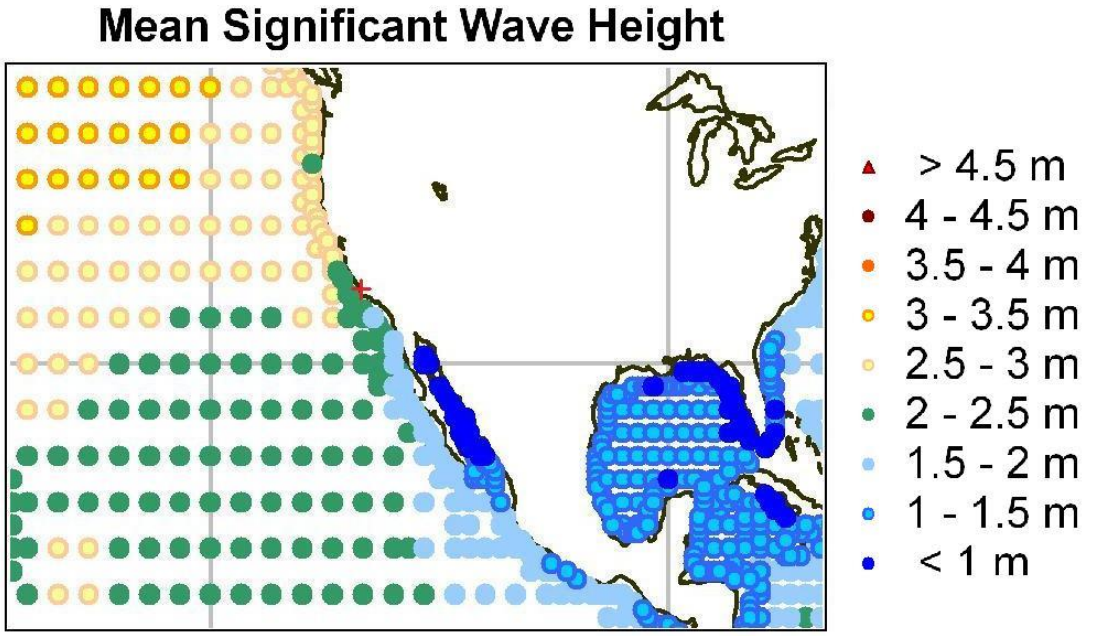

Figure 15 - Mean significant wave height in North America for 1997 to 2006 [53]

A similar approach taking into account the mean wave direction, Dw, can be considered, the size of each bin is then 10°, but the presentation is less obvious as the results depend of three variables: Hs, Ta and Dw. But to give an idea, the most common sea state in 2011 has a significant wave height of 2-2.25m, a wave period of 6-6.25s and a wave mean direction of 300-310°.

The yearly occurrence of the wave mean direction, as seen in Figure 16 for the year 2011, could be a useful factor in choosing the orientation of the OWC inlet. However, it doesn't take into account the significant wave height and the wave period.

Concerning the power assessment, the annual average wave power available is a result of the combination of the wave power per unit of length and the occurrence of each sea state:

$$P_{ave} = \frac{\sum P_i W_i}{\sum W_i} \qquad [3.1]$$

where P is the wave power per unit of crest length (kW/m) and W is the occurrence of each sea state (%). The expression of the wave power per unit of length is:

$$P = 0.49\, {H_s}^2\, T_a = \frac{\rho g^2 {H_s}^2 T_a}{64\,\pi} \qquad [3.2]$$

where ρ is the water density (1025 kg/m^3), g is the gravitational acceleration (9.81 m/s^2), Hs is the significant wave height (m) and Ta is the average wave period (s). The annual average wave power of Santa Maria over the five past years is 19.5 kW/m, details for singular years are presented in Table 6.

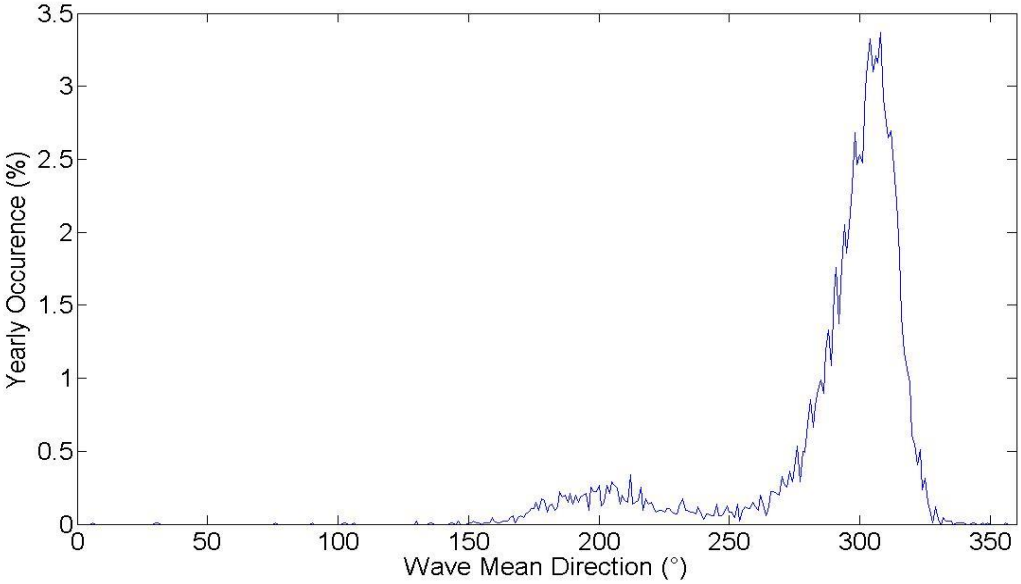

Figure 16 - Santa Maria wave climate directionality (2011)

	2007	2008	2009	2010	2011
Average Annual Power (kW/m)	20.3	20.5	17.0	20.6	18.9

Table 6 – Average annual wave power – Santa Maria

This result can be compared to the global distribution of annual averaged wave power in Figure 17. While deep water records average wave power per unit of crest length between 10-80 kW/m, the values recorded near the shore are generally lower because of the proximity of the coast and the specific geometry of the seabed. Hence, the value recorded close to Santa Maria on the map might is slightly different (20-25 kW/m) from the value calculated above.

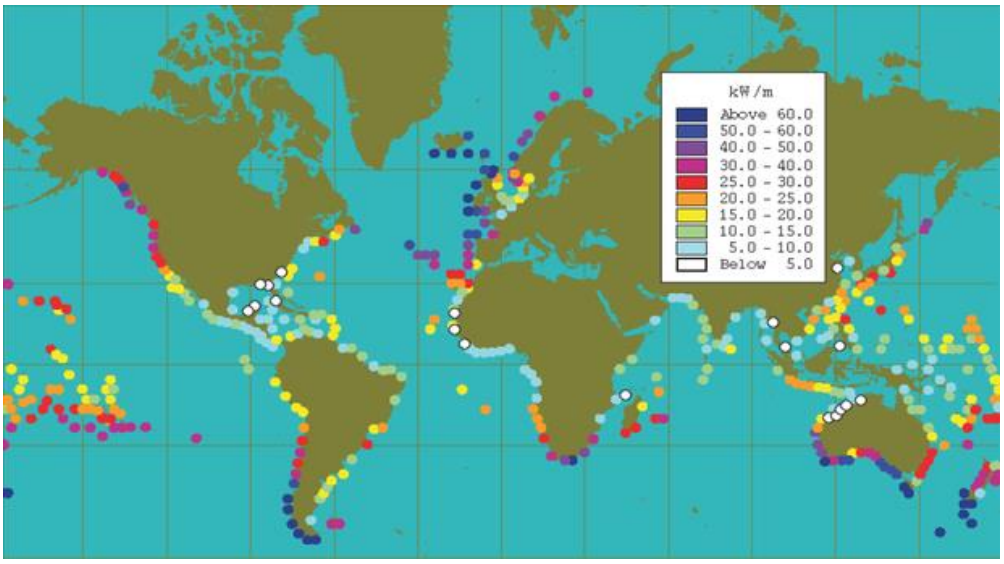

Figure 17 - Global distribution of annual averaged wave power [54]

3. 2. Power Evaluation

However, information is still missing. Indeed, it is important to know if the minimal estimation of power is viable. Hence, the capture efficiency distribution of the device must be taken into account. Its variation depends of the geometry and shape of the device. For instance, the study of different horizontal duct lengths of the BBDB demonstrated the existence of a resonant state for a given wave period [55]. For this exercise, a previous study of the British Department of Trade and Industry on three types of near shore floating device is used as no information is available for fixed offshore units [56]. The DTI produced a report titled *Near Shore Floating Oscillating Wave Column: Prototype Development and Evaluation* where three different types of near shore OWC devices were examined in terms of capture efficiency and cost of build and operation. These devices would be expected to operate in an Atlantic environment. All of the devices employ air turbine power take-off systems. The three configurations are shown in Figure 18. Some tests were tested in full scale configurations while other small scale models results were scaled to full size.

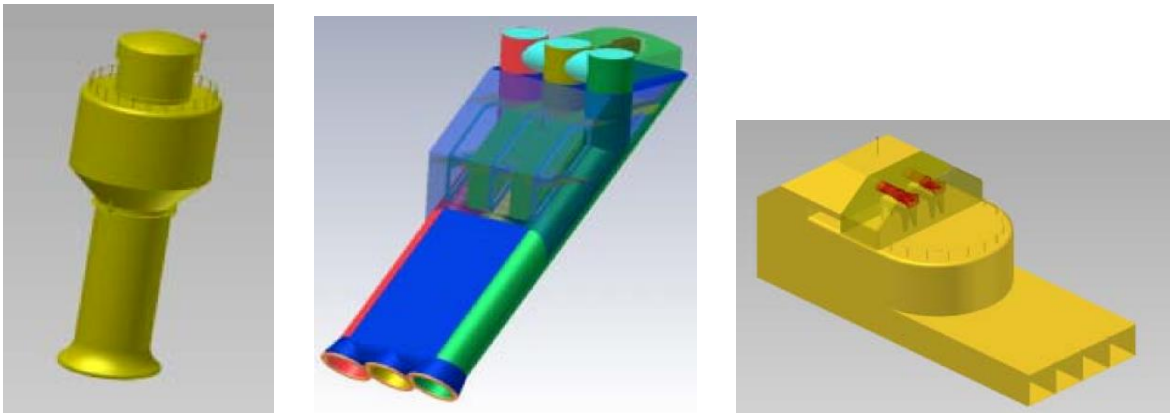

Figure 18 - Spar Buoy (left), Sloped Buoy (middle), BBDB (right)

The conclusions of this comparative analysis, noting that all these devices have evolved since the report was published, are in Table 7.

Spar Buoy	Sloped Buoy	BBDB
Depends on the heave motion and hence the relative motion between the sea surface and the body of the buoy. 1 – Easy, and hence cheaper to build 2 – Omnidirectional power capture 3 – Lower peak capture efficiency **~ 37%** 4 – Large amplitude motions even in moderate sea sates 5 – Poor economics due to low capture efficiency 6 – Best survivability behaviour	This device consisted of three parallel tubes inclined at an angle of 45 degrees which extract energy from the sea from both surge and heave motions. 1 – Good efficiency for a given direction but efficiency falls-off for waves with an approach direction away from buoy alignment 2 – Intermediate survivability	The duct of the device is bent and it is not facing the waves. Hence, the water enters horizontally in the opposite direction to the wave front. 1 – Obtained the highest capture performance of the three devices tested. 2 – Judged to be most adapt for being tuned to sea conditions

Table 7 - Comparison of three devices [56]

Regarding a quantitative comparison, the performance of the three devices is shown in Table 8. The power for a combination of wave heights and periods, together with other characteristics, sea spread and directionality are shown. The wave period used in the table is the peak period, Tp, representing high waves rather than the typical average wave period Ta. As can be seen, the BBDB performs well in unidirectional long crested seas and 10.5s peak periods but less well when the seas are omni-directional.

Pneumatic Performance Comparison for systems on spread mooring in Lewis annual average conditions					**SPAR BUOY**	**SLOPED BUOY**	**BBDB**
Spectral Model	**Hs (m)**	**Tp (s)**	**Sea Directionality**	**Spread Seas**	**(kW)**	**(kW)**	**(kW)**
Bretschneider	3.25	8.7	UNI	Long Crest	177	175	183
Bretschneider	3.25	10.5	UNI	Long Crest	119	144	166
Bretschneider	3.25	10.5	UNI	Cos^10	130	138	142
Bretschneider	3.25	10.5	OMNI	Long Crest	119	133	133
Bretschneider	3.25	10.5	OMNI	Cos^10	130	126	122

Table 8 - Performance comparison of three devices [56]

The projected distribution of the capture efficiency versus wave period of each device is presented in Figure 19. Case 1, called pessimistic case, corresponds to the capture

efficiency measured in tank tests for Spar Buoy, a cylindrical vertical OWC. This is acknowledged as being relatively low capture efficiency with a peak of just 37%. More efficient designs with higher conversion efficiency performance were identified in comparative tank tests. A more reasonable case is represented by Case 2 where the peak of capture efficiency is 51%. Case 3, presented as the optimistic case, has a capture efficiency with a peak of 60%; it is actually lower than the LIMPET shore based device. Both cases 2 and 3 are obtained from the measured Case 1 by a upward shift of the original curve. They represent therefore fictitious but plausible distributions. Besides, the effect of the wave height on the capture efficiency is not predominant.

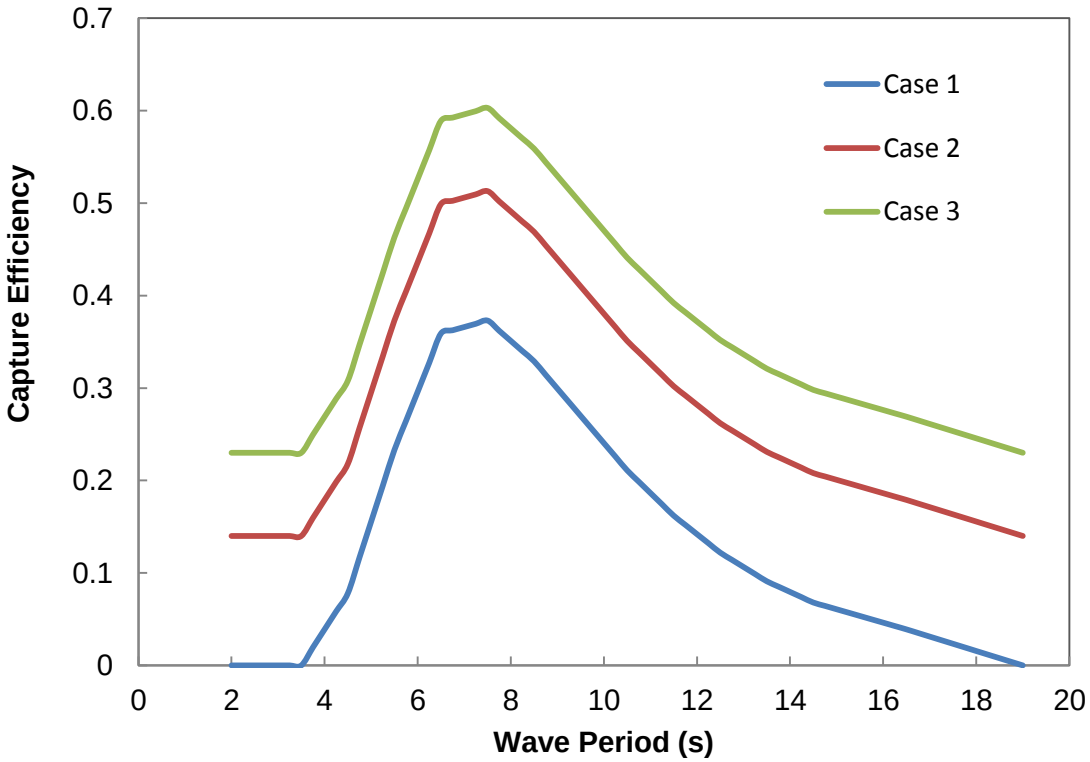

Figure 19 – Capture efficiency distribution

The annual average wave power of Santa Maria site during the chosen period is 19.5 kW/m, thus the three capture efficiencies yield respectively 5.9, 8.7 and 10.4 kW/m; complementary results are presented in Table 9 for years 2007 to 2011. Finally, the annual average output power per unit of length is calculated, with the conversion chain, presented in chapter 2, considering a 65% average turbine efficiency and an efficiency of the rest of the system of 90%; the value ranges 3.5 to 6.1 kW (Table 10). To give an idea, it represents the half of the amount of power available in the North Sea where the wave climate is modestly represented with an annual average wave power per unit of length of 40 kW/m. In conclusion, for a

floating installation, exposed to offshore conditions, even in moderately energetic seas, OWC power production is viable.

Average Annual Power (kW/m)	2007	2008	2009	2010	2011
Capture Efficiency 37%	6.4	6.2	5.3	6.1	5.7
Capture Efficiency 51%	9.3	9.1	7.6	9.0	8.3
Capture Efficiency 60%	11.1	10.9	9.2	10.8	10.0

Table 9 – Average annual power considering capture efficiency – Santa Maria

	case 1		case 2		case 3	
Location	**Santa Maria**	**North Sea**	**Santa Maria**	**North Sea**	**Santa Maria**	**North Sea**
Conversion Efficiency	0.30		0.45		0.53	
Average Turbine Efficiency			0.65			
Other System Components			0.9			
Power (kW/m)	3.5	7.1	5.1	10.4	6.1	12.5
OWC array front – 9.5m	32.8	67.3	48.4	99.2	57.8	118.6

Table 10 – Power estimation for an OWC in Santa Maria and the North Sea

What about a fixed unit exposed to offshore conditions? Could an equivalent viability be expected? To answer these questions experiments were carried out on small scale prototypes: this study is presented in the following chapter.

Chapter 4

TANK EXPERIMENTS AND ANALYTICAL PREDICTIONS EVALUATION

In the previous chapter a theoretical approach based on the capture efficiency of near shore and offshore floating devices [56] was used to assess the wave power extractable with an OWC for a specific location. In the present chapter, two alternative approaches are investigated: an experimental approach and an analytical model, both based on fixed devices.

In a first part, generalities about the conditions of the experiments and the analytical model assumptions are introduced.

Then, a particular interest to wave tank tests studies the effects of a combination of various parameters on the power performance of the OWC. At this step of the study, the analysis inspects the influence of the wave height, the wave period, the geometry and the orifice diameter.

Then, the predictions of the analytical model, and so to say the validity of the model, are evaluated, through a set of wave tank tests employing cylindrical chambers.

Specific tank trials with cylindrical chambers and bent duct buoys are eventually compared with the former theoretical approach for sea conditions equivalent to Santa Maria most frequent sea climate.

4. 1. Test Procedure

This section introduces in more details the specificities of the wave tank tests, the sea conditions, the geometries of OWC studied and the assumptions of the analytical model.

4. 1. 1. Presentation of the Wave Tank

In the 30m x 1.5m x 1.5m wave tank, the waves generated by the paddles of the wave maker are monochromatic. At the end of the canal, the waves are damped by an artificial beach. As

the tests are in small scale, Table 11 presents the Froude scaling employed during the study, where s is the scale employed. The Froude scaling is based on the geometry similitude, all linear dimensions have the same ratio, and thus the model in small scale must have the same shape than the structure in full scale.

Quantity	Scaling
wave height and length	s
wave period	$s^{0.5}$
wave frequency	$s^{-0.5}$
power density	$s^{2.5}$
mass	s^{3}
force	s^{3}
torque	$s^{4.5}$
power	$s^{3.5}$
linear displacement	s
linear velocity	$s^{0.5}$

Table 11 - Froude scaling

The linear wave theory is not fully respected for a 1:50 scale when we consider the combination of water depth, significant wave height and wave period of the most common wave. Thus, the trajectory of the particles is more elliptical than circular in the wave tank (Figure 32). As a result, the model would get a slightly bigger value of water elevation inside the devices.

4. 1. 2. Sea states and geometries

A large range of wave heights and wave periods are tested at a 1:50 scale during the tanks experiments to enlarge the understanding of the phenomena observed; Table 12 and Table 13 present the values used, both in small scale and full scale. Regarding the case of Santa Maria, trials are carried out with a 40mm wave height and a 1s wave period: it corresponds to a wave height of 2m and a wave period of 7s in full scale, closed of the most occurring episode from Santa Maria.

Wave Height (mm) small scale	20	**40**	60	80	100
Wave Height (m) full scale	1	**2**	3	4	5

Table 12 – Wave Heights

Wave Period (s) small scale	0.5	**1**	2
Wave Period (s) full scale	3.5	**7**	14

Table 13 – Wave Periods

The experimental approach gives also the opportunity to compare the power output of various geometries of OWCs. Two shapes are investigated: the first one is a vertical cylindrical bottomless chamber and the second is a bent duct buoy (Figure 20). Tests on the cylinder are carried out on two water drafts (Table 14), while two configurations are considered for the bent duct buoy opening: backward (BBDB) and frontward (FBDB).

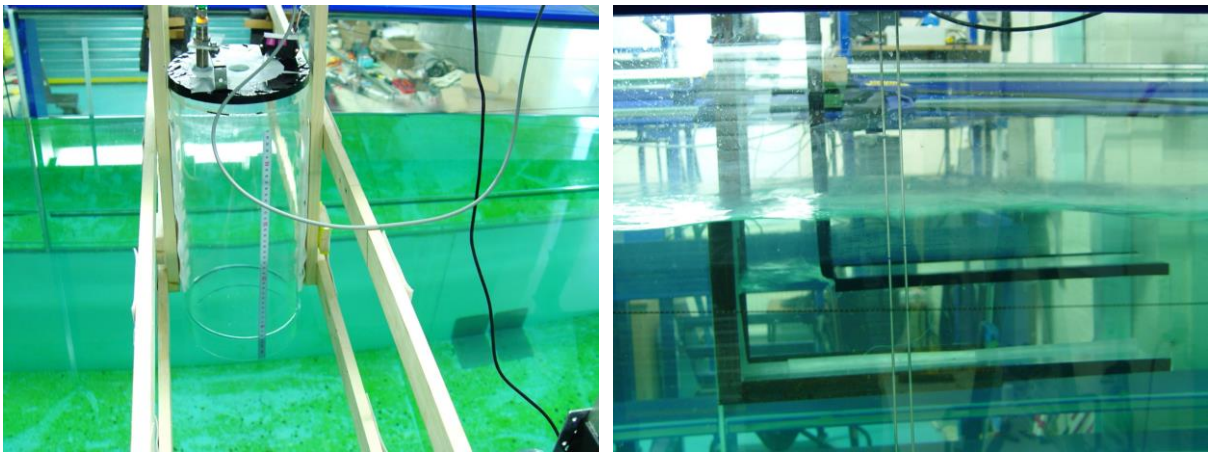

Figure 20 - Cylindrical chamber and bent duct buoy tested in the wave tank

	Cylinder 1	**Cylinder 2**
water draft (mm) small scale	50	75
air draft (mm) small scale	450	425

Table 14 - Drafts dimension in small scale

The cylinder has a length of 500mm and a 190mm diameter what corresponds to a 9.5m diameter in full scale. The open mouth of the bent duct buoy is a 190mm side square (comparable to the cylinder diameter); complementary dimensions are presented in Figure 21. There is no specific reason for the length of the horizontal duct of the bent duct buoy to measure 807mm. However, at this stage the idea was to shorten the length of the duct at the end of the first set of experiments to study the effect on the capture efficiency [55]. Besides, the use of different wave periods allows testing different ratio of wavelength by length of the horizontal duct and studying their influence on the capture efficiency too.

Whatever the geometry, the top of the upper part of the chamber is provided with an orifice symbolizing the turbine. Four orifice diameters (Table 15) were tested to optimize the power output.

Orifice diameter (mm) small scale	**8**	**10**	**20**	**30**
Orifice diameter (m) full scale	**0.4**	**0.5**	**1**	**1.5**

Table 15 - Orifice diameters

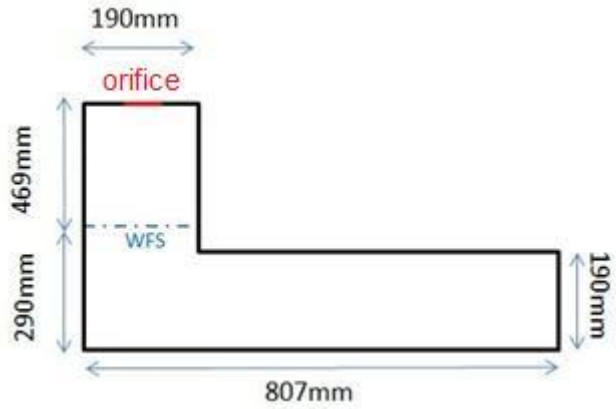

Figure 21 – Dimensions of the bent duct buoy (small scale)

4. 1. 3. A Time-Domain Simulator for an OWC Used for Comparative Results

The chosen analytical model, *Farman 2012*, used for the tests presented here is based on a former analytical model*, Gervelas 2011* [57], itself based on the previous work on trapped air cavities for marine vehicles, describing the coupling between hydrodynamic and thermodynamic problems.

The original model is suitable for both regular and irregular waves and predicts the internal water elevation as well as the pressure variation inside the OWC chamber. It might be used for a preliminary design.

It is inspired by the works on inclusion of pneumatic compliances within marine vehicles [45, 58, 59, 60]. This has been investigated in order to reduce heave, roll and pitch motions of the vessels during excessive wave weather exploring hydrostatic, hydrodynamic approaches.
Indeed, the architecture of a trapped air cavity is quiet similar to an OWC, as the open bottom tank is connected by a valve to the atmosphere. The model used is similar to a mechanical oscillator and solves the equation of motion while the same motion of the water column is observed inside the chamber.

Several assumptions are made: diffraction, turbulence effect, vortex shedding and viscous effects are ignored, instead, a damping coefficient taken as 10% of critical is used. The model applies the linear wave theory and is suitable for small amplitude.

In this 1D time-domain model, Newtons' second law is solved to determine the water elevation inside the chamber, assuming the water column is a solid vertical cylinder with a mass equal to the cylinder of water from the bottom of the cylinder to the internal water level:

$$M\ddot{z} + B\dot{z} + Cz = F(t) \quad [4.1]$$

where M is the mass of the column of water, B is the damping coefficient, C is the hydrostatic restoring coefficient, z is the internal water elevation in the chamber and F(t) is the total force acting on the water column.

The excitation force F(t) is decomposed in three forces:

$$F(t) = F_a(t) + F_{FK}(t) + F_{\delta P_{air}}(t) \quad [4.2]$$

where $F_a(t)$ is the added mass force, $F_{FK}(t)$ is the Froude-Krylov force acting at the bottom of the chamber, $F_{\delta Pair}(t)$ is the vertical force due to the varying air pressure inside the chamber.

The expression of the variation of pressure inside the chamber is obtained considering the ideal gas law, the compression-expansion of the air contained in the chamber is assumed to be an isentropic process.

The problem is reduced to two coupled differential equations, one governing the heave motion of the water column and the other governing the pressure inside the chamber:

$$\begin{cases} \ddot{z} = -0.2\sqrt{\dfrac{g}{\alpha + z}}\,\dot{z} - \dfrac{g}{\alpha + z}\,z + \dfrac{1}{\alpha + z}\displaystyle\sum_{i=1}^{N} \beta_i a_i \cos(\omega_i t + \phi_i) - \dfrac{\Delta P}{\rho(\alpha + z)} \\ \Delta\dot{P} = \dfrac{-{c_s}^2 C_d A_0}{\pi R^2 (h_{a0} - z)}\sqrt{2\,\Delta P\,\rho_{air}} + \gamma\dfrac{(\Delta P + P_{atm})\dot{z}}{h_{a0} - z} \end{cases} \quad [4.3]$$

where ΔP is the difference between the inner pressure and the atmospheric pressure, g is the gravitational acceleration (9.81m/s^{-2}), P_{atm} is the atmospheric pressure, R is the radius of the chamber, a_i is the amplitude, ω_i is the angular frequency, ϕ_i is the phase of the wave, ρ is the water density, ρ_{air} is the air density, h_{a0} is the air draft, C_d is the coefficient of discharge, A_0 is the orifice area, C_s is the speed of sound is the air , α and β are simplifications and γ is the heat capacity ratio.

The model has been compared to wave tank tests of a fixed scaled OWC (1:20) fitted with 3 floating chambers of equal draft [27]. The geometry of the numerical chamber is cylindrical.

As experimental and numerical geometries are different, the dimension of the orifice on the top is calibrated for numerical simulation to reproduce the flow rate measured during the tests.

The comparison of the experimental and the numerical results show a good agreement except when diffraction effects are predominant. The numerical model overestimates the pressure drop at the resonant period in regular waves. The non-linear effects are not taken into account by our analytical model, indeed.

4. 2. Influence of different parameters on the performance of OWC during wave tank tests

During the wave tank tests a combination of parameters have been tested to study the performance of OWC. Even if the tests were carried out in small scale, the results are presented in full scale according to the Froude scaling. Thus, for the purpose of the exercise, 5 wave heights (1; 2; 3; 4; 5m), 3 wave periods (3.5; 7; 14s) , 4 geometries (cylinder 1, cylinder 2, BBDB and FBDB) and 4 orifice diameters (0.4; 0.5; 1; 1.5m) are used.

In the context of the analysis, the expression of the power output is calculated with the flow rate Q (m^3/s) and the root mean square of the pressure drop, ΔP, measured at the orifice exhaust of the chamber (Pa):

$$P = \Delta P\, Q \qquad [4.4]$$

The flow rate expression is:

$$Q = C_d\, A_{orifice} \sqrt{\frac{2\,\Delta P}{\rho_{air}}} \qquad [4.5]$$

where Cd=0.61 is the coefficient of discharge, $A_{orifice}$ is the orifice area (m^2) and ρ_{air}=1.25 kg/m^3 is the air density.

Figure 22, Figure 23 and Figure 24 present the evolution of power extracted with a 2m wave height depending of the size of the orifice diameter and the geometry for 3 different wave periods (3.5; 7 and 14s). Complementary results concerning the behaviour of the rest of the wave heights are presenting in the appendix A.

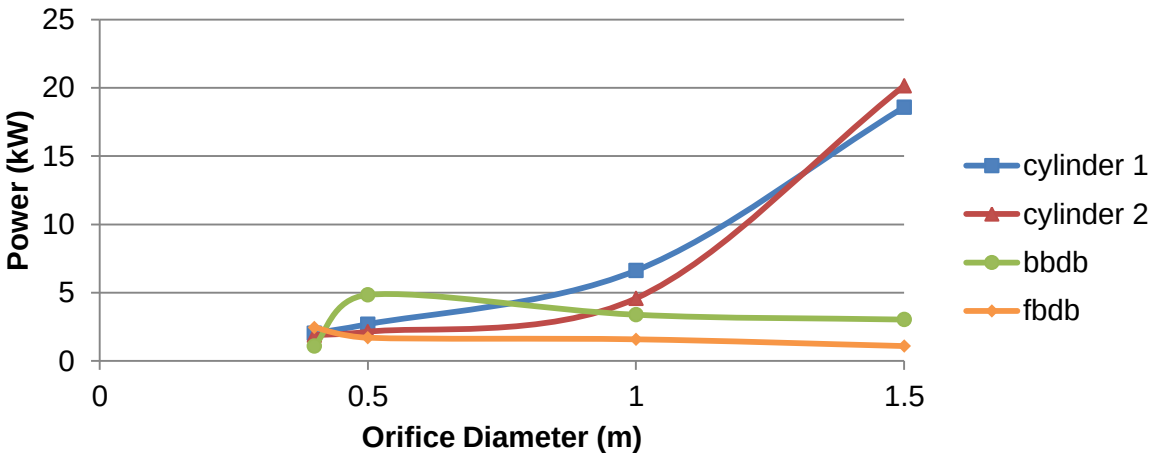

Figure 22 - Power estimation depending of the orifice diameter and the geometry (H=2m; T=3.5s)

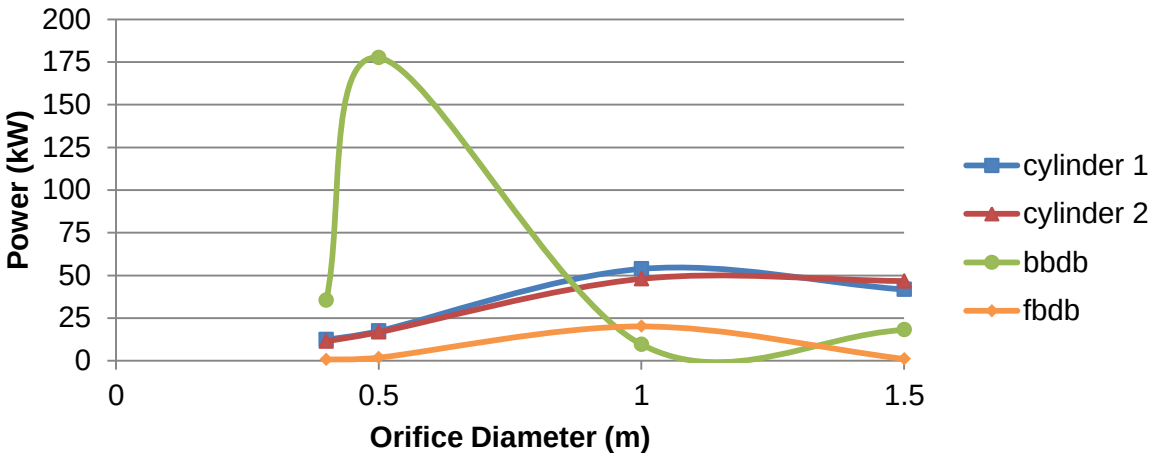

Figure 23 - Power estimation depending of the orifice diameter and the geometry (H=2m; T=7s)

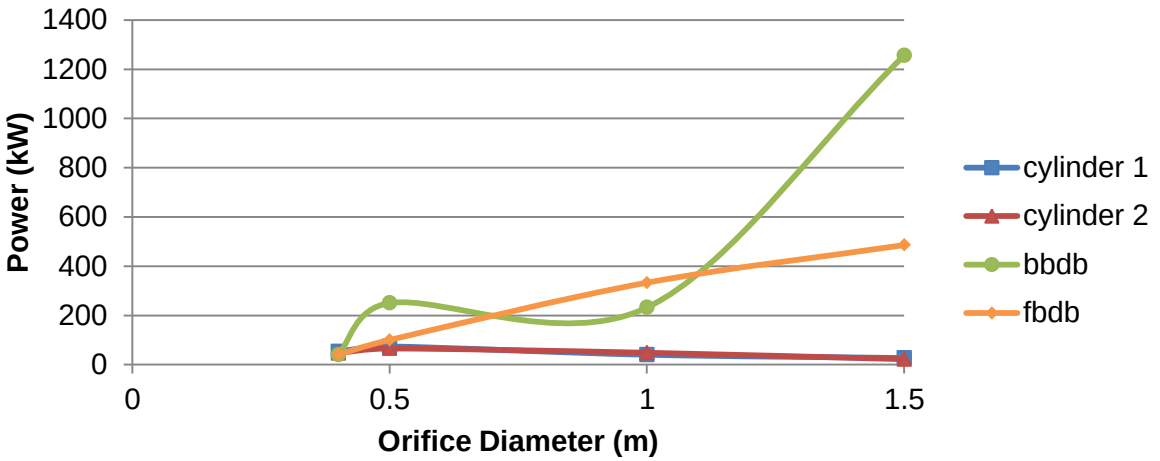

Figure 24 - Power estimation depending of the orifice diameter and the geometry (H=2m; T=14s)

First, it appears that for a fixed wave height (2m), the amount of power extractable grows with the increase of the wave period. For instance, the power extracted by the BBDB with an orifice of 1m takes successively the value of 4 kW, 9.6 kW and 232 kW for wave periods from 3.5 to 14s. Indeed, the more the wave period is long the more the wave length increases. As a result, the slope of the inner free surface becomes smaller, and the amount of pressure reached is bigger.

Regarding the influence of the orifice diameter, the response is specific to each chamber and varies depending of the wave period. The highest performance of each configuration is characterised by a bump in the curve which corresponds to the locus of the resonant phenomenon for the particular geometry and sea state, denoted as: the damping of the device.

In the case of the cylinders which both adopt a similar behaviour, the optimal orifice size decreases when the wave period increases. Indeed, the peak of power is successively associated to the 1.5m, then 1m and 0.5m orifice diameters, respectively with 20, 54 and 74 kW.

In the case of the BBDB, the resonant phenomenon occurs for the 0.5m orifice diameter at two wave periods, 3.5s and 7s, with the corresponding power of 5 and 178 kW respectively. For a wave period of 14s, the recorded peak reaches 1256 kW for a1.5m orifice diameter.
There are two assumptions concerning the origin of the peak associated to the BBDB in Figure 23. The first one assumes that the device is working with a geometry closed to the resonant state specific to the sea climate predefined. The other one would question the presence of reflective waves coming from the wave tank paddle interfering with the incoming wave programmed.

When the wave period increases, the optimal orifice size in favour of the damping of the FBDB increases too; successively from 0.4, 1 to 1.5m. The associated power outputs are 2.5, 20 and 486 kW.

Overall, the cylinders with a 1.5m orifice provide the best performance for a small wave period: ~20 kW (Figure 22). However, for medium and long wave periods, the optimum selection is the BBDB successively with an orifice of 0.5 and 1.5m (Figure 23 and Figure 24); the power generated is evaluated respectively to 178 and 1256 kW. Finally, the addition of a horizontal duct (BBDB and FBDB) optimized the performance of the device working in long wave period (Figure 24). All these observations, also applicable to the figures in appendix A, highlight the dependency of the performance with the geometry. Hence, it is important to remind that additive orifice sizes not tested here might get greater power output.

Considering the length of the horizontal duct of the bent buoy, the experiments were repeated later in the test campaign at a location further away from the tank paddle to avoid any interaction with potential reflective waves. At the time of the investigation, the study was focusing especially on one sea condition hence the new tests were only carried out for every chamber with a 2m wave height and 2 wave periods (7 and 14s). The results from this new set of experiments are presented later in the section comparing the tank tests with the theoretical predictions based on Santa Maria wave climate.

4. 3. Evaluation of the analytical model in comparison with tank tests carried out on cylindrical chambers

The analytical model evaluated in this part, has been presented earlier. As previously suggested, the model used a vertical cylindrical chamber; hence the predictions are only compared with 1:50 scale experiments carried out on the bottomless cylinder and its two water drafts.

Among the analysis only a part of the results in small scale is presented as the trend observed looks the same. The values used for the comparison are the pressure drop, ΔP, and its resulting power output [equation 6]. The following figures of the variation of pressure drop over the time (Figure 25 to Figure 27) were obtained for the cylinder 1 with a water draft of 50mm, an orifice of 8mm and a wave height of 40mm. The changing parameter is the wave period, successively fixed at 0.5s, 1s and finally 2s; they can be respectively called short, medium and long wave periods. In annexe, additional figures are presented in appendix B for wave height of 60, 70 and 80mm.

As seen from Figure 25 to Figure 27, the wave period has a lot of influence on the agreement between the experiments and the predictions of the model. It appears that the analytical model underestimates the pressure drop for shorts waves (0.5s) and has a good agreement for longer waves (2s). Meanwhile, the medium wave of 1s overestimates the pressure.

The wavelength, λ, associated to these three wave periods (0.5, 1 and 2s) are respectively 0.39, 1.56 and 5.8m. They are calculated from the expression of the wave period valid for any water depth:

$$T = \sqrt{\frac{2\pi\,\lambda}{g\ tanh(\frac{2\pi\,h}{\lambda})}}$$

[4.6]

where g is the gravitational acceleration (9.81 m/s^2) and h is the water depth.

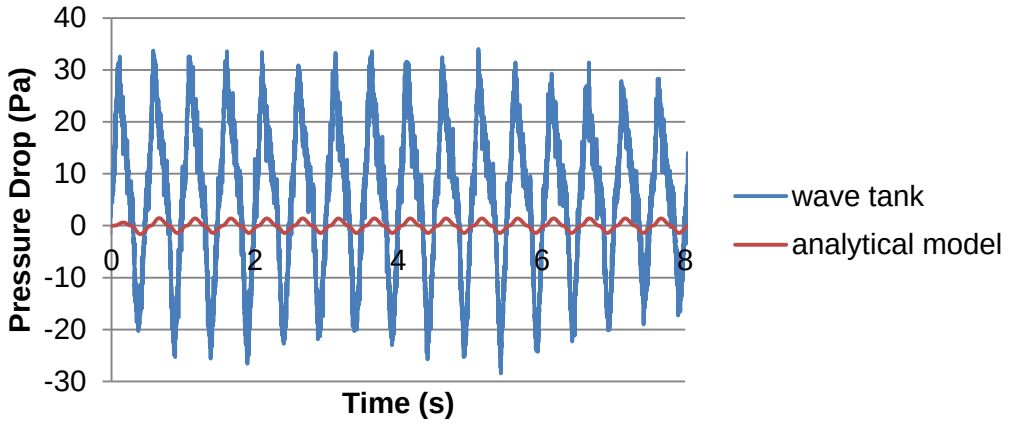

Figure 25 - Pressure drop measured for a 50mm water draft cylinder with an 8mm orifice diameter (Hs=40mm; T=0.5s)

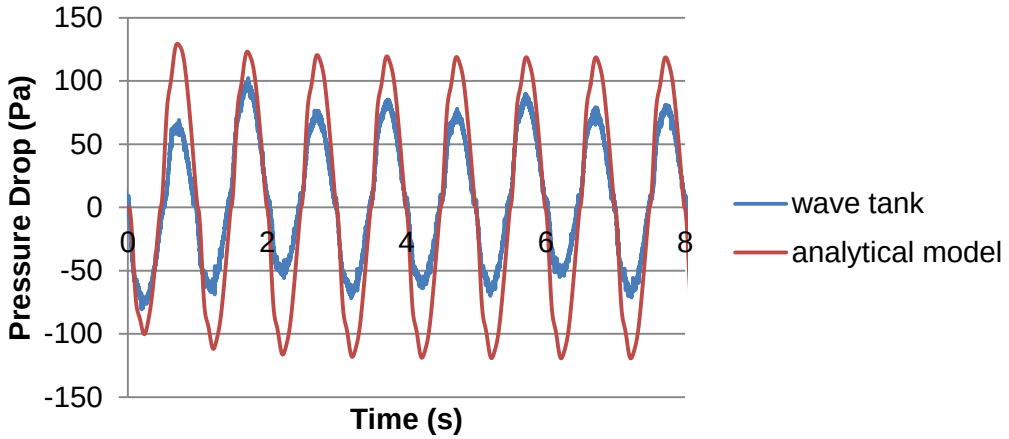

Figure 26 - Pressure drop measured for a 50mm water draft cylinder with an 8mm orifice diameter (Hs=40mm; T=1s)

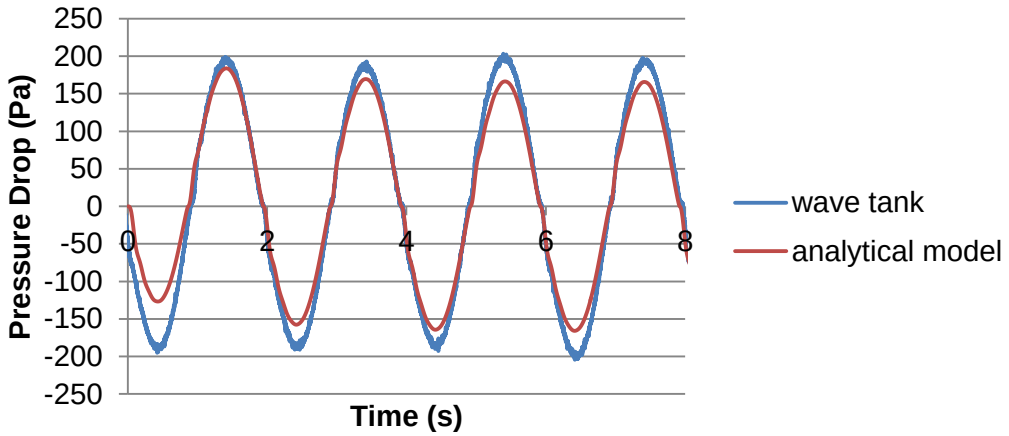

Figure 27 - Pressure drop measured for a 50mm water draft cylinder with an 8mm orifice diameter (Hs=40mm; T=2s)

As a matter of fact, the numerical model doesn't take into account viscous effects. However, these effects are particularly important and have an impact on the water elevation inside the cylinder when the device (diameter of 190mm) has the same order than the wavelength. In the studied case, this is what happens for the short wave period which has a wavelength of 390mm, so to say only two times the diameter of the chamber (Figure 25). As a result, the analytical model underestimates the pressure drop and shows smaller results than the ones achieved with the experiment.

Besides, in the case of a long wave period the device is approximately 30 times smaller than the wavelength (5.8m). Thus the flow around and inside the chamber is less perturbed by the presence of the structure; hence the viscous effects are less important. As a consequence, the model, which is inviscid, is more able to reproduce the physics and is in good agreement with the wave tank tests (Figure 27).

These previous observations can be emphasised by Figure 28 and Figure 29. They compare the power extracted (W) for the experimental and the analytical tests for medium and long wave periods in small scale. Cases 1 and 2 refer to the water drafts of cylinder 1 and cylinder 2 [Table 14]. Indeed, the trends of the pressure drop can be translated to the power [equation 4.5]. Hence, the model obtains up to three times the value of power of the wave tank tests for a 1s wave period in Figure 28. In the meantime, a better agreement is notable for a 2s wave period in Figure 29 especially for the peak of power corresponding to the resonant phenomenon. More generally, even though the amount of power predicted by the model is sometimes far from the tank test expectations, the phenomenon of resonance is fairly well reproduced by the model.

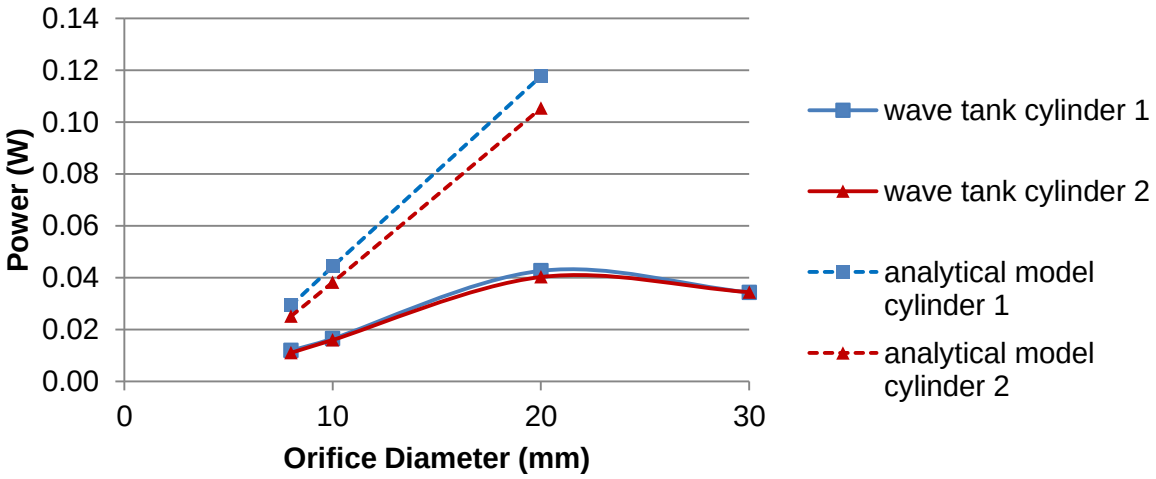

Figure 28 - Comparison of experimental and analytical predictions of power (W) for a 190mm diameter cylinder (Hs=0.04m; T=1s)

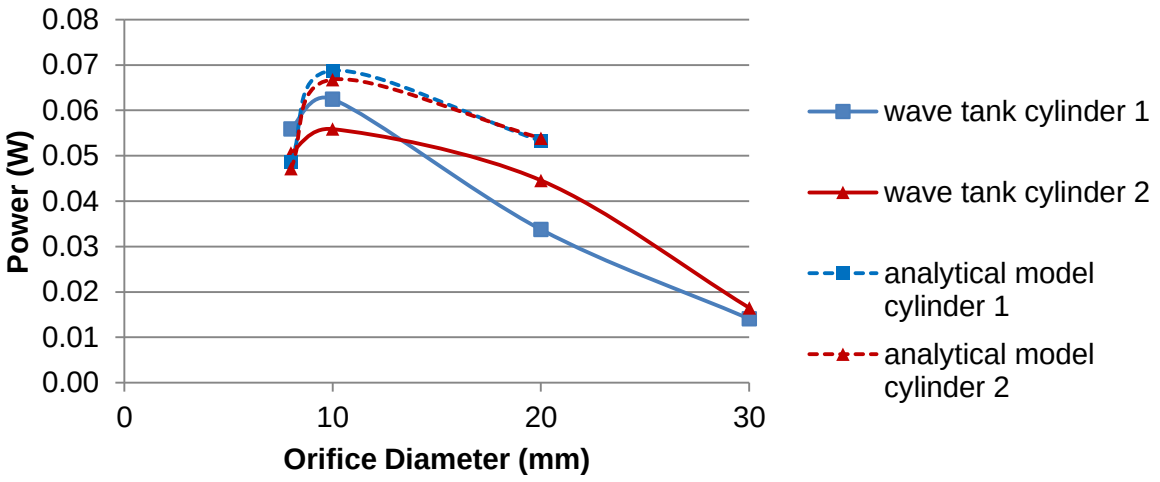

Figure 29 - Comparison of experimental and analytical predictions of power (W) for a 190mm diameter cylinder (Hs=0.04m; T=2s)

Therefore, the analytical model is not suitable for medium wave period. So to say it is not appropriate to predict the power extractable from device installed in Santa Maria wave climate. Thus, it is preferable to use the experimental approach for this specific purpose.

4. 4. Performance of the cylinders and the bent duct buoys compared to Santa Maria predictions

In this last section, the Santa Maria power estimation based on near shore floating devices [56] is compared with the experimental results on fixed chambers. Hence, the sea conditions used are a wave height of 2m and a wave period of 7s. An extension to long wave period is also presented. The estimation of the power extractable from both cylindrical and bent duct buoy shapes calculated from the measurement of the pressure drop during the tests is converted into full scale.

As specified earlier, the results presented here come from tests carried out at a location further from the paddles to avoid any interference with reflective waves. Table 16 shows the results and Figure 30 highlights the trends of the curves for a 7s wave period.

It appears that both cylindrical chambers get the maximum of power, around 35.6-37.7 kW, for an orifice/turbine with a diameter of 1m. However the BBDB gets a bigger amount, 57.9 kW, for a smaller orifice of 0.4m. Meanwhile, the FBDB has pour results reaching 4.1kW for an orifice size of 1.5m.

Orifice diameter (m)	0.4	0.5	1	1.5
Power (kW) $_{\text{Cylinder water draft=case 1}}$	10.5	14.6	37.7	30.3
Power (kW) $_{\text{Cylinder water draft=case 2}}$	9.8	14.1	35.6	30.4
Power (kW) $_{\text{BBDB}}$	57.9	48.0	14.8	5.0
Power (kW) $_{\text{FBDB}}$	0.9	2.2	2.8	4.1

Table 16 - Comparison of power estimation (full scale) for different chambers (H = 2m; T = 7s)

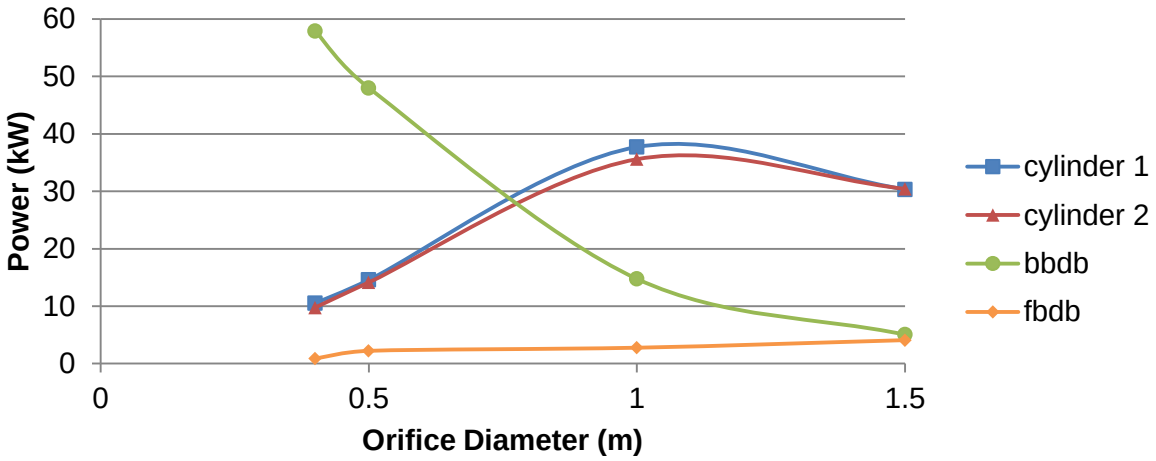

Figure 30 - Power estimation depending of the orifice diameter and the geometry (H = 2m; T = 7s)

In comparison with the tests carried out at a location closer to the paddles (Figure 23), the maximum power outputs are: 1.5 times lower for the cylindrical chambers, 3 times lower for the BBDB, and 4 lower for the FBDB. The appearance of a peak in the power output provided by the cylindrical chamber as a function of the orifice size is to be expected. Indeed, this locus corresponds to the resonance phenomenon associated to the combination of the geometry and the sea conditions predefined. As no peak is clearly observed in the bent duct buoys behaviour, it suggests that the shapes considered do not favour the occurrence of this phenomenon at the conditions tested. It might occur for a smaller orifice than 0.4 in the case of the BBDB, and a bigger orifice than 1.5m in the case of the FBDB.

Indeed, this geometry has not been subjected to variation yet, as would suggest a study carried out on 2D and 3D tank tests, drawing the attention to different key parameters which are governing the primary energy conversion of floating BBDB [55]. Elements such as the length of the horizontal duct, the draft, and the direction of incident waves have a deep impact on the performance. It appeared that wavelength, for which energy conversion

efficiency is maximum, is about four times the length of the BBDB horizontal duct. The maximum value of efficiency of 70% was obtained with the backward configuration of the bent duct buoy, while the frontward configuration reached a peak of capture efficiency of 10%. Finally, passing from 2D to 3D cases suggested an increase of the peak of capture efficiency of 40% supposing an improvement due to wave diffracted by the BBDB.
Thus, a next campaign might be carried out to optimize the capture efficiency and so to say the power output

As tank tests were carried out for sea conditions closed to the most common sea state observed in Santa Maria over the five past years, a comparison of the power estimation is possible. However, it must be kept in mind that the first estimations based on capture efficiencies of floating devices whereas the estimation based on tank tests are for fixed devices.
According to the 1:50 scale used for the tank tests, the OWC considered has a diameter of 9.5m in full scale. The power for such dimensions was previously calculated for Santa Maria site and is presented in Table 10.

The power expected for the lowest capture efficiency (37%) in Santa Maria, 32.8 kW, is closed to the peak of power estimated for the tank fixed cylinders, 35.6-37.7 kW. Indeed, the lowest capture efficiency was associated to the Spar Buoy, a floating cylindrical OWC. Besides, the highest capture efficiency (60%) in Santa Maria, 57.8 kW, and the maximum amount of power estimated for the tank fixed BBDB, 57.9 kW are similar. In the DTI report, a better capture efficiency was noticed for the BBDB [56].

In on hand this good agreement is encouraging and leads to believe that the wave climate of Santa Maria would be viable for a fixed offshore OWC. It might also suggest that a bigger amount of power could be supplied if the device is optimised.
In the other hand the peak of power is obtained for a turbine diameter of 0.4m what is quite small. This last observation questions the feasibility of a turbine of such dimension. Thus, an additional campaign would be highly recommended to optimize a BBDB chamber with a bigger diameter.

To go further in the understanding of the behaviour of the geometries, the tests have been repeated for a longer wave period of 14s (Figure 31). First, the bent duct buoy performs better than the cylinder for orifices bigger than 0.5m, and it can even produce up to 30 times the power extracted by the cylinder for a 1.5m orifice size. Besides, the phenomenon of resonance of the two bent duct buoy configurations doesn’t occur for the selected range of orifice diameters unlike the cylinders. According to the tendency of the curves, it might rather

happen for bigger orifice diameters and could even reach amount of power bigger than 500 kW. Finally, it is interesting to notice that the FBDB response overtakes the performance of the BBDB, which was not the case for the wave period of 7s. Thus, one configuration might be preferable to another depending of the wave period and so to say the most occurring wave climate of a location.

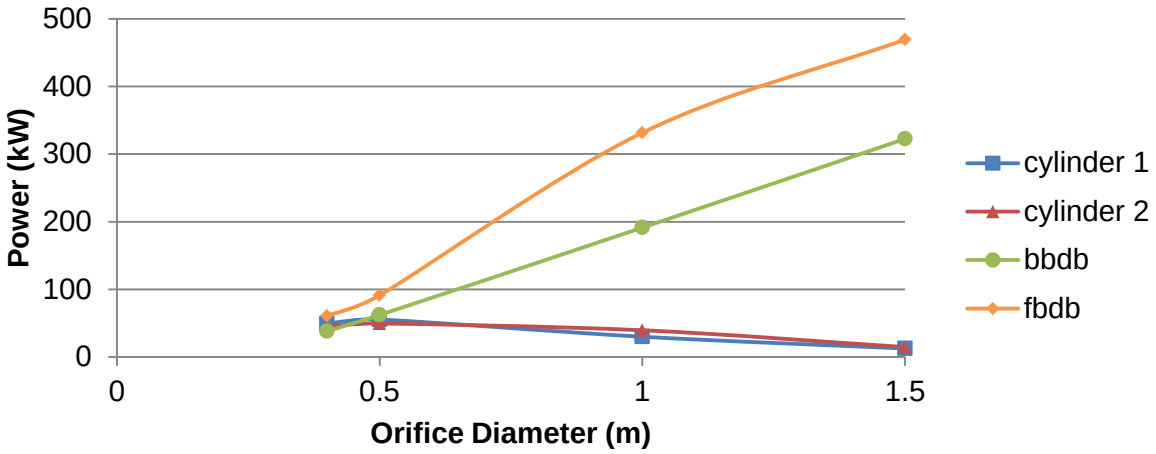

Figure 31 - Power estimation depending of the orifice diameter and the geometry (H = 2m; T = 14s)

Chapter 5

NUMERICAL INVESTIGATIONS

After assessing the power of an OWC for a specific location, first based on the capture efficiency of floating devices, and then from tank tests on fixed prototypes in small scale, a numerical investigations are presented. In fact, the use of CFD should intend to offer the possibility to demonstrate the viability of the unit studied and evaluate the wave tank tests precision by getting a better accuracy of the power estimation.

This chapter introduced investigations on an alternative wave generation method using a numerical wave maker. The first part brings the attention of the reader attention the the different wave theories, wave generation and damping methods. In a second part, the settings of the new method are presenting. In a third part, the results are analysed before making recommendations for a CFD approach of the Santa Maria case.

Before continuing a short introduction to the main settings of an OWC simulation with CFD is presented. More generally, CFD uses numerical methods to solve Reynolds Average Navier-Stokes Equations (RANSE) problems which can be simplified into Euler equations by removing terms of viscosity. The treatment of the interface between air and water which is characteristic to any wave problem is possible thanks to the use of the Volume Of Fluid method (VOF). It is an advection scheme which describes the shape and location of the free surface by considering a two-phase flow and the water free surface. In this model, each cell of the grid is defined by a fraction function comprises between 0 and 1.
As the wave propagation is a complex concept, in order to precisely describe the behaviour of the flows inside and outside the chamber, such as the free surface motions, the airflow, or the motions of the water particles, extensive cell refinements would be needed at the locations previously mentioned. For the same reasons, the simulation is transient. These characteristics are associated to expensive computational requirement and time consuming solutions. Hence, to reduce the computational cost, sometimes there will be the possibility to run quasi 2D simulations or to resolve the problem for the half of the device if it is symmetric, as long as the convergence and the accuracy of the solution are respected.

5. 1. Wave Generation

There are various ways to generate waves inside a fluid domain. The following sections explore the different methods used during the previous works undertaken at Cranfield University, and introduce an alternative method.

5. 1. 1. Regular Waves: Linear Wave Theory

Up to now, the Airy Wave Theory commonly called Linear Wave Theory (LWT) has been privileged to generate regular waves as it is a good compromise between accuracy and implementation ease [17, 18, 19, 20]. The LWT makes various assumptions; it is valid for small wave amplitudes and in deep water where the particles trajectory is described as circular (Figure 32). Surface tension and viscosity are neglected and the fluid has a constant density and is irrotational.

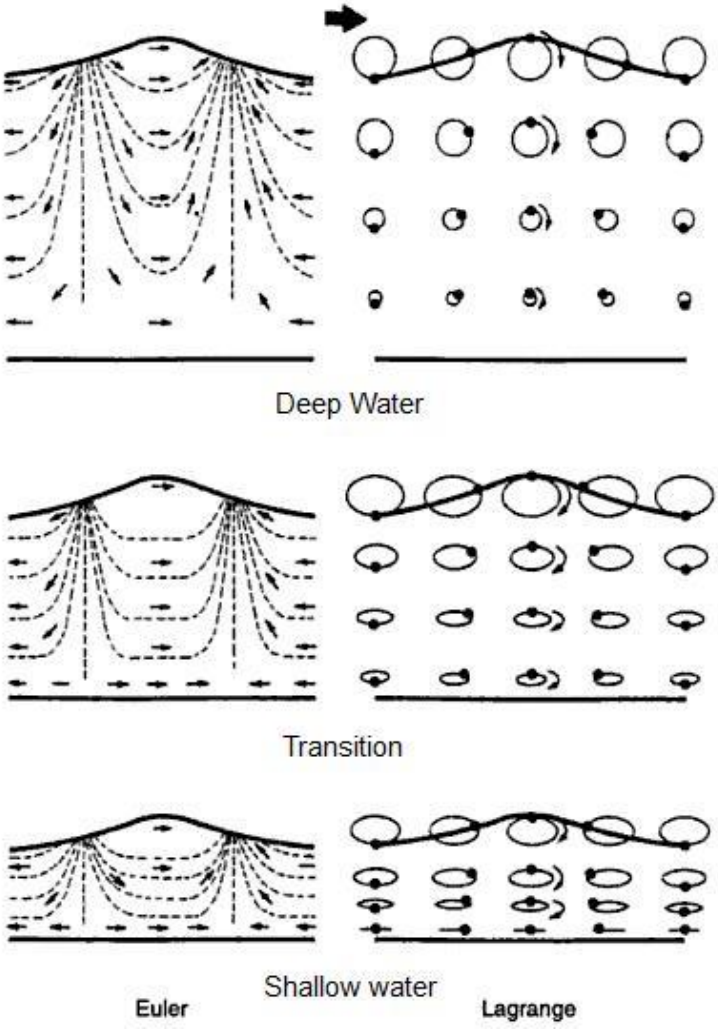

Figure 32 - Particles motion [44]

In this method, the horizontal and vertical components of the orbital velocity, u and v, are implemented at the initial inlet and other boundary, while the expression of the water surface elevation, η, is defined in inlet:

$$u = Aw\, e^{ky} \cos(kx - wt) \quad [5.1]$$

$$v = -Aw\, e^{ky} \sin(kx - wt) \quad [5.2]$$

$$\eta = A \cos(kx - wt) \quad [5.3]$$

Where A is the wave amplitude (m), A = H/2 with H the wave height (m), ω is the pulsation (rad.s^{-1}), **K** is the wave number and k is the magnitude of the wave number (m^{-1}), y is the distance between the point at the water free surface and the seabed and h is the water depth without wave.

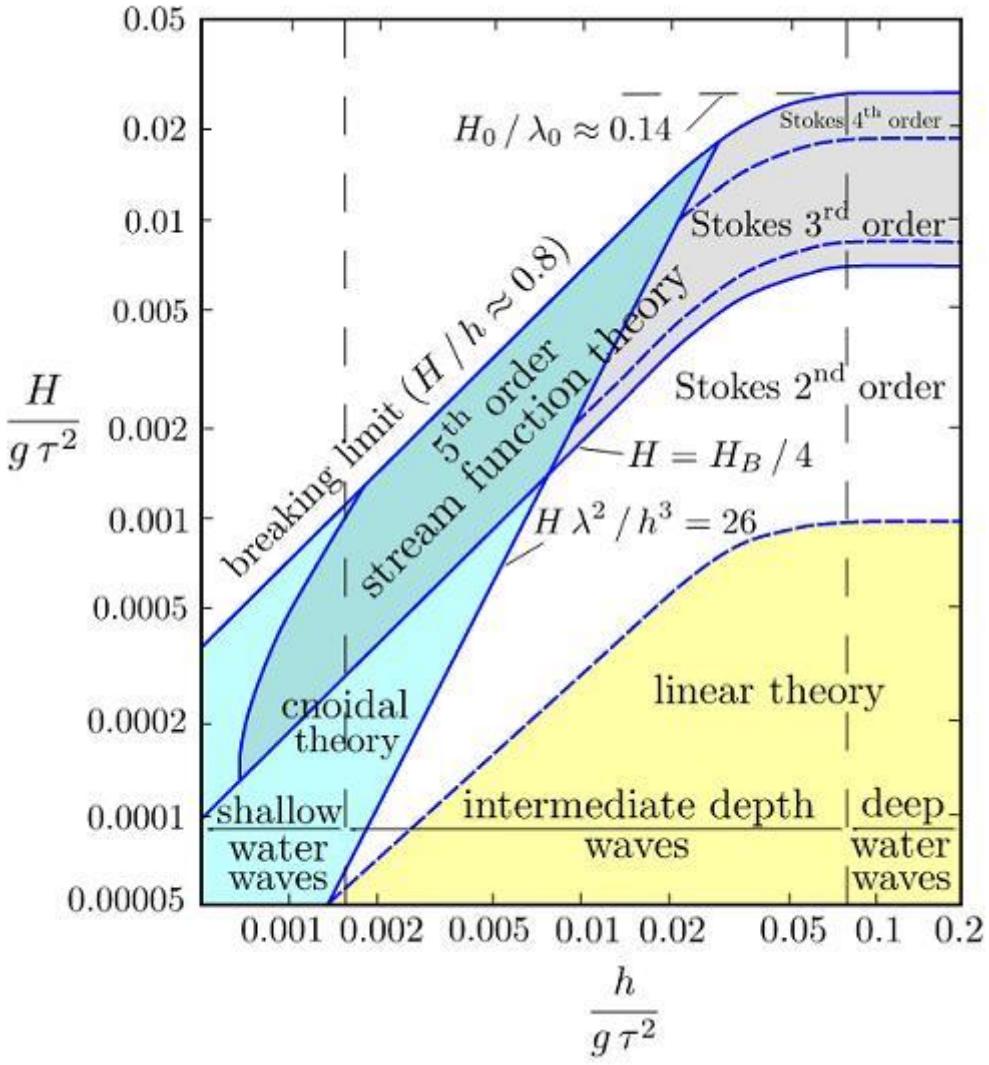

Figure 33 – Limits of validity for various wave theories according to [61]

Figure 33 presents the domain of validity of different wave theories where H is the wave height (m), τ is the wave period (s), g is the gravitational acceleration ($m.s^{-2}$), h is the water depth (m). From a trio of wave height, wave period and water depth, the diagram determines the wave theory suitable to model the wave according to two ratio $H/(g\,\tau^2)$ and $h/(g\,\tau^2)$. As previously mentioned, the LWT is a sinusoidal wave valid in deep water for small wave amplitudes. Wave theories of Stokes up to the 5^{th} order allow to model complex waves in the limit of validity of the model; they result of a combination of different sinusoidal signals. Some extreme waves break inevitably because of their steepness. Theoretically, they can't be modelled by any of the wave theories mentioned on the diagram as the ratio of H/λ is over or equal to 0.14 [44, 61].

Concerning the application of LWT in a CFD simulation, if the steepness of the implemented wave is not valid in LWT, the inlet boundary condition is not respected inside the domain and can engendered discontinuities at the boundaries and even formation of non-linear effects such as breaking waves.

5. 1. 2. Irregular Waves: Wave Spectrum

The random behaviour of the sea was investigated by De Miguel who implemented the model of JONSWAP inside CFX [17]. This model, following the Fourier transform concept, assumes that the wave elevation distribution is a superposition of sinusoidal waves with different heights, periods and phases. The equations used won't be presented here as the model has not been used during the work of the thesis but they are available in [17].

5. 1. 3. Wave Makers

An alternative approach to generate waves in CFX is proposed to the previous methods used by Cranfield students. It consists to reproduce the movement of a wave maker at the inlet of the fluid domain. As a consequence, one of the boundaries is in motion, and the domain is equivalent to a numerical wave tank.

Two models of wave makers are presented below. The first, a piston type, compresses and decompresses the flow along the x axis; it is easier to implement. The second, a flap type, generates the motion with a paddle rotating around the z axis (Figure 34).

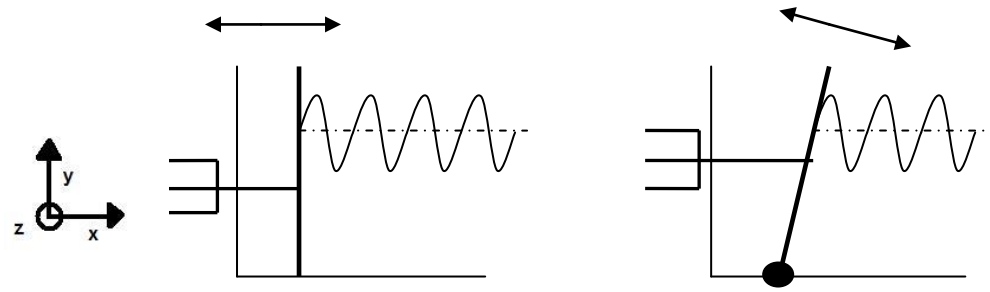

Figure 34 - Wake makers generating waves: a piston (left), a paddle or flap (right)

The wave maker law used for the simulation consider the amplitude of the movement of a wave maker (piston or paddle), x_0, linked to the wave amplitude, A, by a transfer function. The law of the piston wave maker is:

$$\frac{A}{x_0} = \frac{4\,sinh^2\,kh}{2kh + sinh\,2kh}$$

[5.4]

Where h is the water depth and k is the wave number. The expression describing the motion of the piston is x_0*sin(ωt).

The law of the flap type wave maker is:

$$\frac{A}{x_0} = \frac{4\,sinh\,kh\,(kh\,sinh\,kh - cosh\,kh + 1)}{kh\,(2kh + sinh\,2kh)}$$

[5.5]

Where h is the water depth and k is the wave number. The expression describing the angular motion of the paddle is Θ$_0$*sin(ωt), where $\Theta_0 = \frac{x_0}{h}$ (rad), corresponds to the angle made by the height of the domain and the paddle of the wave maker.

For instance, studies already validated a 2D flap type wave maker in CFX [50]. This study checked the good agreement with the Wave Maker Theory (WMT), evaluated the wave propagation and optimised the slope of the beach (Figure 35).

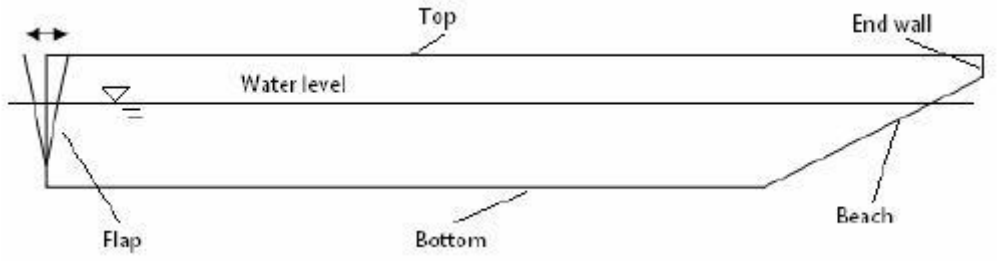

Figure 35 – 2D schematic diagram for flap wave maker [50]

Experiments with physical wave makers demonstrate that it is nearly impossible to generate regular waves with a ratio H/λ closed to 0.1 and over as some nonlinear effects appear during the propagation. Indeed, over a ratio of 0.1, the waves break inevitably [44].

5. 2. Wave Damping

The method to dissipate the energy is as much important as the method to generate waves. The natural dissipation of the surface waves engendered by the beach is a process generally used at the end of experimental wave tank. Such implementation at the end of the numerical domain has already been investigated in CFD. More especially, [50] shows that the quasi 2D tank, with a height of 2.5m and a length of 35m, must be equipped with a beach with a 1/3 slope ratio to optimize the damping of the waves (Figure 35). Alternatively, in the following section, the physics governing the implementation of an absorbing volume is presented.

5. 2. 1. Porous Absorber

The use of a porous absorber in numerical simulations has been mentioned in different papers and Guerrini [19] was the first to introduce it at Cranfield University. This technic is used to avoid any wave reflection which might disturb the incident wave propagation. Indeed, by absorbing the surface waves reaching the end of the domain, the behaviour of an hidden is simulated. An absorbing volume is defined upstream of the outlet boundary by the implementation of “momentum sources”. The equations governing this subdomain force pressure loss in all directions resulting of a decrease in the velocity. In the general momentum equation, the source term corresponds to the vector $\mathbf{S}_M$:

$$\frac{\partial(\rho \boldsymbol{U})}{\partial t} + \nabla \bullet (\rho \boldsymbol{U} \otimes \boldsymbol{U}) = -\nabla p + \nabla \bullet \tau + \boldsymbol{S}_M \quad [5.6]$$

Where ρ is the water density, **U** is the water velocity vector $\mathbf{U}_{x, y, z}$, t is the time, p is the static pressure and τ is the stress tensor. Among all the loss models, the isotropic model has been chosen to introduce a uniform loss in all directions:

$$\boldsymbol{S}_{M,x} = -\frac{\mu}{K_{perm}} U_x - K_{loss} \frac{\rho}{2} |\boldsymbol{U}| U_x \quad [5.7]$$

$$\boldsymbol{S}_{M,y} = -\frac{\mu}{K_{perm}} U_y - K_{loss} \frac{\rho}{2} |\boldsymbol{U}| U_y \quad [5.8]$$

$$\boldsymbol{S}_{M,z} = -\frac{\mu}{K_{perm}} U_z - K_{loss} \frac{\rho}{2} |\boldsymbol{U}| U_z$$

[5.9]

Where K_{perm} is the permeability, K_{loss} is the loss coefficient, μ is the dynamic viscosity and $\mathbf{U}_{x, y, z}$ are the components of the velocity vector **U**. The components of the source can be also expressed using linear and quadratic coefficients C_{R1} and C_{R2}:

$$C_{R1} = \frac{\mu}{K_{perm}}$$

[5.10]

$$C_{R2} = K_{loss} \frac{\rho}{2}$$

[5.11]

It is important to note that not necessary both permeability and loss coefficients have to be defined. For instance, if the purpose is to introduce a linear pressure loss, C_{R1} will be the only coefficient defined, while C_{R2} will be equal to zero.

The successive investigations of Guerrini and Rigosi about the linear coefficient leads to retain a value of 3000 kg/(m^3.s), corresponding to a linear pressure drop of 3000 Pa per meter of absorber length per meter per second. Indeed, it is assimilated to the minimum error introduced for a wide range of wavelengths [20].

To conclude, this implementation in the CFD code showed different advantages. First, the problem has no more velocity profile defined at both sides of the domain absorbing zone. Then in the case of OWC simulations, the dissipation of energy through the domain can be represented by the extraction of the wave energy by the device and finally the waves simulated are independent of the domain size.

5. 3. Simulation Settings

Over the last years, Cranfield students working on marine energy projects have been used to generate numerical waves thanks to the implementation of the horizontal and vertical components of the orbital velocity, u and v, and the water surface elevation, η, characteristic of the LWT at the inlet boundary. These expressions and their associated assumptions have been introduced earlier.

The alternative approach investigated for this thesis considers the inlet boundary as a wall with a moving mesh reproducing the displacement of a physical piston wave maker. The motion of the particles of water is comparable to the one observed in a wave flume.

In this section, the two methods of wave generation are confronted to each other and compared to the LWT. In order to damp the waves before, a porous absorber is implemented before the end of the domain. Then, a study of mesh convergence is undertaken with the piston wave maker in order to optimize the evolution of the water elevation over the time and along the domain.

5. 3. 1. Studied case

The wave chosen for this investigation has a wave height of 100mm and a wave period of 1.5s. It refers to a ratio of H/λ equal to 0.028 meaning that the wave is not expected to break and can be generated with a wave maker [44]. According to Figure 33,with a water depth of 2m, the theory suitable to model the case is the wave of Stokes of 2nd order ($H/(gT^2)$ = 0.0045 and $h/(gT^2)$ = 0.091). From this assumption, it is already possible to say that the LWT which has been used for the former OWCs simulations might not be suitable in the present case; hence the use of the wave maker might look more appropriate.

The fluid domain can be considered as a numerical wave tank which has a length of 8m, a height of 3m, a width of 0.03m and a water depth of 2m. As a result, the length of the domain is slightly bigger than 2 wavelengths (λ = 3.5m). The waves propagate normally during the first wavelength until they reach the absorbing zone located at 6m from the inlet and 1.5m from the outlet boundary. A representation of the quasi-2D domain is shown in Figure 36.

5. 3. 2. Boundary conditions

A first part presents the boundary conditions common to both wave generation methods, while a second part focuses on the inlet boundary condition characteristics and reports a resume of the overall settings of the boundary conditions.

The boundary conditions are chosen on the basis of the previous work undertaken in [17, 18, 19, 20] concerning the case following the behaviour of the LWT.

The bottom of the domain is defined as a *wall with no slip* to describe the seabed, while the top and the outlet of the domain are defined as *openings*. Since both inflow and outflow are allowed with the opening boundary condition, the value of the velocity at the outlet is set to zero. In the case of planar 2D geometries, a *symmetry* boundary condition is applied at the back and the front boundaries as the *free slip walls* degrades the accuracy of the results, since control volume gradients are not computed [20].The subdomain, constituting the porous absorber, is a volume with a length of 0.5m located between 6 and 6.5m from the inlet boundary. It applies an isotropic loss is with a *resistance coefficient of 3000 kg/(m^3.s*). Finally, the boundary condition of the inlet is defined with CEL (CFX Expression Language).

Case of the LWT – The waves are generating thanks to the implementation of the expression of the orbital velocity coming from the LWT [eq. 5.1 & 5.2] at the inlet boundary, meanwhile the water free surface elevation is defined as a sinusoid [eq. 5.3] along the domain as an initial condition. The overall boundary conditions governing the simulation are reported in Table 17.

BOUNDARY CONDITIONS – ORBITAL VELOCITIES	
Inlet	**Opening**
	Cartesian Velocity Components
	u from LWT
	v from LWT
	w = 0[m/s]
	Low Turbulence
Outlet	**Opening**
	Cartesian velocity Components
	u = 0[m/s]
	v = 0[m/s]
	w = 0[m/s]
	Low Turbulence
Top	**Opening**
	Static Pressure (Entrainment)
	Relative Pressure = 0 Pa
	Zero Gradient Turbulence
Bottom	**Wall**
	No Slip Wall
	Smooth Wall
Front	**Symmetry**
Back	**Symmetry**
SUBDOMAIN	
Sponge	**Isotropic Loss**
	Linear Resistance Coefficient
	3000[kg/m^3/s]

Table 17 – Boundary conditions and subdomain imposed in the model for waves generated with the LWT

Case of the wave maker – The waves are generated by the transversal motion of the inlet boundary. The user defines a number of CEL to define the motion of the piston along the x axis as a mesh motion at the inlet boundary. At t=0, the water free surface elevation adopted the expression of the water elevation presented in equation 5.3. The law of the piston

displacement is using a ramp on three wave period to introduce gently the motion of the flow inside the domain. The overall boundary conditions governing the simulation are reported in Table 18.

BOUNDARY CONDITIONS - PISTON	
Inlet	**Wall**
	Mesh Motion – Specified Displacement
	Cartesian Components
	X Component = PistonLaw
	Y Component = 0[m]
	Z Component = 0[m]
	No Slip Wall
	Smooth Wall
Outlet	**Opening**
	Cartesian velocity Components
	u = 0[m/s]
	v = 0[m/s]
	w = 0[m/s]
	Low Turbulence
Top	**Opening**
	Mesh Motion – Specified Displacement
	Cartesian Components
	X Component = PistonLaw
	Y Component = 0[m]
	Z Component = 0[m]
	Static Pressure (Entrainment)
	Relative Pressure = 0 Pa
	Zero Gradient Turbulence
Bottom	**Wall**
	No Slip Wall
	Smooth Wall
Front	**Symmetry**
Back	**Symmetry**
SUBDOMAIN	
Sponge	**Isotropic Loss**
	Linear Resistance Coefficient
	3000[kg/m^3/s]

Table 18 - Boundary conditions and subdomain imposed in the model for waves generated with a wave maker

5. 3. 3. Meshing approach

In this section, a general mesh setting is introduced before focusing on the specificities of three different meshes generated to optimize the evolution of the water elevation along the domain. The discretization in space of the domain consists of a structured mesh of hexahedra elements.

Every mesh includes two refined zones. The first one is defined around the interface between the air and the water, considering the water level when the sea is still. The refinement of this region is required in order to describe properly the hydrodynamic of the wave close to the interface. Indeed, it is important to transcribe efficiently the evolution of the orbital velocity profile at the crests and the troughs of the wave as this component drives the whole motion studied. In this region, the mesh consists of a regular refinement along y axis and it has a different density distribution along the x axis.
The second zone is located at the exact position of the porous absorber. In this area, high regular refinement along the x axis is applied to improve the effect of the resistance coefficient on the dissipation of energy. However, due to the method of “blocking” used during the meshing with ICEM, the mesh distribution along the y axis adopted the same definition than in the rest of the domain.

In particular, the refinement becomes less important when moving away from the interface both in the air and in the water. This choice can be accounted for the fact that in deep water the particles motion is expected to be circles whose diameters decrease with the water depth until it reaches the seabed. By referring to Figure 32, at this location the vertical component of the velocity is expected to be equal to zero. Concerning the air, the assumption made considers that the air flow is less influenced by the motion of the water when it is far from the interface.

Up to know, the mesh described a planar 2D domain; however CFX simulations run with 3D meshes only. Hence, a quasi-2D domain is generated with an extrusion distance along the z axis of the order of magnitude of the smallest mesh dimension (0.03m). As a result the domain is very thin and less time consuming than a real 3D domain; it consists of one layer of elements and two layers of nodes. Figure 36 resumes fairly well the mesh construction.

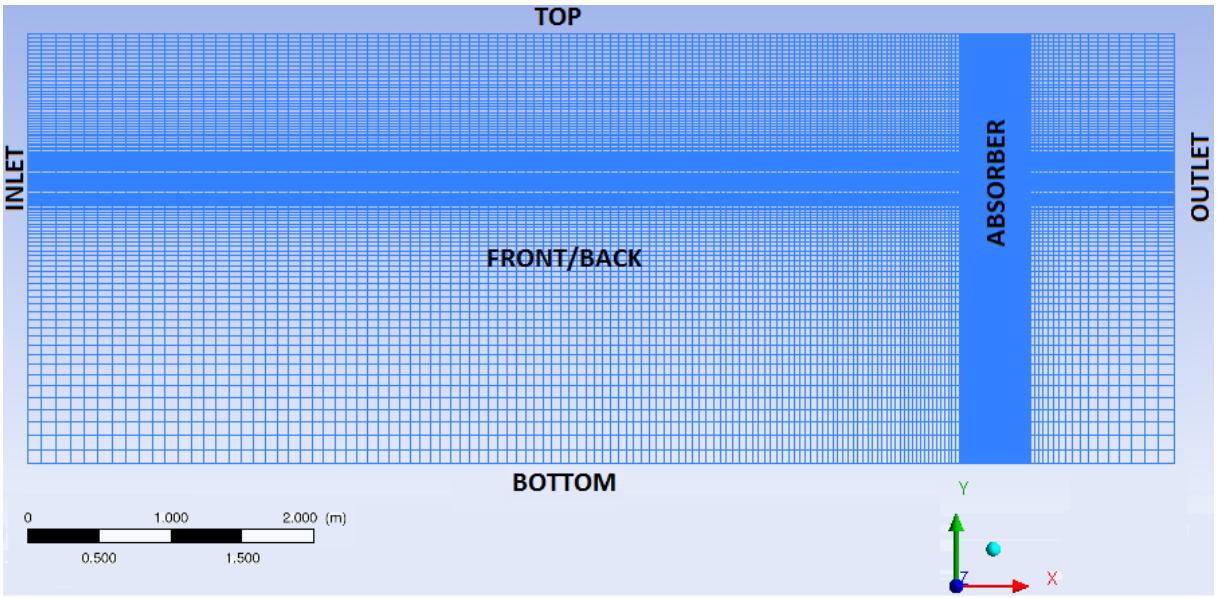

Figure 36 - Domain layout, boundary conditions and medium mesh

A study of mesh convergence is undertaken with three different meshes respectively called coarse, medium and fine; the total amount of nodes and elements required for each mesh is reported in Table 19. The purpose is to compare the relative error of the water elevation measured in CFD with the LWT at different locations along the x axis for every mesh. In complement, the numerical water velocity of the crest of the wave is compared with the theoretical value for every mesh.

The 3 meshes are tested with the wave maker boundary condition, while the medium model is used for the comparison between the two methods to generate waves. Every mesh is defined with 10 points per wave height in the refined region surrounding the water free surface. Far from this region the number of cells along the y axis decreases. The difference between the coarse, the medium and the fine meshes depends of the number of cells used to describe the wavelength; the smallest amount of cells per wavelength is located close to the inlet while the highest distribution concentrated in the absorbing zone. In other words, the number of points used to describe a wavelength is varying from:

- 16 to 128 *(coarse mesh)*
- 35 to 128 *(medium mesh)*
- 70 to 128 *(fine mesh)*

The minimal and maximal cell sizes are reported in Table 19.

	Coarse mesh	Medium mesh	Fine mesh
Total Mesh Nodes	**8058**	**35880**	**51980**
Total Elements	**3800**	**17442**	**25650**
Type of Elements	**Hexahedra**	**Hexahedra**	**Hexahedra**
Time step	**0.02s**	**0.02s**	**0.02s**
dx min	**0.025m**	**0.025m**	**0.025m**
dx max	**0.225m**	**0.1m**	**0.05m**
dy min	**0.01m**	**0.01m**	**0.01m**
dy max	**0.225m**	**0.1m**	**0.1m**

Table 19 – Structured mesh properties

5. 3. 4. Data Handling

The post processing of the results was undertaken in two steps. First, the results of the simulation are visualized with the interface CFX-Post. Since the simulation ran in transient scheme, the results have been written in output file (*.trn) for every time step. As the purpose of the study is to assess the two wave generation methods, the idea is to compare the free surface elevation over the time at different locations of the tank. In this context, the use of a procedure (*.cse) written in CCL (CFX Command Language) is necessary to automate the extraction of the data given the high number of time steps otherwise it would be time consuming. Thus, the procedure suggested by the author extracted the location of the isosurface associated to a volume fraction of water equal to 0.5 for every time step. Indeed, this volume fraction value corresponds to the interface between the two fluids of air and water. As a result, (*.txt) files are produced for every time step containing combinations of x axis value and y axis value associated to the volume fraction of water specified.

Finally, these files are post processed with a MATLAB routine written by the author. In one hand, it put some order in the data which have been randomly classified inside the (*.txt) file during the procedure, and in the other hand, it extracts the variation of water elevation for x abscise values specified by the user.

In fact, this method is convenient as it doesn't require determining all the locations (along x axis) suitable for data recording before running the simulation. In other words, there is always the possibility to check the variation of free surface elevation for a specific x abscise in the limit of the domain and mesh definitions.

5. 4. Simulation Results

In this section, the water propagation and free surface elevation are verified against the LWT for the comparison of the two wave generation methods for regular waves. After demonstrating a good efficiency of the numerical wave maker, two parameters are analysed to undertake the study of mesh convergence: the water elevation and the water velocity at the crest of the wave.

For avoidance of doubt, the different expressions mentioned in the following analysis *"Orbital velocity"*, *"Piston"* and *"LWT"* refer respectively to:

- the first method of wave generation based on the definition of the orbital velocity and the free surface elevation of the Linear Wave Theory presented in 5.1.1. (CFD approach)
- the second method of wave generation using the numerical wave maker presented in 5.1.3. (CFD approach)
- the Linear Wave Theory predictions (theoretical approach)

5. 4. 1. Comparison of Two Wave Generation Methods

The results presented to compare the two methods have been obtained with the medium mesh. The five locations chosen along the x axis to assess the water elevation over the time are at *0.3, 1, 3, 6 and 7.2m* from the inlet.

Instead of considering a fixed residual value generally associated to transient simulation, the convergence criteria of the current simulations can be defined as the repeatability of the wave oscillations as the physic studied is about a periodic phenomenon.

From a qualitative to a quantitative comparison – Figure 37 and Figure 38 represent the water elevation numerically predicted by the two generating methods respectively at 1m and 7.2m from the inlet. Complementary figures are presented in Appendix C for the other locations.

In the case of the wave generation governed by the equations of the LWT, the average of the water free surface (=average between the crest and the trough of the wave) has a tendency to increase over the time. Indeed, the average of the water elevation at 1m from the inlet is equal to 2m at t=0s, while it is equal to 2.03m at t=50s (Figure 37). So to speak the difference with the initial average value of the water elevation represents one third of the wave height implemented. In fact, this case is not isolated; on the contrary it can be identified in Figure 38 and in appendix C at the other locations along the x axis.

This phenomenon of displacement of the average water surface has already been observed in the work of Guerrini generating waves with the LWT [19].

Even though the boundary conditions applied at the outlet are similar for both simulations run, this behaviour doesn't occur in the case of the numerical wave maker; the average water elevation remains the same independently of the time.

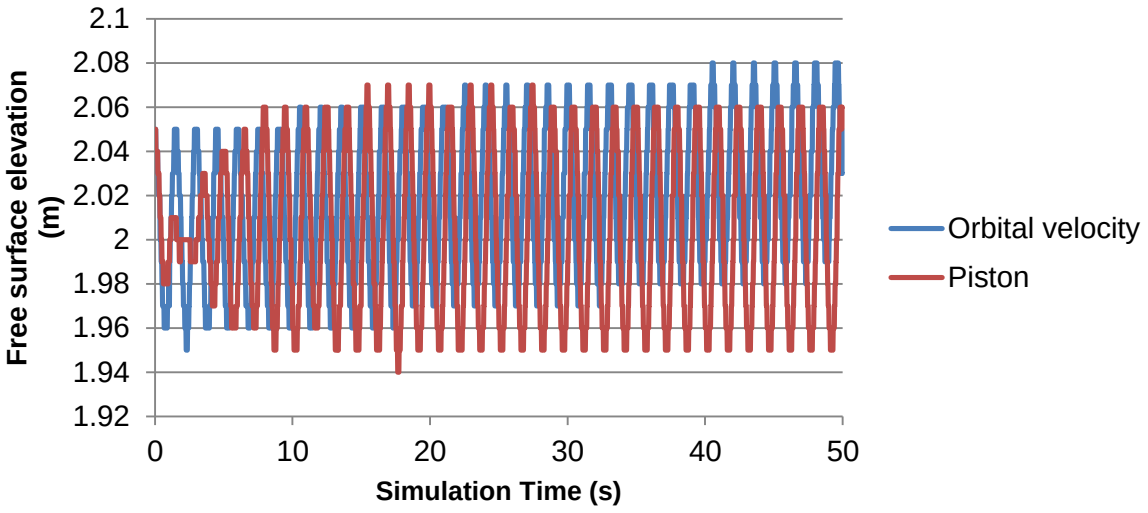

Figure 37 - CFD orbital velocity and CFD piston free surface elevation at 1m from the inlet

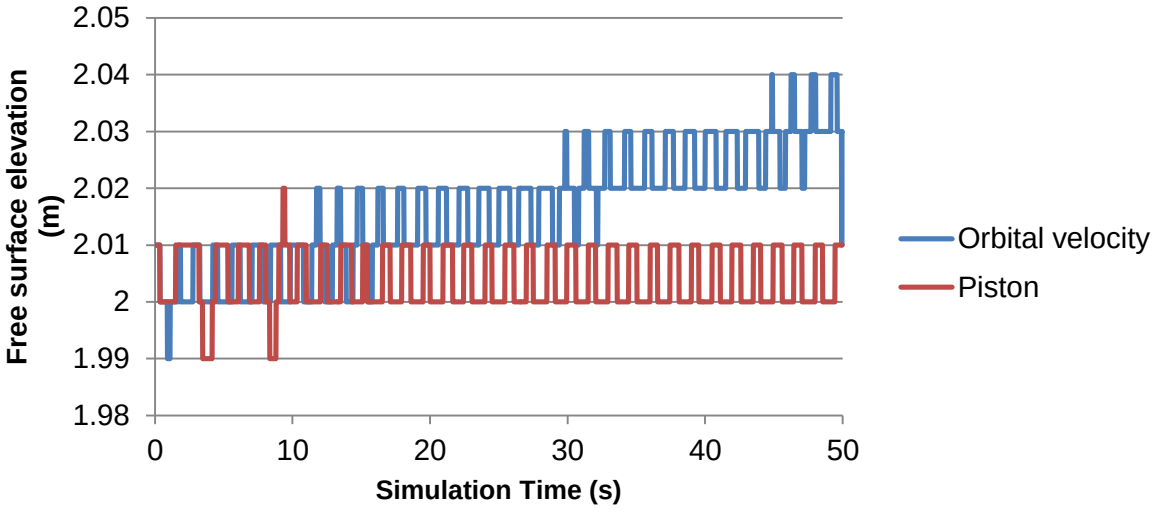

Figure 38 - CFD orbital velocity and CFD piston free surface elevation at 7.2m from the inlet

Meanwhile, the water elevation recorded in both cases at 7.2m from the inlet demonstrates fairly well the action of the porous absorber located between 6 and 6.5m from the inlet boundary. Indeed, the initial wave height of 0.1m has been divided by 10 before reaching the

outlet boundary (Figure 38). Moreover, the evolution of the free surface elevation over the time draws the attention to the absence of reflective waves.

More specifically in Appendix C, the two approaches are evaluating by comparing the water elevation of CFD predictions (obtained by the implementation of the orbital velocity and the water elevation based on the LWT or the motion of a piston wave maker) with the theoretical water elevation of the LWT. The average relative errors associated to the two CFD approaches presented in Appendix C are reported in Table 20 according to the expression of the relative error:

$$err\% = \frac{Abs(LWT_{value} - CFD_{value})}{Abs(LWT_{value})} \quad [5.16]$$

Where LWT_{value} corresponds to the theoretical prediction of the water elevation based on LWT and CFD_{value} corresponds to the water elevation recorded during the CFD simulations.

Abscises	Orbital Velocity	Piston
x = 0.3m	**0.98**	**0.43**
x = 1m	**0.87**	**0.45**
x = 3m	**0.97**	**0.56**
x = 6m	**0.97**	**0.48**
x = 7.2m	**1.57**	**1.41**

Table 20 - Average relative errors (%) between the water free surface elevation CFD predictions and the LWT (H=0.1m, T=1.5s)

The values reported in Table 20 demonstrate a better matching between the CFD predictions of the wave maker with the LWT. Indeed, the average relative error calculated with the CFD predictions based on the LWT represents up to two times the average relative error associated to the piston. This result is mostly explained by the previous observation made about the increase of the average water elevation observed over the time for the usual wave generation method based on LWT. Besides, equivalent value of the average relative error can be noticed for both CFD predictions at 7.2m from the inlet: this tends to remind us that the porous absorber has already damped the wave.

In Appendix C, the evolution of the water elevation recorded in the case of the wave maker reveals that the water elevation overestimates the LWT predictions during the first wave periods at the location of 0.3m from the inlet boundary. Meanwhile, it underestimates the LWT predictions during the first three wave periods at the locations further from the inlet

boundary (at 1, 3 and 6m). This phenomenon can be explained by the fact that the water free surface is initially defined according to the LWT, thus at t=0s the wave profile inside the tank isn't matching the motion of the paddle and it takes time to adapt before stabilizing. Besides, the time taken by the signal to stabilize at further locations from the inlet is due to the ramp of 3 wave periods set during the implementation of the wave maker to gently introduce the wave inside the domain. The location at 7.2m from this inlet doesn't witness this phenomenon as the wave has already been damped by the porous absorber.
As a result, the relative error associated to the wave maker is generally more important during the first wave periods.

Finally, the piston wave maker demonstrated better capabilities than the usual wave generation based on the LWT. Hence, it is sensible to advise its use for next simulations dealing with wave-structure interaction.

5. 4. 2. Mesh Convergence Study for the Piston Wave Maker

Since the best match between the LWT and the CFD predictions occurs with the piston wave maker, this last method has been retained to realize a mesh convergence study. Two parameters have been retained for the analysis: the water elevation and the water velocity.

Influence of the mesh refinement on the water elevation – The comparison of the evolution of the water elevation along the domain has been undertaken between three different meshes introduced in section 5.3.3. Figure 39 presents the water elevation recorded at 1m from the inlet: there is a good agreement between the medium and the fine meshes. On the contrary, the coarse mesh loses a part of the wave information as it is not enough refined along the x axis (only 15 points per wavelength close to the inlet boundary). This observation can be expanded to complementary figures in Appendix D for locations at 0.3, 3 and 6m from the inlet boundary. As a result, a minimum of 35 points per wavelength, corresponding to the medium mesh, seems to describe fairly enough the wave. Switching to a minimum of 70 points per wavelength close to the inlet, doesn't worth it in term of time requirement.

In addition, the CFD predictions of the water elevation have been compared to the LWT following the same procedure than the one presented in section 5.5.1. Table 21 reported the average relative error between the numerical water elevation and the LWT prediction associated to each mesh depending of the location along the x axis.
The main observation focuses on the comparison between the values obtained with the medium and the fine meshes. The results of the fine mesh highlights the fact that the porous

absorber hasn't perform effectively since the wave hasn't been damped when it reaches x=7.2m. As a result, higher average relative errors than the ones obtained for the medium mesh are reported for locations at 3 and 6m from the inlet. However, at 0.3 and 1m from the inlet the water elevation is closer from the LWT predictions. These observations might induce that the porous absorber indirectly influences the water elevation upstream. This last aspect is recommended to be studied in more depth in future investigations.

To conclude, the medium mesh appears like a good compromise between accuracy of the results and reduction of the time requirement.

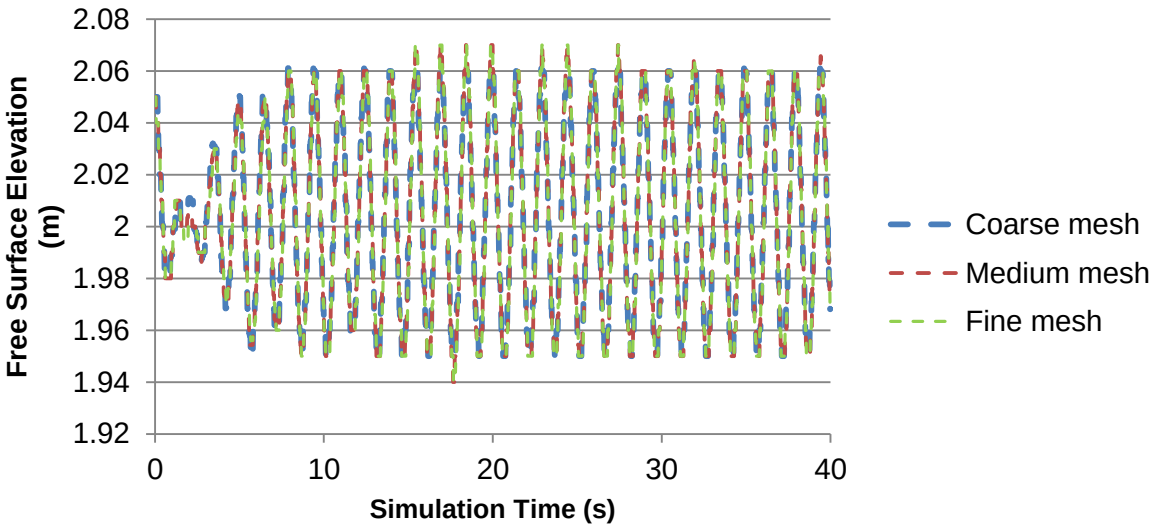

Figure 39 - Free surface elevation of three meshes at 1m form the inlet (H=0.1m; T=1.5s)

Abscises	Mesh 1 - Coarse	Mesh 2 - Medium	Mesh 3 - Fine
x = 0.3m	**0.44**	**0.43**	**0.39**
x = 1m	**0.38**	**0.45**	**0.42**
x = 3m	**0.68**	**0.56**	**0.59**
x = 6m	**0.78**	**0.48**	**0.56**
x = 7.2m	**1.63**	**1.41**	**0.76**

Table 21 - Average relative errors (%) between the water free surface elevation CFD piston predictions and the LWT depending of the mesh (H=0.1m, T=1.5s)

Influence of the mesh refinement on the water velocity – A last parameter allows studying the mesh convergence: the water velocity. The horizontal and vertical components

of the orbital velocity, u and v, introduced earlier can also be given for a specific location under or at the water free surface (x = 0) by the following expression [62]:

$$u = u_0 \cos(wt) \quad [5.13]$$

$$v = - v_0 \sin(wt) \quad [5.14]$$

$$u_0 = \frac{Aw \cosh(k(y+h))}{\sinh(kh)} \quad [5.15]$$

$$v_0 = \frac{Aw \sinh(k(y+h))}{\sinh(kh)} \quad [5.16]$$

Where A is the wave amplitude (m), w is the pulsation (rad.s^{-1}), k is the wave number (m^{-1}), y is the vertical coordinate of the point of interest relative to the calm water surface and h is water depth. In the present case (H=0.1m, T=1.5s, h=2m), the location of interest is located at the interface which means that the value of y is equal to zero and $u_{max} = -v_{max} = 0.21$ m.s^{-1}.

The velocity plotted from Figure 40 to Figure 42 is the superficial water velocity, measured with the 3 different meshes. The maximum value of the colour scale has been fixed to 0.21m.s^{-1}. By definition, the superficial velocity is a volume fraction weighted velocity, for instance the superficial velocity of an element consisting of 100% water is the same as its velocity, however the superficial velocity of an element consisting of 0% of water is zero. Thus, in the following figures, the air flow has a superficial water velocity equal to zero, while the maximum of water superficial velocity, which is equivalent to the water velocity according to the definition, occurs at the crest of the wave. At this location, the horizontal component of the orbital velocity, u, is maximal while the vertical component, v, is equal to zero. In opposition, the slowest particles of the water free surface are located at the trough of the wave.

Every figure has been taken after the repeatability of the wave has been demonstrated *(40s ≤ t ≤ 50s)* and it appears that the maximum of the water velocity tends to its theoretical value of 0.21m.s^{-1} more the mesh is refined. Indeed, with a coarse mesh the maximum of the water velocity is slightly overestimated; the red zone associated to the maximum of the colour scale is spread on the crest of the wave. However from the medium mesh, this area starts to decrease. Thus, by comparing the representation of the water superficial velocity of the medium and the fine meshes and considering the previous conclusion about the accuracy of the water elevation description depending of the mesh, it is sensible to confirm the sufficiency of the medium mesh.

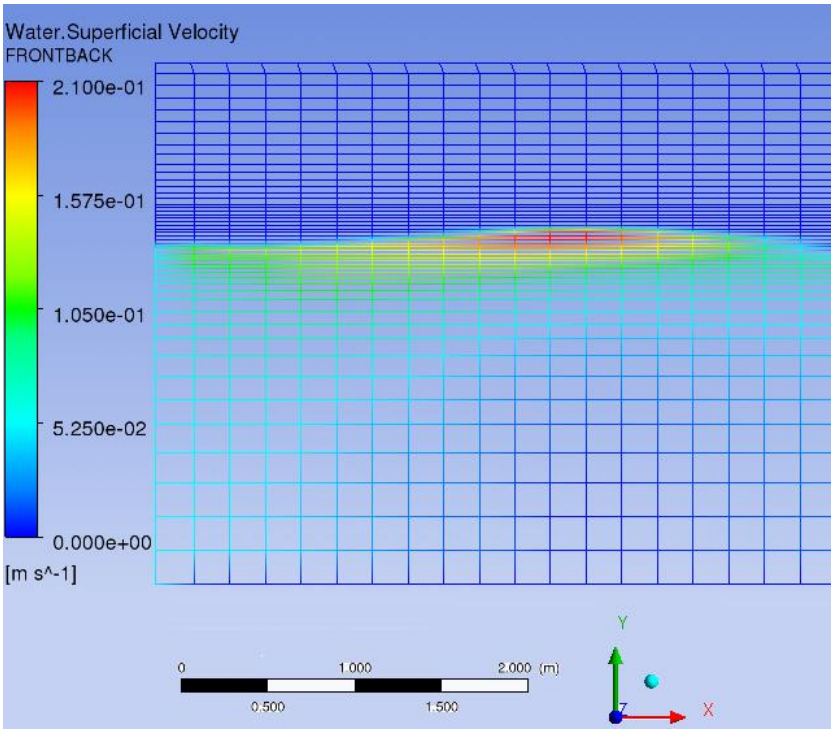

Figure 40 - Water superficial velocity with coarse mesh at t=40s

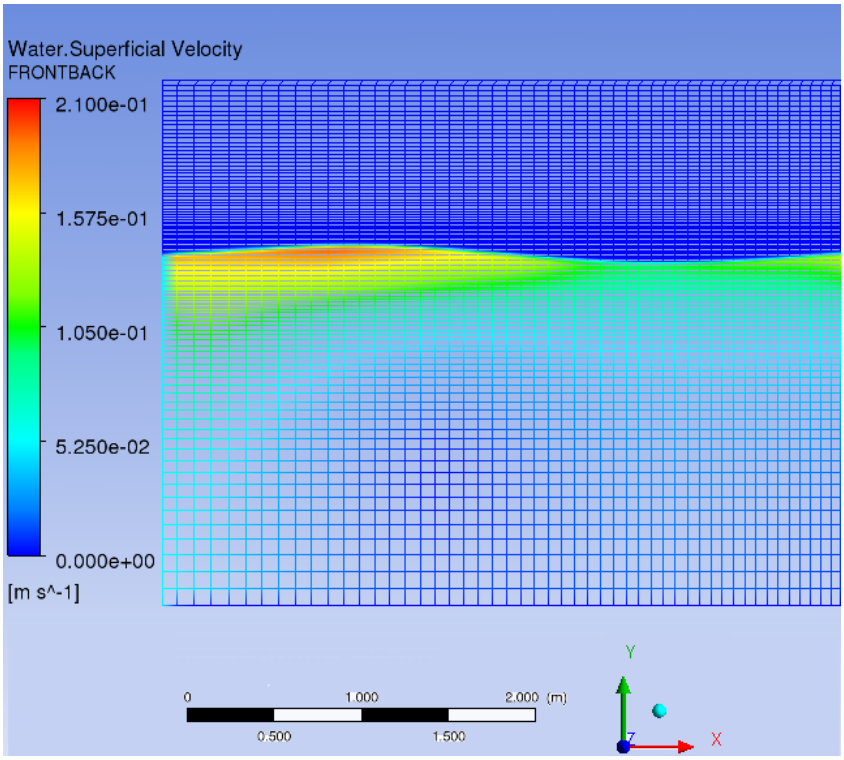

Figure 41 - Water superficial velocity with medium mesh at t=50s

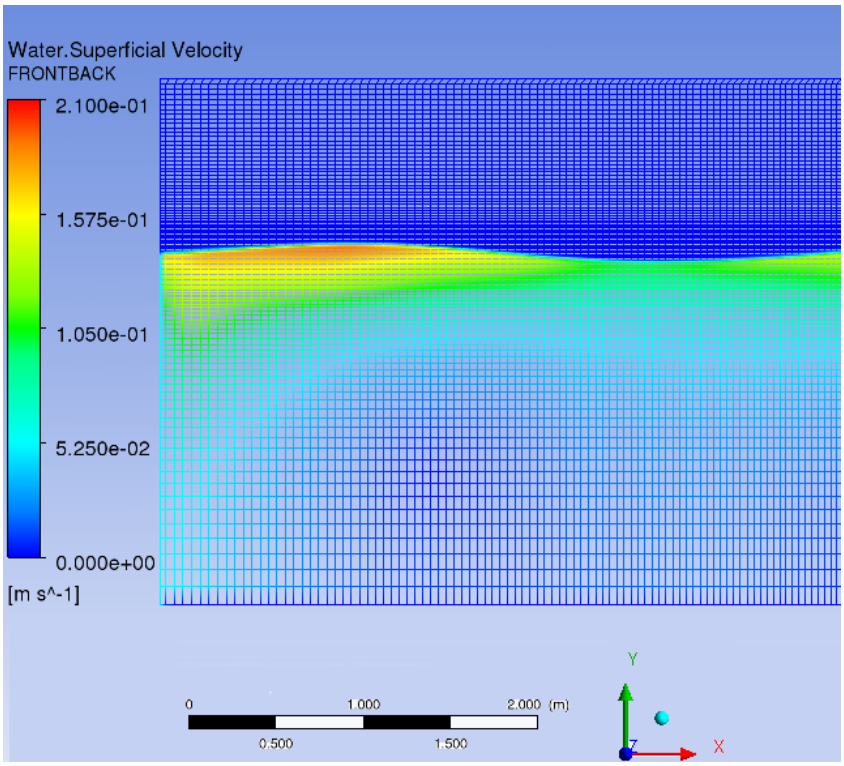

Figure 42 - Water superficial velocity with fine mesh at t=50s

5. 5. Suggestions for Further Investigations

CFD investigations were intended to complete the theoretical and the experimental approaches to validate the feasibility of the installation of a fixed offshore OWC device in the wave climate of Santa Maria, however due to lack of time the project has not been completed. The purpose of this section is to give recommendations to proceed to the CFD power predictions.

5. 4. 1. Numerical Flap Wave Maker

At first, it is suggested to implement the principle of the flap type wave maker inside the model. It has been presenting in 5.1.3. but not investigated due to lack of time and priorities. However, the motion of the paddle is much closer to the motion of the wave maker used during the experimental tests. Hence, a complementary study could be considered in the future to compare this type of wave maker with the piston type presented in the thesis. The idea would be to replace the inlet boundary condition, and run the simulation with the medium mesh. It is already possible to predict some problem with the deformation of the mesh occurring when the angle between the imaginary fixed inlet and the paddle will increase.

5. 5. 2. Power Predictions of Santa Maria with a CFD Approach

Since the combination of numerical wave maker and porous absorber demonstrates good agreement in wave generation, propagation and damping, it is suggested to retain these boundary conditions to complete the power predictions study of Santa Maria site with a CFD approach.

To have a consistent reasoning, the simulations set in CFX should have the same parameters than the experiments trialled in the wave tank with the different chambers (cylinder, BBDB and FBDD) for the most occurring sea state of Santa Maria (Hs=2m, T=7s). The modelling of full scale devices could be considered with CFD; however carrying out small scales simulations make easier and more coherent the comparison with the experimental data already available. The numerical predictions could be converted in full scale with the same method used for the analytical and the experimental results.
Thus, the wave chosen for the numerical simulation has a wave height of 40mm and a wave period of 1s. It refers to a ratio of H/λ equal to 0.026 meaning that the wave is not expected to break and can be generated with a wave maker [44]. According to Figure 33, with a water depth of 1.5m, which is equivalent to the water depth of the wave tank tests presented in section 4.4., the theory suitable to model the case is the wave of Stokes of 2nd order ($H/(gT^2)$ = 0.0042 and $h/(gT^2)$ = 0.156).

It is suggested that the numerical domain keeps the same wave length of 8m since the simulations previously run showed a good response to the porous absorber with the use of the medium mesh. The height of the domain might be reduced to 2.5m since the water depth has changed.

The location of the device inside the domain must be defined carefully, especially concerning the bent duct buoy as the horizontal duct (807mm) might produce reflective waves that could interact with the incoming waves. According to the analysis of the water elevation undertaken in 5.3., it would be appropriate to position the chamber at ~2m from the inlet. Indeed, the water elevation recorded between x=1m and x=3m demonstrated good agreement with LWT predictions.

It is advised to follow the characteristics of the medium mesh. In other words, it is suggested to define an area around the free surface which describes the wave height with at least 10 points/cells. 35 points/cells per wavelength are suggested to define the mesh close to the inlet boundary. Besides, additional refined zones must be added at the surrounding of the device especially to capture the variation of the free surface elevation inside the chamber but also to record the fluctuations of pressure drop through the orifice.

Chapter 6

CONCLUSION

6. 1. Considerations and Achievements

This thesis is part of the broad research project about performance and development of OWC technologies which started in 2007 at Cranfield University and has been carried out over time thanks to the work of a number of MSc students [16, 17, 18, 19, 20].

The present work is intended to investigate the viability and assess the power estimation of a fixed offshore OWC as there is a lack of performance predictions for such a device in the literature.
For the purpose of this study, a fictional scenario takes place in the Santa Maria sea region, off the coast of California, as this location is surrounded by fixed offshore structures.

The first investigations based on a theoretical approach show encouraging results. The methodology developed to assess the power of the specific location revealed an annual wave power, averaged over the five past years, of 19,5kW/m. This value corresponds to half the amount observed in the North Sea near offshore structures; it is certainly less but still worthy of commercial exploitation as the present work demonstrates.

Then, by combining the capture efficiencies of three near and offshore floating devices, with peak efficiencies of 37, 51 and 60% respectively, the associated annual average wave power per unit length of crest ranged from 3.5 to 6.1kW/m.

To complete the predictions for fixed devices, Santa Maria most occurring sea conditions were applied to small scale wave tank experiments, and an analytical model, of a bottomless cylinder and a bent duct buoy. Complementary wave heights and wave periods have been explored to improve the understanding of a fixed offshore OWC.
The results of the comparison between the wave tank tests and the analytical model demonstrated different interesting observations. Although the analytical model is recommended for early design of these devices, it seems not wholly suitable for the current study. In fact, the wave period chosen is too short to agree with the assumptions of the

model. More generally, even though the amount of power predicted by the model is sometimes far from the tank test expectations, the phenomenon of resonance is fairly well reproduced by the model.

The experimental approach demonstrates that the BBDD shape appeared to have the best capture efficiency among all the prototypes trialled in the tank for the most occurring wave climate of Santa Maria.

In particular, the comparison between the power assessment of Santa Maria with a peak of capture efficiency of 60% and the tank tests operating in similar sea conditions with the BBDB for a mouth of 9.5m shows good agreement ~58kW.This result suggests that a fixed offshore device would be viable in terms of power production were it to be located in the same site as the data buoy. In addition it points to the fact that a better capture efficiency could be reached if an improvement was made in the OWC collector geometry. Notwithstanding, the optimal orifice diameter associated to the BBDB best performance is quite small, 0.4m, compared to the diameter of the turbine generally found in the literature. Hence, a complementary campaign of experiments is recommended to study the feasibility of the turbine.

The CFD investigations were intended to complement the theoretical and the experimental approaches to confirm the feasibility of the installation of a fixed offshore OWC unit in the wave climate of Santa Maria. However due to lack of time another axis of investigations has been pursued. However recommendations have been made for further investigations on this subject. The numerical approach presented in the thesis tends to corroborate the capabilities of a numerical wave maker of the piston type against the theoretical LWT predictions and the usual method used to generate regular waves in the former works undertaken at Cranfield University.

The piston wave maker demonstrated better capabilities than the usual wave generation method using the implementation of the orbital velocity and the free surface elevation based on the LWT. In fact, its use managed to overcome a problem which appears in previous work such as the increase of the average water elevation over the time. Besides according to literature, it offers larger domain validity, in other words, a larger number of waves can be modelled with a numerical wave maker.

An additional mesh convergence study has been carried out with the piston wave maker. It especially highlights the fact that the model reproduced fairly well the physics of the phenomenon. Indeed, the numerical water velocity matches the theoretical expectations. Besides, it defined the mesh requirements with the intention to undertake further investigations on wave-structure interaction with OWC devices that could be carried out in the future.

6. 2. Recommendations

As mentioned earlier, the numerical investigations intended to focus on the feasibility of a fixed offshore OWC installation in the wave climate of Santa Maria; hence this section presented some recommendations to complete the actual theoretical and experimental predictions of power.

Flap type wave maker – At first, it could be interesting to investigate the response of an alternative to the piston wave maker: the flap type presented in 5.1.3. Indeed, the rotation induced by the paddle in this model is closer to the motion of the paddle of a wave maker used in a wave tank. The new model could be checked against the results of the actual numerical piston wave maker and even get better results as it better reproduces the physical phenomenon.

CFD simulations based on wave tank experiments – To have a consistent reasoning, the simulations set in CFX should have the same parameters than the experiments carried out in the wave tank with the different chambers (cylinder, BBDB and FBDD) for the most occurring sea state of Santa Maria converting in small scale (Hs=40mm; T=1s). The dimensions suggested for the numerical domain are a water depth of 1.5m, a domain height of 2.5m, a length of 8m and a width of the order of the smallest mesh cell (quasi-2D domain). Even though the length of the tank is reduced compared to wave tank tests, the porous absorber presents in the numerical model intends to damp the wave to avoid any reflection coming from the outlet boundary.

Definition of the mesh – The mesh convergence study undertaken during the numerical investigations demonstrates that a refinement of 10 cells per wave height at the surroundings of the interface and at least 35 cells per wavelength close to the inlet boundary are a good compromise between accuracy and time requirement. Away from the interface the mesh is less refined as most of the physics is determined close to the free surface of the flow. Besides, the porous absorber requires a high mesh refinement to improve its effect on the wave; hence the refinement from the inlet to the absorbing zone increases along the x axis. Since the OWC will be added to the CFD model, the mesh will require extra refinement especially inside the chamber and at the surroundings of the orifice to describe precisely the variation of the water elevation and the fluctuations of the pressure drop.

Post processing of the result – In order to undertake a good comparison between the numerical calculations, the theoretical predictions and the experimental measurements, it is highly suggested to calculate the power extractable of the different chambers with the methodology presented in Chapter 4.

REFERENCES

[1] Commission of the European Comities, *Renewable Energy Road Map – Renewable Energies in the 21st Century: Building a More Sustainable Future,* (2007).

[2] Circle of Blue, http://circleofblue.org (accessed June 2012).

[3] European Ocean Energy Association, *Oceans of Energy: European Ocean Energy Roadmap 2010-2050* (2010).

[4] Mørk, G., Barstow, S., Kabuth, A., Pontes, M.T., *Assessing the Global Wave Energy Potential,* 29th International Conference on Ocean, Offshore Mechanics and Arctic Engineering, Shangai, China (2010).

[5] European Renewable Energy Council, *Renewable Energy in Europe: Markets, Trends and Technologies* (2012).

[6] Carbon Trust, *UK Wave Energy Resource* (2012).

[7] World Energy Council, *2010 Survey of Energy Resources* (2010).

[8] (US) Energy Information Administration, *Annual Energy Outlook 2012 with projections to 2035* (2012).

[9] Department of Energy & Climate Change, *UK Renewable Energy Roadmap* (2011).

[10] Mattarolo, G., Lafon, F., Michel, B., *Wave energy resource off the French coasts: the ANEMOC database applied to the energy yield evaluation of Wave Energy Converters,*10th European Wave and Tidal Conference (EWTEC), Uppsala, Sweden (2009).

[11] (US) Energy Information Administration, *Annual Energy Review 2011* (2012).

[12] Hammons, T.J., *Electricity Infrastructure in the Global Market Place* - Chapter 4: *Energy Potential of the Oceans in Europe and North America: Tidal, Wave, Currents, OTEC and Offshore Wind* (2011).

[13] Electric Power Research Institute, Bedard, R., *Overview of US Ocean Wave and Current Energy; Resource, Technology, Environmental and Business Issues and Barriers* (2007).

[14] Ricketts, M., (*Wood Mackenzie), Basemap of Hydrocarbon Fields* (2009).

[15] Greg Croft Inc., http://www.gregcroft.com (accessed October 2012).

[16] Brighenti, A., *Numerical Investigation of Oscillating Water Column Buoys*, MSc Thesis, Cranfield University (2008).

[17] De Miguel, B., *Investigation of OWC Buoys for Offshore Power Generation,* MSc thesis,

Cranfield University (2010).

[18] Fantini, E., *Free Surface Flow CFD Simulation for Developing the Oscillating Water Column Technology, MSc Thesis,* Cranfield University, (2007).

[19] Guerrini, F., *Numerical Analysis of OWC Devices for Offshore Application, MSc Thesis,* Cranfield University (2009).

[20] Rigosi, S., *Hydrodynamic CDF Modelling for Floating OWC Technology,* MSc Thesis, Cranfield University (2011).

[21] Carbon Trust, *Marine Energy Challenge: Oscillating Water Column Wave Energy Converter Evaluation Report* (2005).

[22] Pico Power Plant, http://pico-owc.net (accessed December 2011).

[23] Torre-Enciso, Y., Ortubia, I., Lopez de Aguileta, L.I., Marques, J., *Mutriku Wave Power Plant: form the Thinking out to the Reality,* 10th European Wave and Tidal Conference (EWTEC), Uppsala, Sweden (2009).

[24] Japan Agency for Marine Earth Science and Technologies, http://www.jamstec.go.jp (accessed December 2011).

[25] GhuangZhou Institute of Energy Conversion, http://english.ciec.cas.cn (accessed December 2011).

[26] SeWave, *Tunnelled Wave Energy Converter Presentation: Invisible at Energetic Sites* (2007).

[27] RWE, *Siadar Wave Power Scheme*, http://www.rwe.com (accessed December 2011).

[28] Oceanlinx, http://www.oceanlinx.com (accessed December 2011).

[29] Oceanlinx, *Brochure from Conception Commercial reality* (2011).

[30] Miyazaki, T., Masuda, Y., JAMSTEC, *Tests on the Wave Power Generator Kaimei*, Offshore Technology Conference, Houston, Texas (1980).

[31] National Science Foundation Tokyo Regional office, *Report on Ocean wave Energy Conversion Projects,* http://www.nsftokyo.org/ssr98-08.html (accessed December 2011).

[32] World Energy Council, (1994).

[33] Toyota, K., Nagata, S., Imai, Y. and Setoguchi, T., *Research for Evaluating Performance of OWC-Type Wave Energy Converter "Backward Bent Duct Buoy",* 10th European Wave and Tidal Conference (EWTEC), Uppsala, Sweden (2009).

[34] Embley Energy, http://sperboy.com (accessed December 2011).

[35] Philips, J.W., Rayney, R.C.T., *Sperboy Design Evolution* (2005).

[36] Orecon, Ridingthe Wave Cornwall Pure Business (2008), http://www.investincornwall.co.uk (accessed January 2012).

[37] Ocean Energy, http://www.oceanenergy.ie (accessed December 2011).

[38] Leancon Wave Energy, http://www.leancon.com (accessed December 2011).

[39] Offshore Wave Energy, http://www.owel.co.uk (accessed December 2011).

[40] Green, W.L., Campo, J.J., Miles, J.A., Parker, J.E., *Wave Energy Conversion with an Oscillating Water Column on a Fixed offshore Platform,* Journal of Energy Resources Technology, December (1983), Vol. 105/487.

[41] Evans, D.V., *The Oscillating Water Column Wave Energy Device* (1978).

[42] Folley, M., Whittaker, T, *The Effect of Plenum Chamber Volume and Air Turbine Hysteresis on the Optimal Performance of Oscillating Water Columns, Proceedings of 24th International Conference on Offshore Mechanics and Arctic Engineering (OMAE), Halkidiki, Greece (*2005).

[43] Stappenbelt, B., *Mechanical Model of a Floating Oscillating Water Column Wave Energy Conversion Device,* 2009 Annual Bulletin of the Australian Institute of High Energetic Materials, 1 34-45 (2010).

[44] Molin, B., *Hydrodynamique des Structures Offshore* (2002).

[45] Patel, M.H., Witz, H.A., *Compliant Offshore Structure* (1991). pp. 45, 104

[46] Lee, C.-H., Nielsen, F.G., *Analysis of Oscillating Water Column Device Using a Panel Method,* 11th International Workshop on Water Waves and Floating Bodies, Hamburg, Germany(1996).

[47] Brito-Melo, A., Sarmento, A.J.N.A., *Numerical Modelling of OWC Wave Power Plants of the Oscillating Water Column Type,* Advances in Boundary Elements, WIT Press, pp. 25-34 (2002).

[48] Delauré, Y.M.C., Lewis, A., *3D Hydrodynamic Modelling of Fixed Oscillating Water Column Wave Power Plant by a Boundary Element Methods*, Ocean Engineering, Vol. 30, Issue 3, pp. 309-330 (2003).

[49] Josset, S., Clément, A.H., *A Time-Domain Numerical Simulator for an Oscillating Water Column Wave Power Plants,* Renewable Energy, Vol. 32, Issue 8, pp. 1379-1402 (2007).

[50] Lal, A., Elangovan, M., *CFD Simulation and Validation of Flap Type Wave-Maker,* World Academy of Science, Engineering and Technology 22 (2008).

[51] Spinneken, J., Heller, V., Kramer, S., Piggott, M., Viré, A., *Assessment of an Advanced Finite Element Tool for the Simulation of Fully-Nonlinear Gravity Water Waves,* Proceedings of the 22nd International Offshore and Polar Engineering Conference, Rhodes, Greece (2012).

[52] National Data Buoy Center, http://www.ndbc.noaa.gov/station_page.php?station=46011(accessed May 2012).

[53] Barstow, S., Mørk, Lønseth G., L., Mathisen, J.P., *World Waves Wave Energy Resource Assessments from the DeepOcean to the Coast,* 10th European Wave and Tidal Conference (EWTEC), Uppsala, Sweden (2009).

[54] Hagerman, G., *Overview of U.S. Ocean Wave Energy Resources*, presented at the Capital Hill Ocean Energy Briefing, Washington D.C. (2004).

[55] Toyota, K., and al., *Primary Energy Conversion Characteristics of a Floating OWC "Backward Bent Duct Buoy"*, Proceedings of the 20th International Offshore and Polar Engineering Conference, Beijing, China (2010).

[56] Department of Trade and Industry, *Near Shore Floating Oscillating Wave Column: Prototype Development and Evaluation.*

[57] Gervelas, R., Trarieux, F., Patel, M., *A Time-Domain Simulator for an Oscillating Water Column in Irregular Waves at Model Scale,* Ocean Engineering, Vol. 38, Issue 8-9, pp. 1007-1013 (2011).

[58] Harrison, J.H., Patel, M.H., Brown, D.T., *Hydrodynamic Analysis of Marine Vehicles with Pneumatic Compliance,* Royal Institution of Naval Architects Transactions, Vol. 129 (1986).

[59] Patel, M.H., *Hydrostatic Analysis of Marine Vehicles with Trapped Air Cavities*, International Shipbuilding Progress, Vol. 34, Issue 392 (1987).

[60] Witz, J.A., Patel, M.H., *Control of Marine Vehicles with Pneumatic Compliances,* Engineering Structures, Vol. 9, Issue 2, pp. 124-133 *(1986).*

[61] Le Méhauté, B., *An Introduction to Hydrodynamic and Water Waves* (1976).

[62] Lewandowski, E. M., *Experimental Study of an Automatic Pitch Control System on a Swath Model* (1994).

[63] ANYSYS-CFX, *Post user's manual, Ansys CFX Release 13.0 ed* (2010).

[64] ANYSYS-CFX, *Pre user's manual, Ansys CFX Release 13.0 ed* (2010).

[65] ANYSYS-CFX, *Solver modelling guides, Ansys CFX Release 13.0 ed* (2010).

[66] NYSYS-CFX, *Solver Theory Guide, Ansys CFX Release 13.0 ed* (2010).

Appendix A

ANALYTICAL MODEL PREDICTIONS AND WAVE TANK TESTS MEASUREMENTS

In this appendix, the capabilities of the analytical model developed by Farman are assessed in comparison with wave tank tests carried out at Cranfield University.

The two approaches are compared with one parameter: the variation of pressure drop which is measured by the sensors at the outlet of the orifice during the tank tests and is analytically predicted with the model.

Because of the nature of the geometry designed inside the model, only tank results obtained with the cylindrical chambers are subjected to comparison with the analytical model.

The results are presented in small scale for three wave periods of (0.5, 1 and 2s) and three wave heights (20, 60 and 80mm), as the 40mm one is already presented in Chapter 4.

This survey draws the attention to the actual capabilities and limits of the analytical model; the evaluation of the analytical model is presented in Chapter 4 section 3.

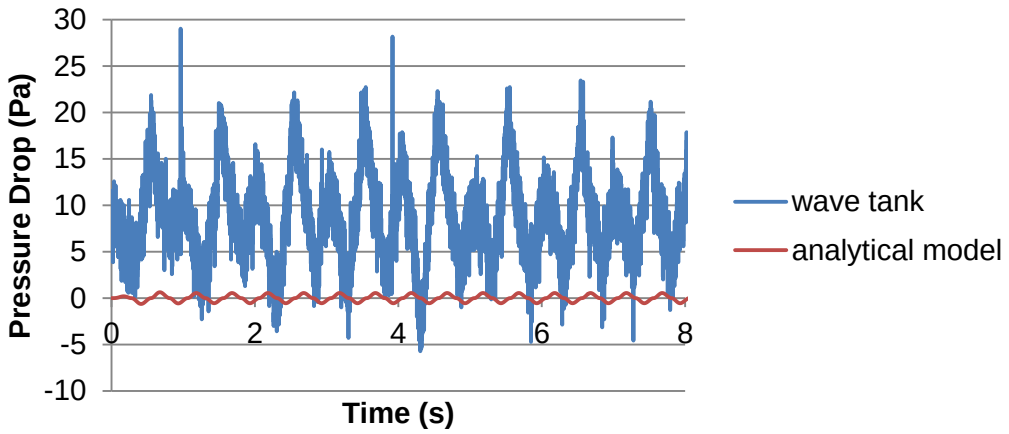

Figure 43 - Pressure drop measured for a 50mm water draft cylinder with an 8mm orifice diameter (Hs=20mm; T=0.5s)

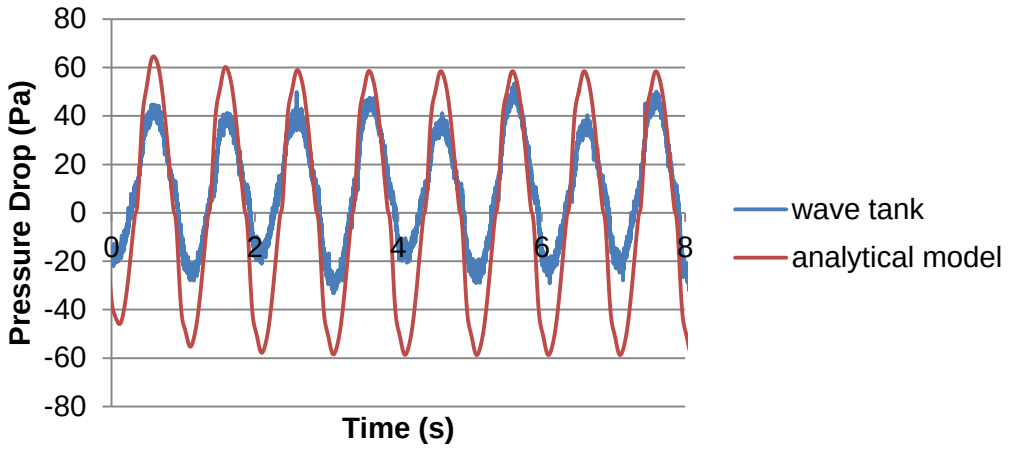

Figure 44 - Pressure drop measured for a 50mm water draft cylinder with an 8mm orifice diameter (Hs=20mm; T=1s)

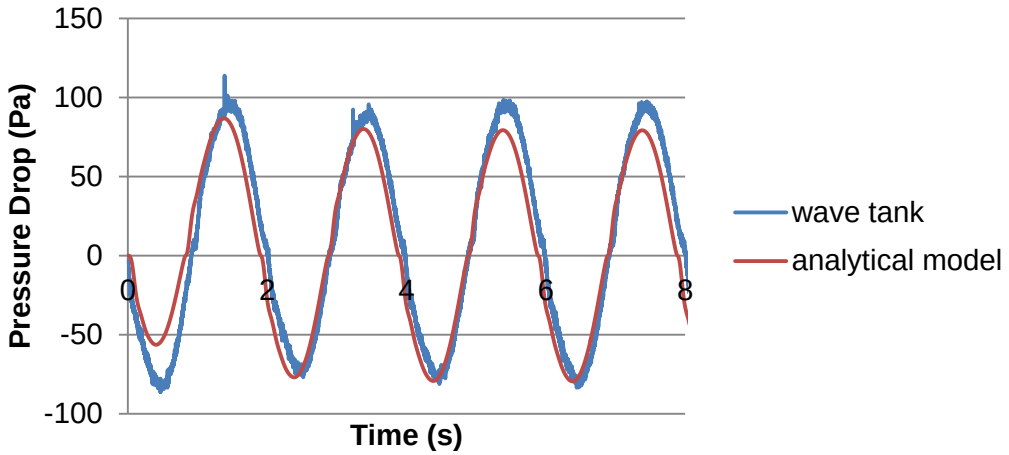

Figure 45 - Pressure drop measured for a 50mm water draft cylinder with an 8mm orifice diameter (Hs=20mm; T=2s)

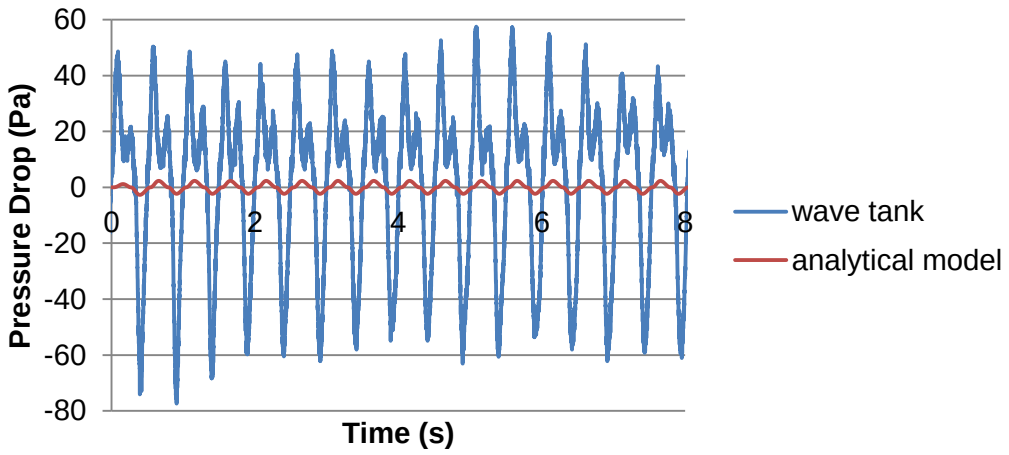

Figure 46 - Pressure drop measured for a 50mm water draft cylinder with an 8mm orifice diameter (Hs=60mm; T=0.5s)

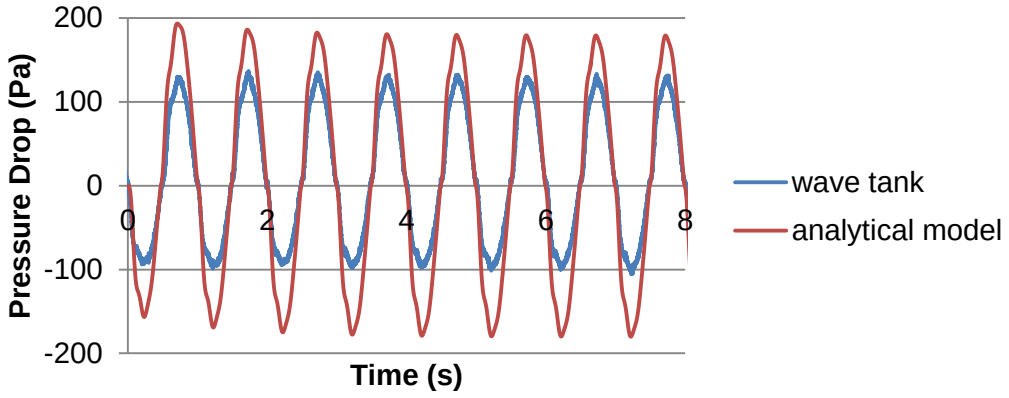

Figure 47 - Pressure drop measured for a 50mm water draft cylinder with an 8mm orifice diameter (Hs=60mm; T=1s)

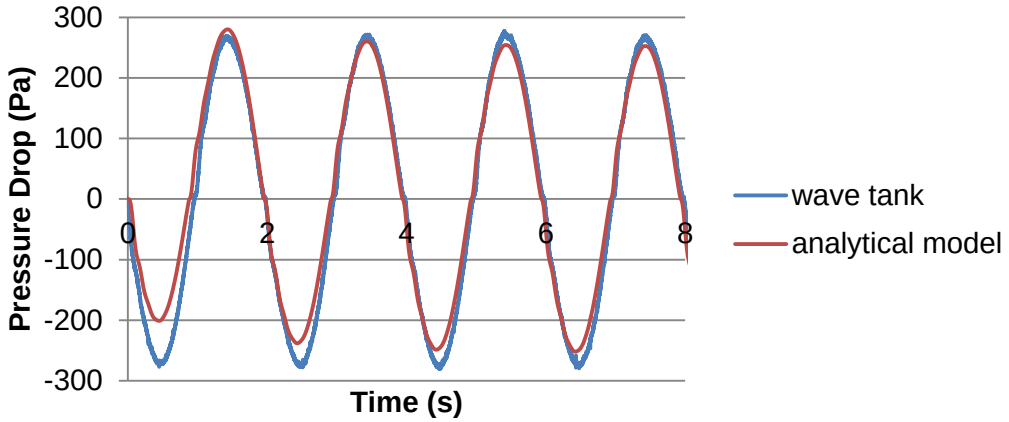

Figure 48 - Pressure drop measured for a 50mm water draft cylinder with an 8mm orifice diameter (Hs=60mm; T=2s)

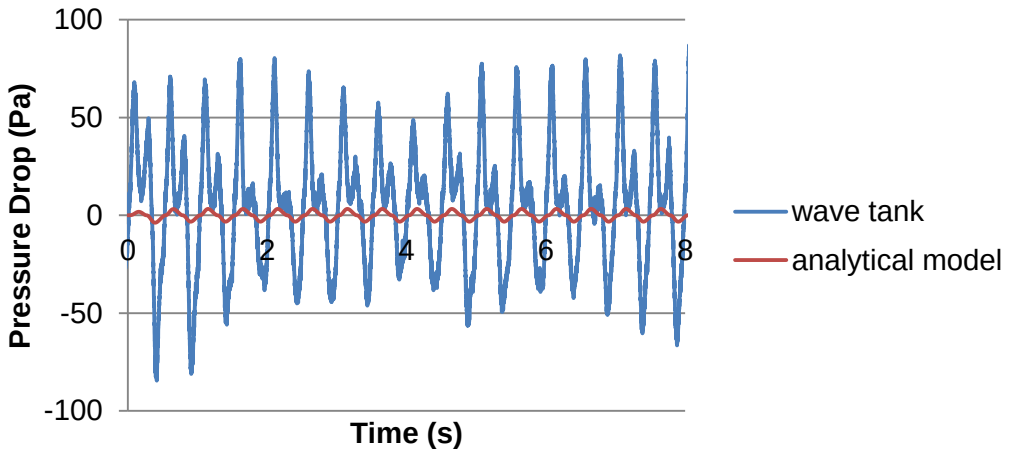

Figure 49 - Pressure drop measured for a 50mm water draft cylinder with an 8mm orifice diameter (Hs=80mm; T=0.5s)

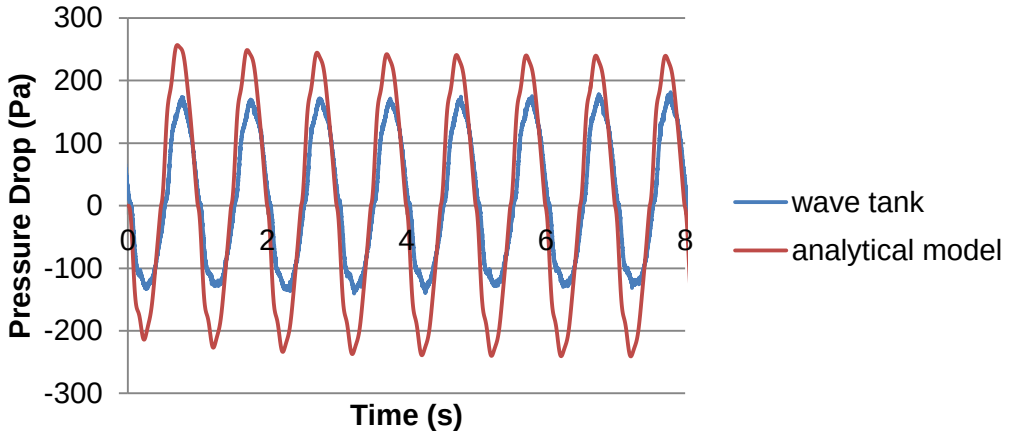

Figure 50 - Pressure drop measured for a 50mm water draft cylinder with an 8mm orifice diameter (Hs=80mm; T=1s)

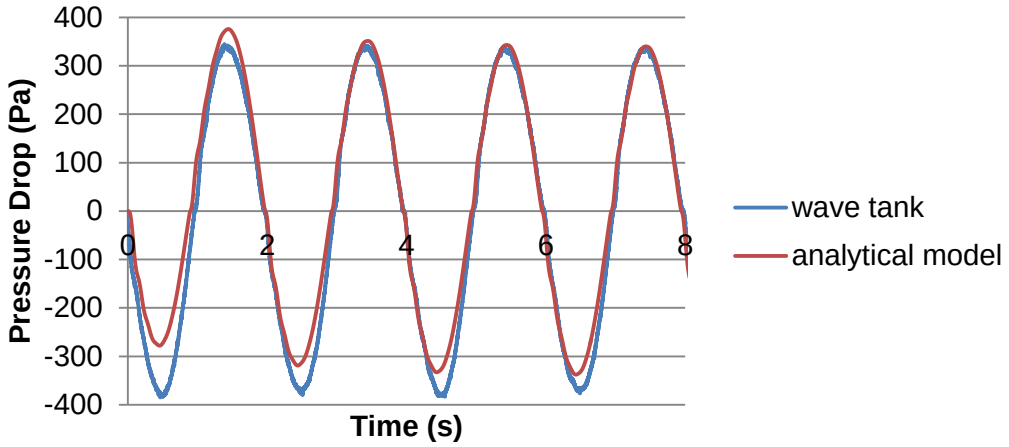

Figure 51 - Pressure drop measured for a 50mm water draft cylinder with an 8mm orifice diameter (Hs=80mm; T=2s)

Appendix B

INVESTIGATION ABOUT OWCs PERFORMANCE AND RESPONSE DURING WAVE TANK TESTS

In this appendix, the power extractable for different geometries and sea climate is estimated theoretically in full scale from the measurements of pressure drop recorded during the tank tests. The survey considers 4 parameters subjected to variation such as the chamber shape (cylinder, water draft, BBDB, FBDB), the orifice diameter (0.4, 0.5, 1 and 1.5m), the wave periods (3.5, 7 and 14s) and the wave height (1, 2, 3, 4 and 5m).

This full part, presenting in Chapter 4 section 2, brings a better understanding of OWC behaviour and variation of performance.

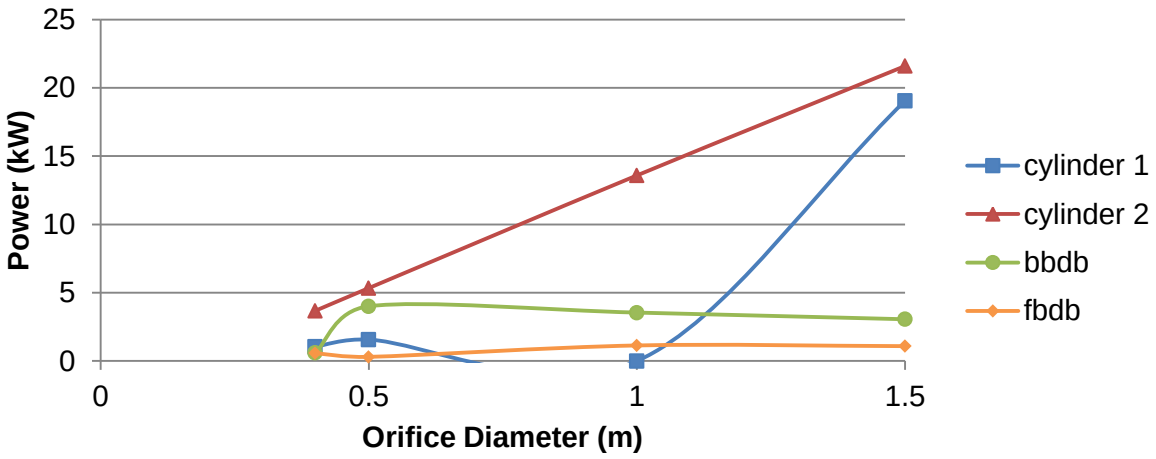

Figure 52 - Power estimation depending of the orifice diameter and the geometry (H=1m; T=3.5s)

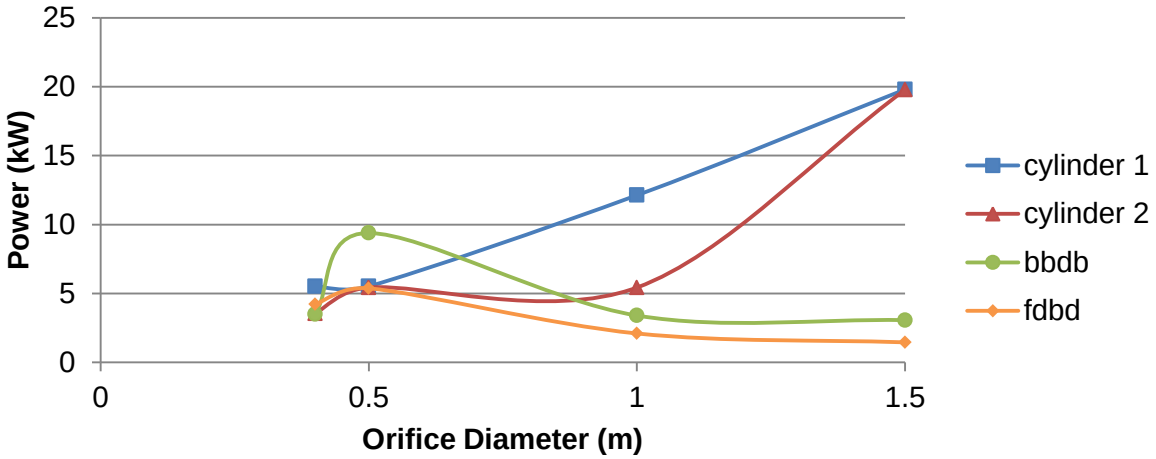

Figure 53 - Power estimation depending of the orifice diameter and the geometry (H=3m; T=3.5s)

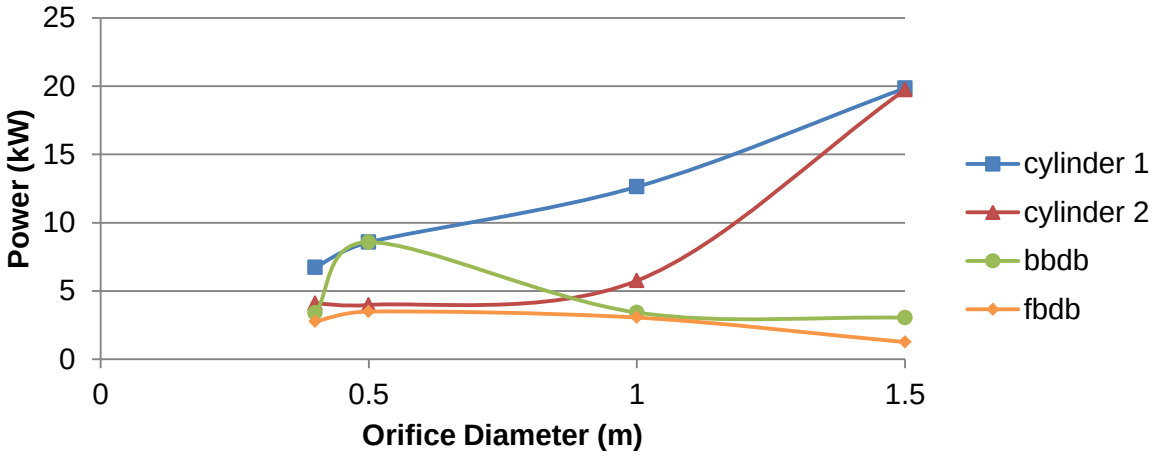

Figure 54 - Power estimation depending of the orifice diameter and the geometry (H=4m; T=3.5s)

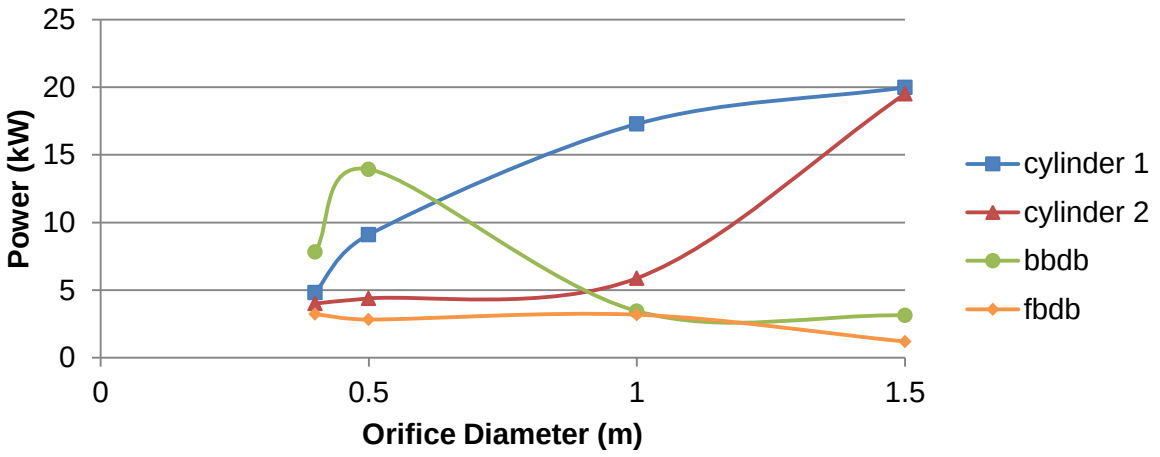

Figure 55 - Power estimation depending of the orifice diameter and the geometry (H=5m; T=3.5s)

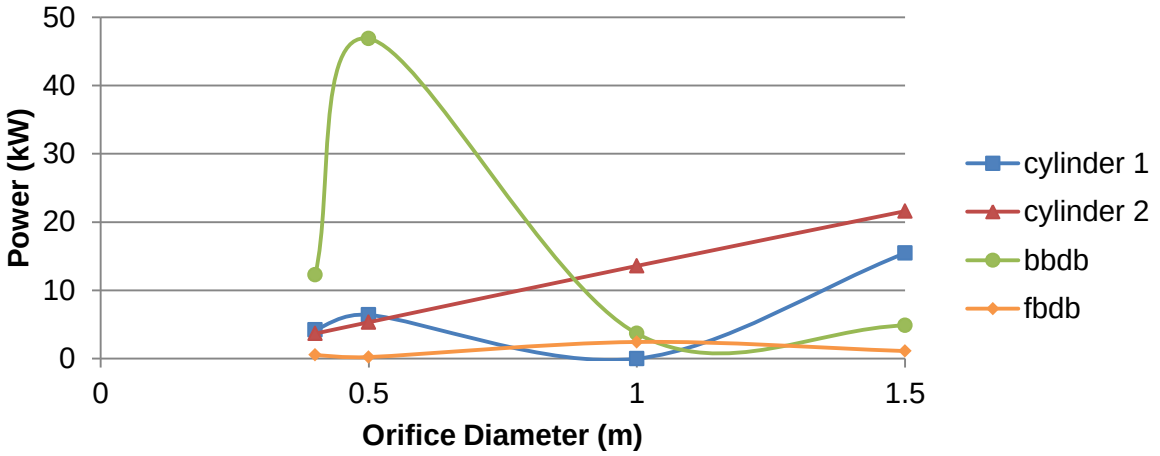

Figure 56 - Power estimation depending of the orifice diameter and the geometry (H=1m; T=7s)

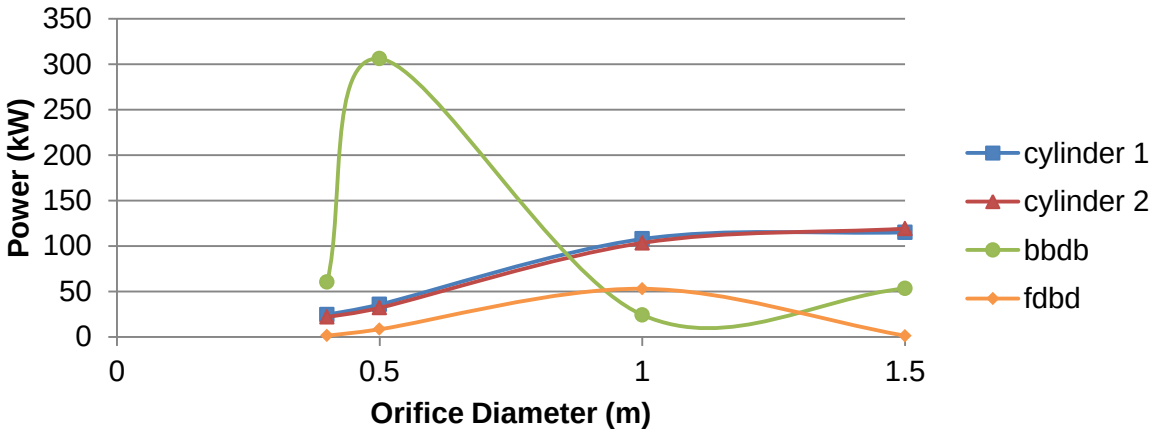

Figure 57 - Power estimation depending of the orifice diameter and the geometry (H=3m; T=7s)

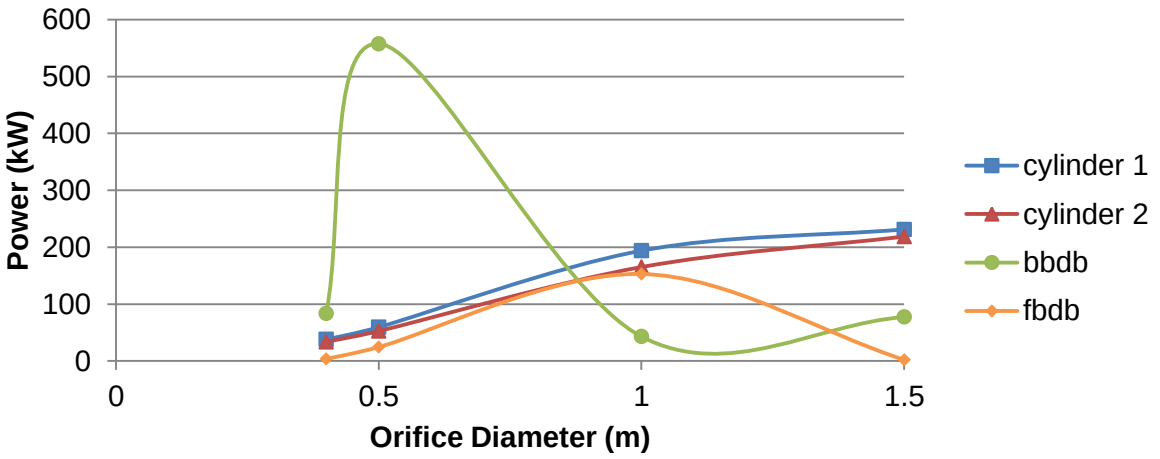

Figure 58 - Power estimation depending of the orifice diameter and the geometry (H=4m; T=7s)

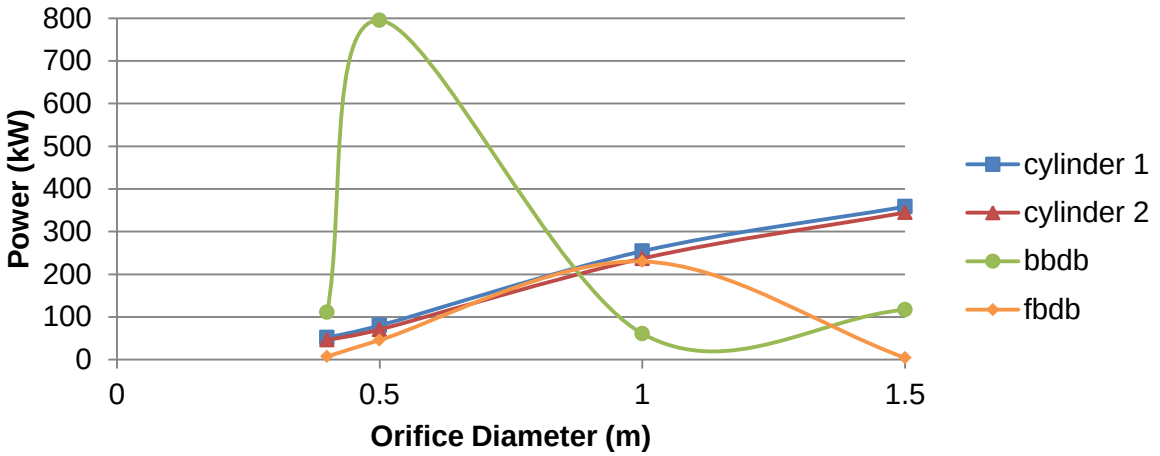

Figure 59 - Power estimation depending of the orifice diameter and the geometry (H=5m; T=7s)

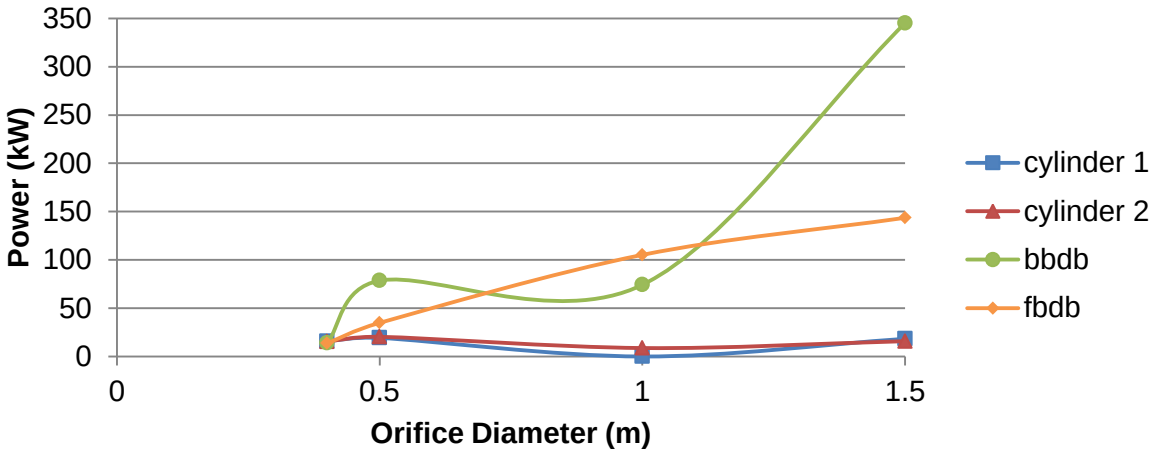

Figure 60 - Power estimation depending of the orifice diameter and the geometry (H=1m; T=14s)

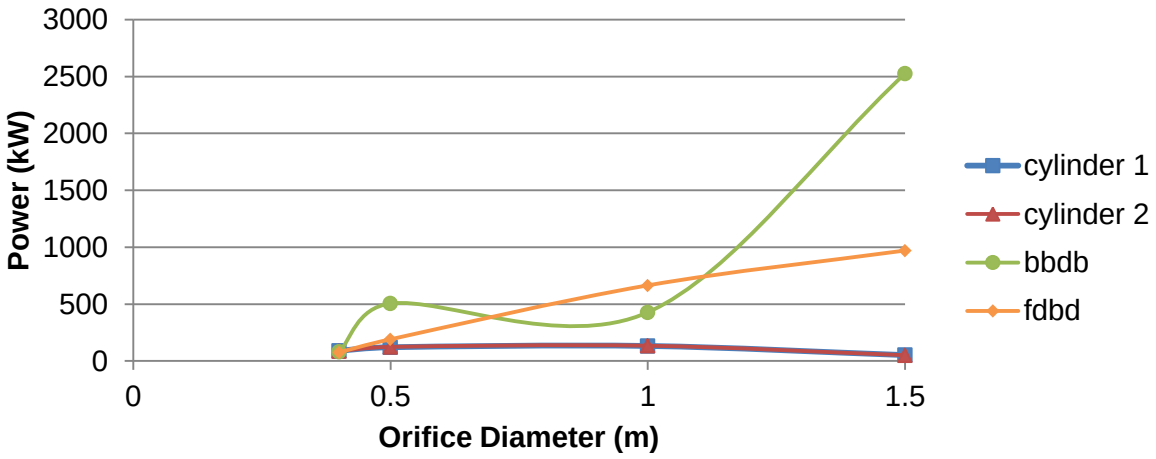

Figure 61 - Power estimation depending of the orifice diameter and the geometry (H=3m; T=14s)

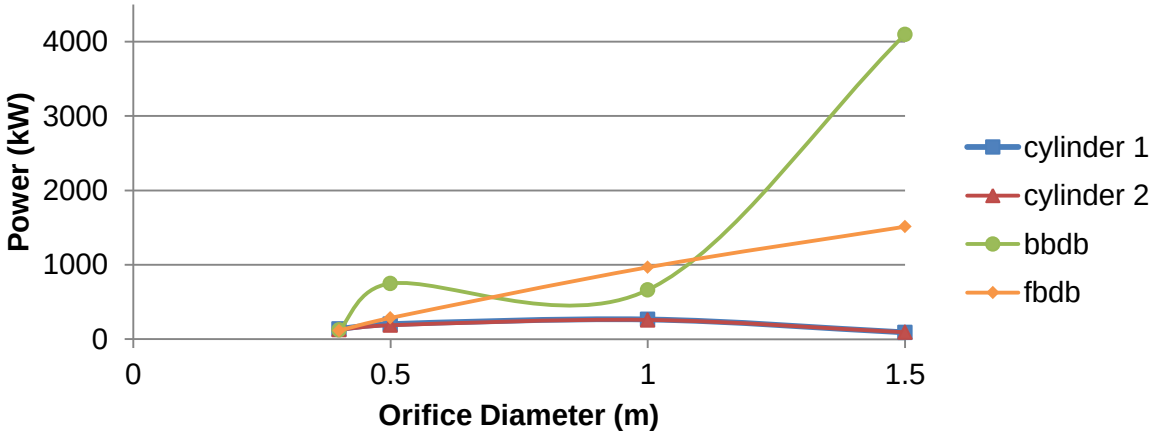

Figure 62 - Power estimation depending of the orifice diameter and the geometry (H=4m; T=14s)

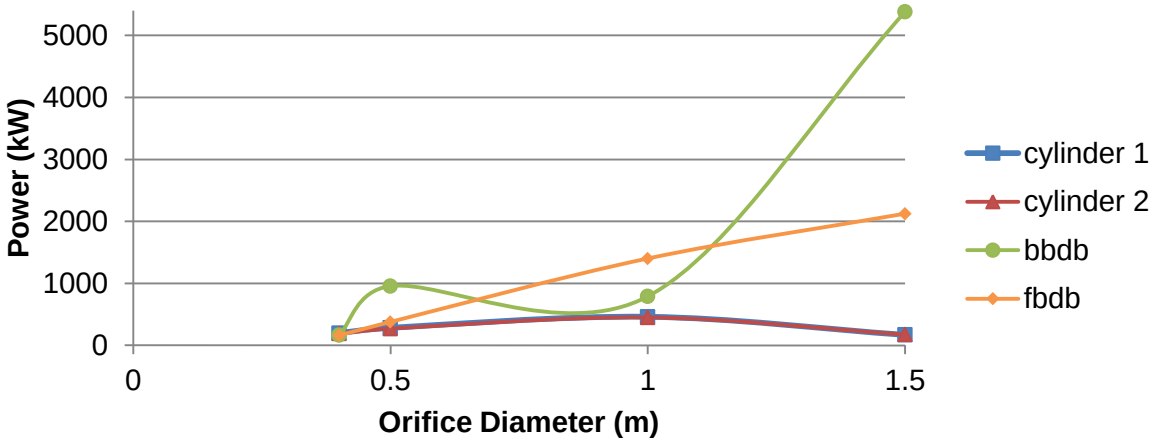

Figure 63 - Power estimation depending of the orifice diameter and the geometry (H=5m; T=14s)

Appendix C

COMPARISON OF TWO WAVE GENERATION METHODS IN CFD

In this appendix, the method which has been used at Cranfield University until now to generate regular waves is confronted to another one. These approaches are evaluating by comparing water elevation of CFD predictions (obtained by the implementation of the orbital velocity and the water elevation based on the LWT or the motion of a piston wave maker) with the theoretical water elevation of the LWT. From this data, the average relative error with the LWT is determined

The wave considered (H=0.1m, T=1.5s) propagates along a 2m water depth domain and its water elevation is recorder at 5 different locations along the x axis (0.3, 1, 3, 6 and 7.2m).

This full part, presenting in Chapter 5 section 4.1., draws the attention to the capabilities of the piston wave maker. All the relative error data are reported in Table 20.

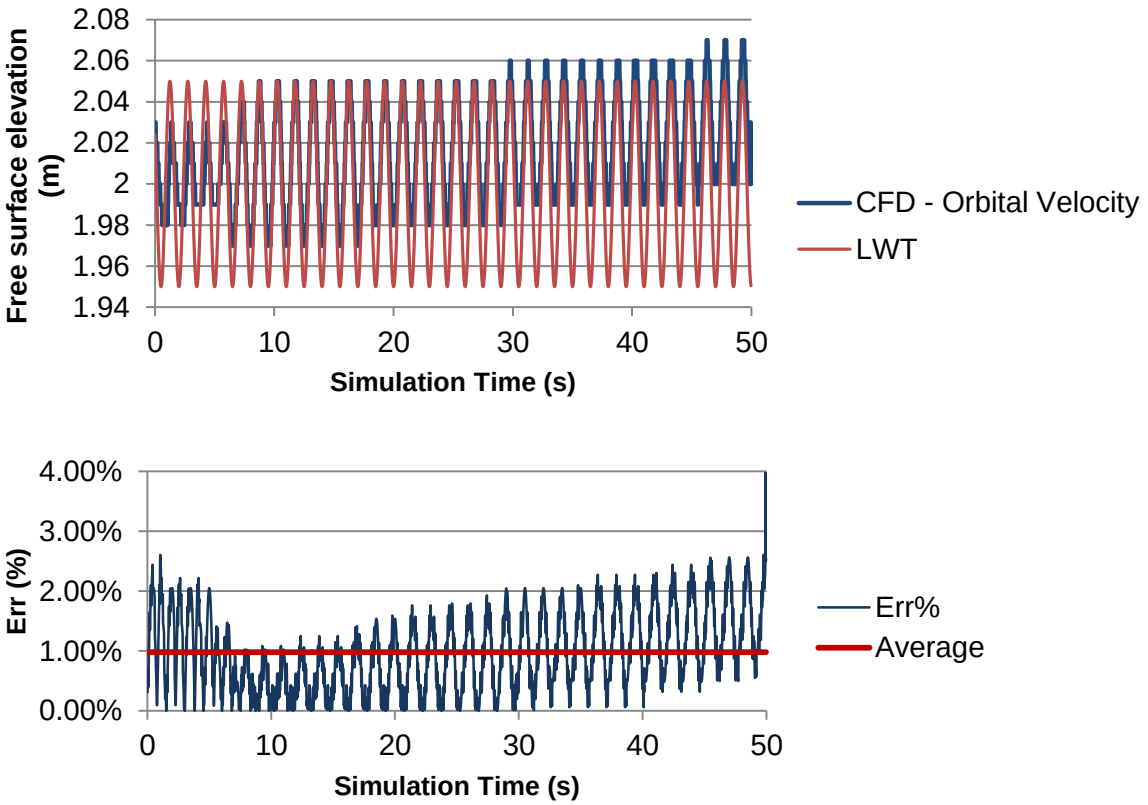

Figure 64 – CFD orbital velocity and LWT free surface elevation (a) and relative error CFD against LWT (b) at 0.3m from the inlet (H=0.1m, T=1.5s)

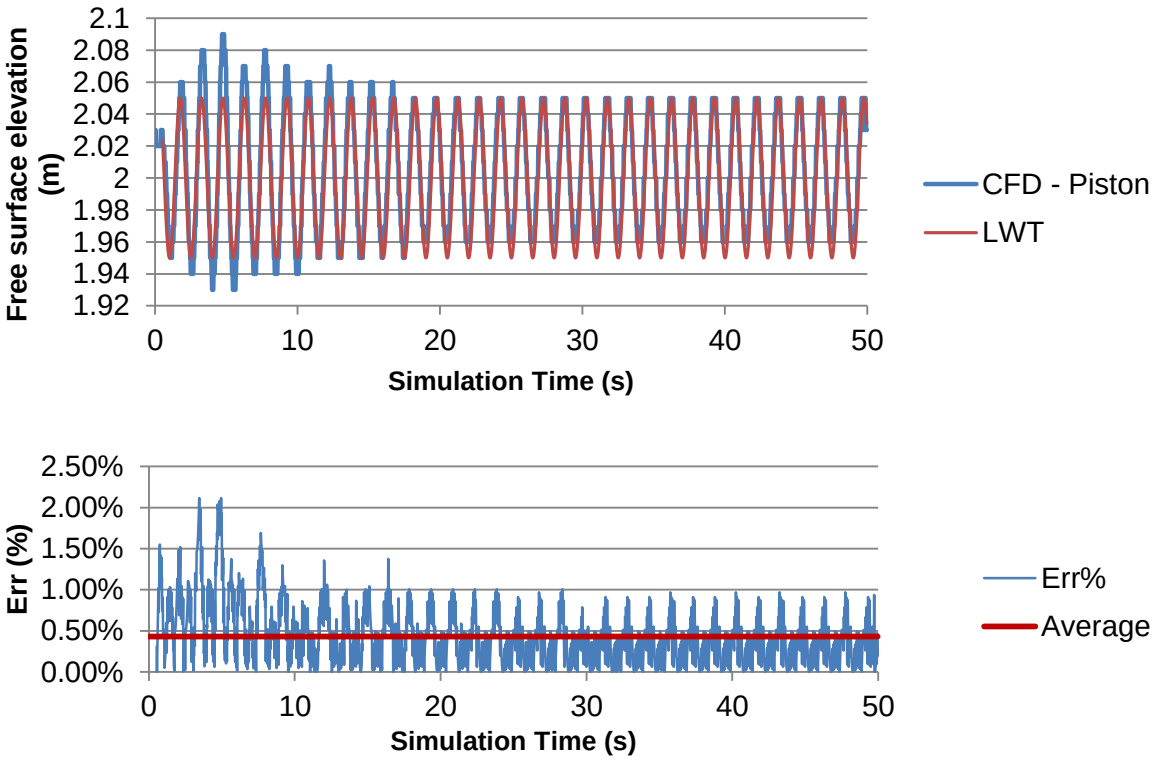

Figure 65 - CFD piston and LWT free surface elevation (a) and relative error CFD against LWT (b) at 0.3m from the inlet (H=0.1m, T=1.5s)

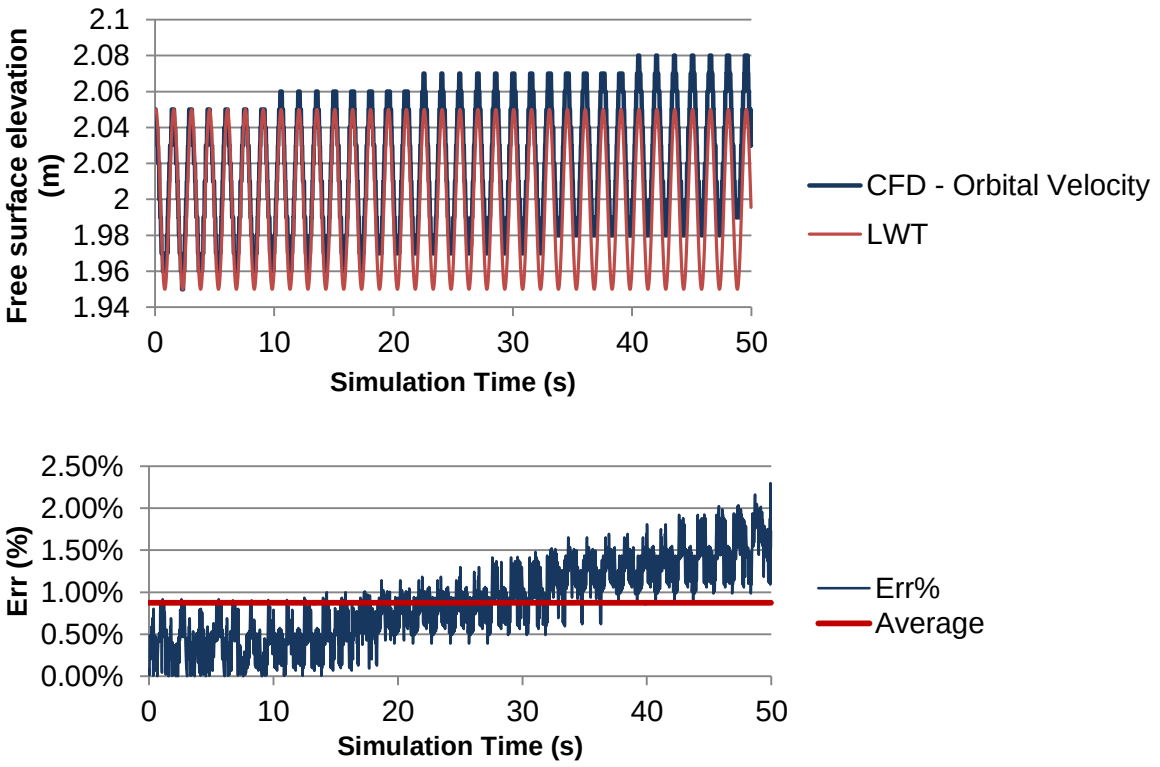

Figure 66 - CFD orbital velocity and LWT free surface elevation (a) and relative error CFD against LWT (b) at 1m from the inlet (H=0.1m, T=1.5s)

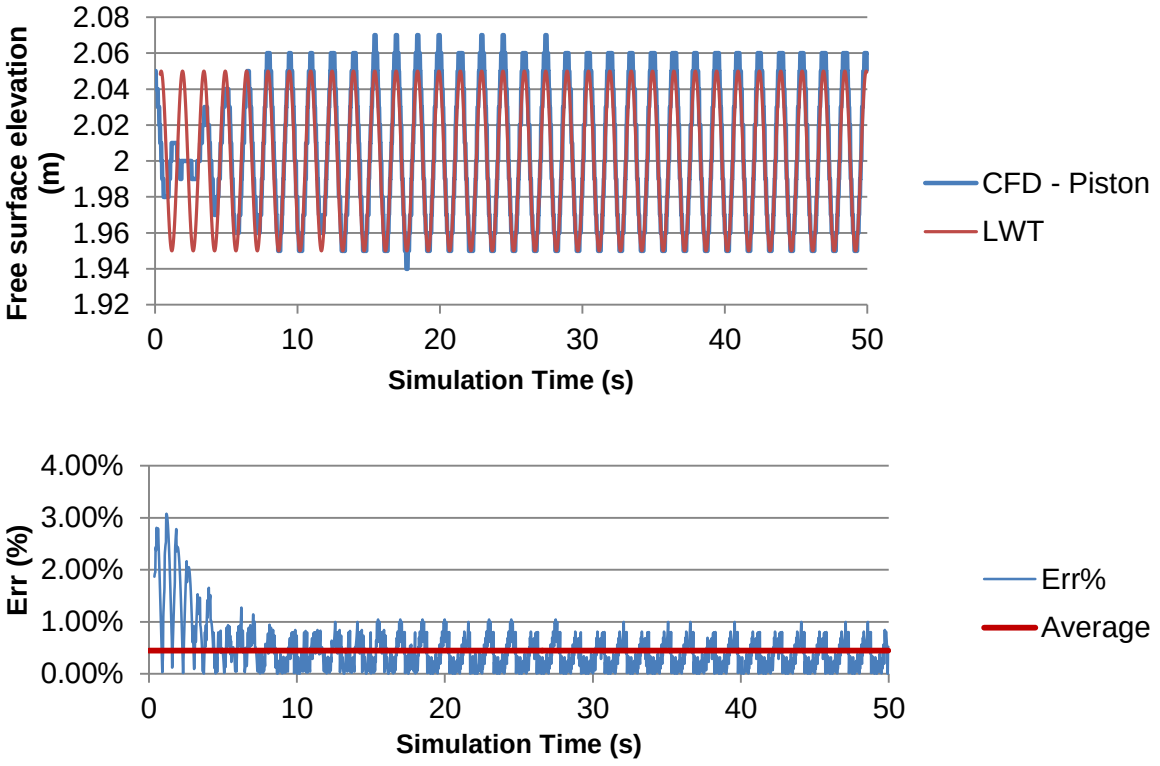

Figure 67 - CFD piston and LWT free surface elevation (a) and relative error CFD against LWT (b) at 1m from the inlet (H=0.1m, T=1.5s)

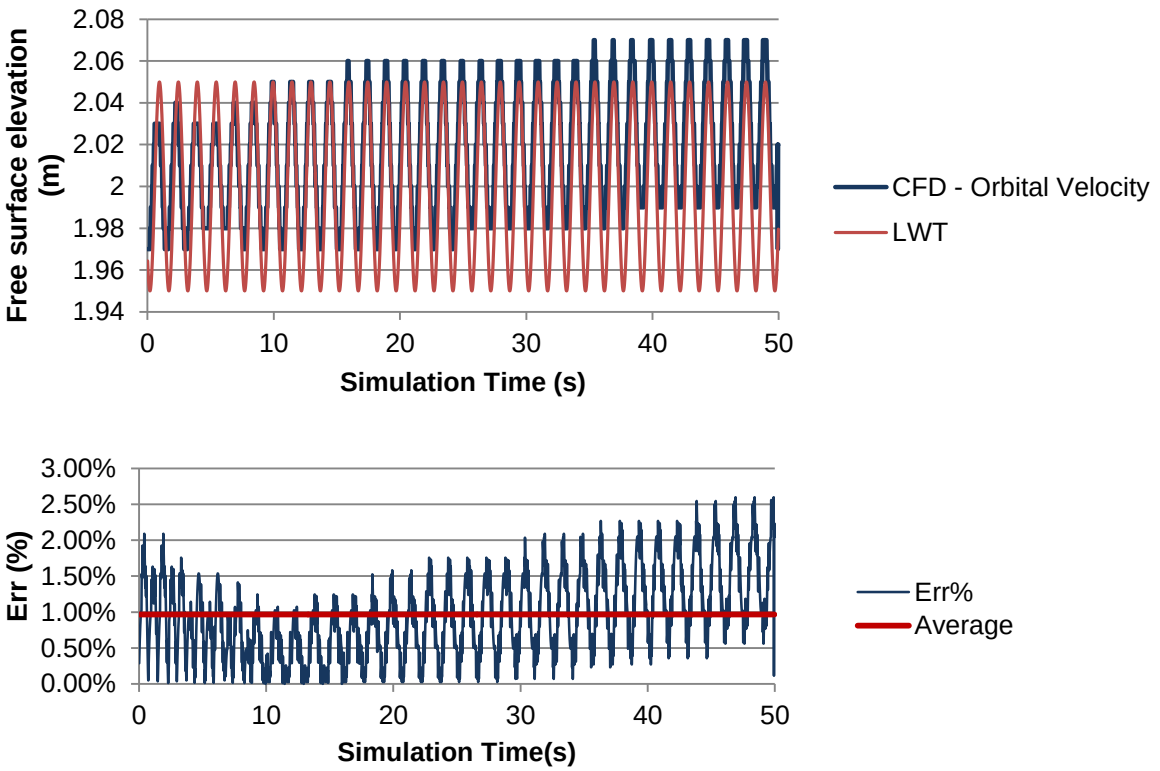

Figure 68 - CFD orbital velocity and LWT free surface elevation (a) and relative error CFD against LWT (b) at 3m from the inlet (H=0.1m, T=1.5s)

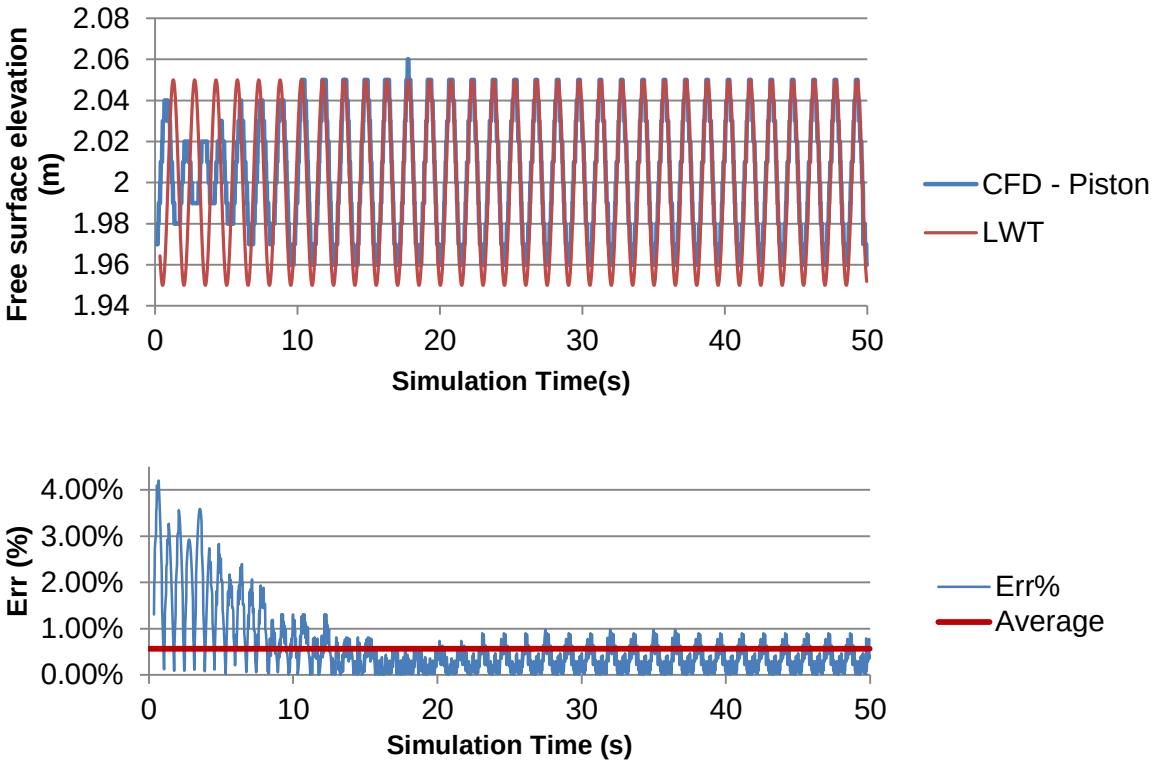

Figure 69 - CFD piston and LWT free surface elevation (a) and relative error CFD against LWT (b) at 3m from the inlet (H=0.1m, T=1.5s)

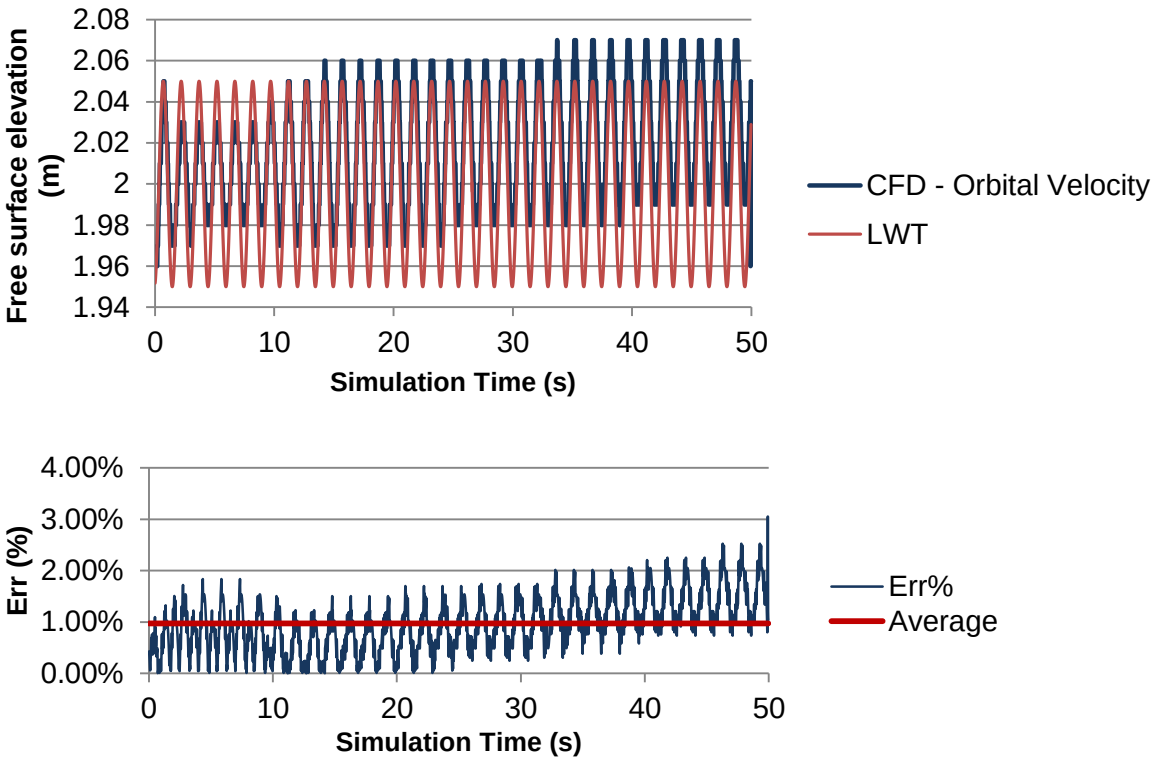

Figure 70 - CFD orbital velocity and LWT free surface elevation (a) and relative error CFD against LWT (b) at 6m from the inlet (H=0.1m, T=1.5s)

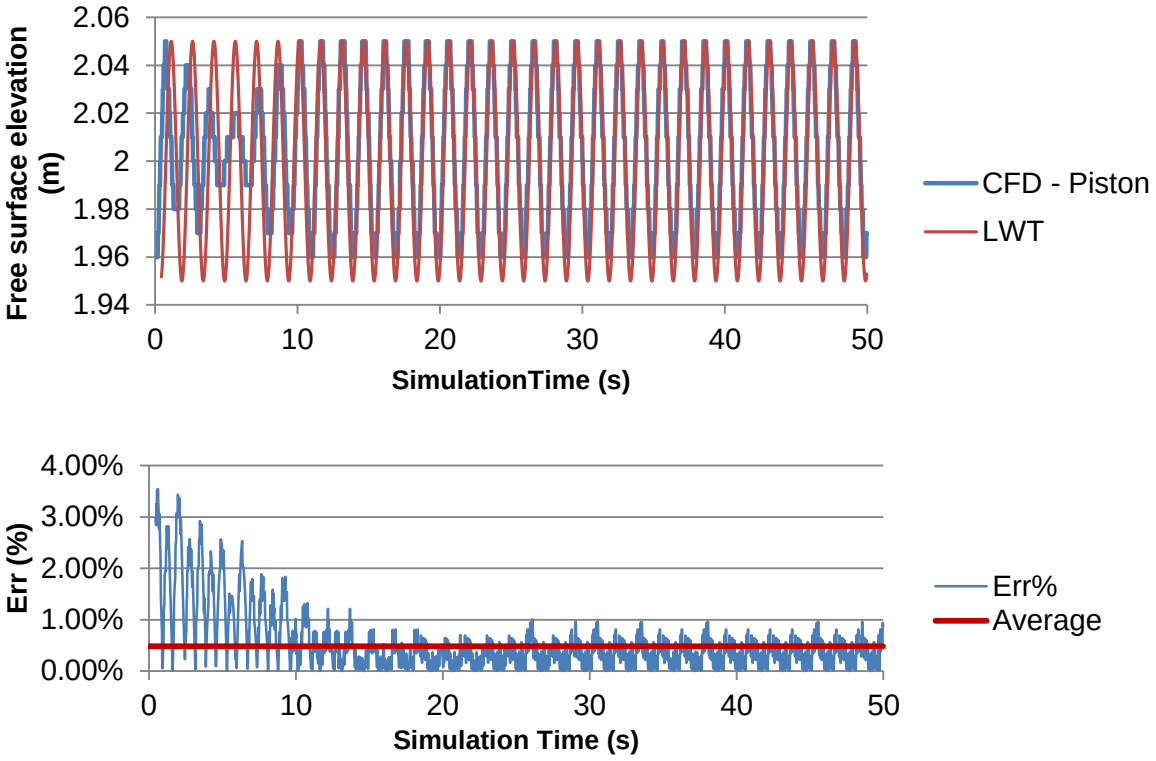

Figure 71 - CFD piston and LWT free surface elevation (a) and relative error CFD against LWT (b) at 6m from the inlet (H=0.1m, T=1.5s)

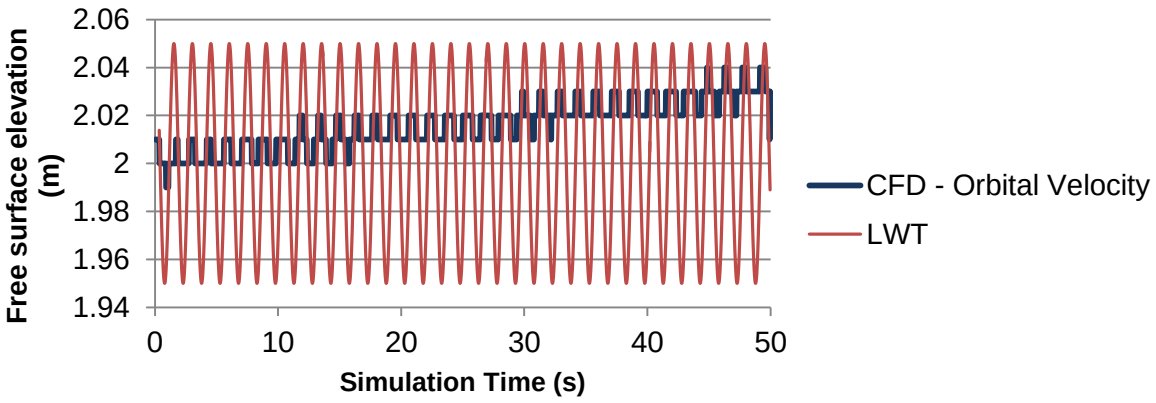

Figure 72 - CFD orbital velocity and LWT free surface elevation at 7m from the inlet (H=0.1m, T=1.5s)

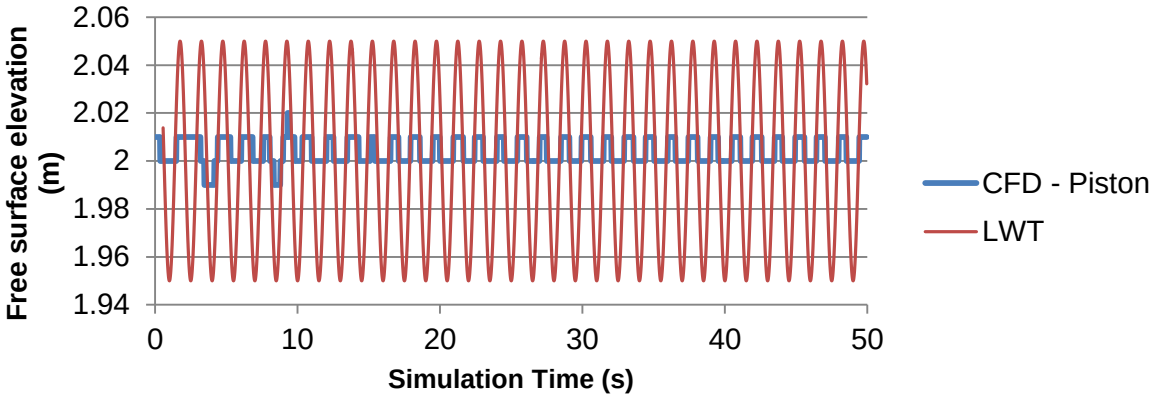

Figure 73 - CFD piston and LWT free surface elevation at 7.2m from the inlet (H=0.1m, T=1.5s)

Appendix D

MESH CONVERGENCE STUDY

In this appendix, figures comparing the water elevation recorded at five different locations (0.3, 1, 3, 6 and 7.2m from the inlet) of the three different meshes presented in Chapter 5 section 3.3. are reported. The wave considered (H=0.1m, T=1.5s) propagates along a 2m water depth.

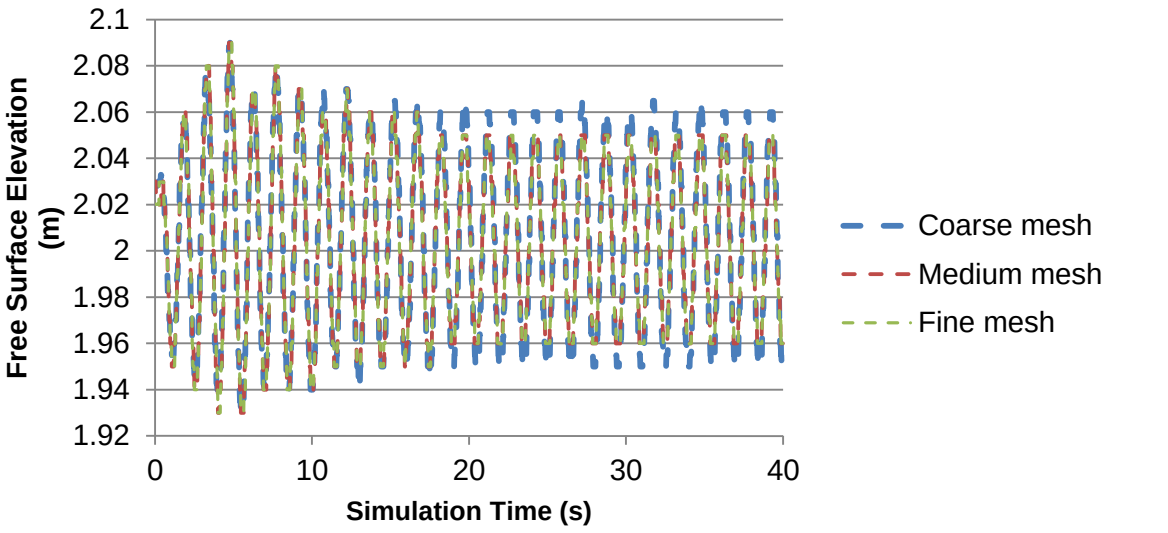

(a)

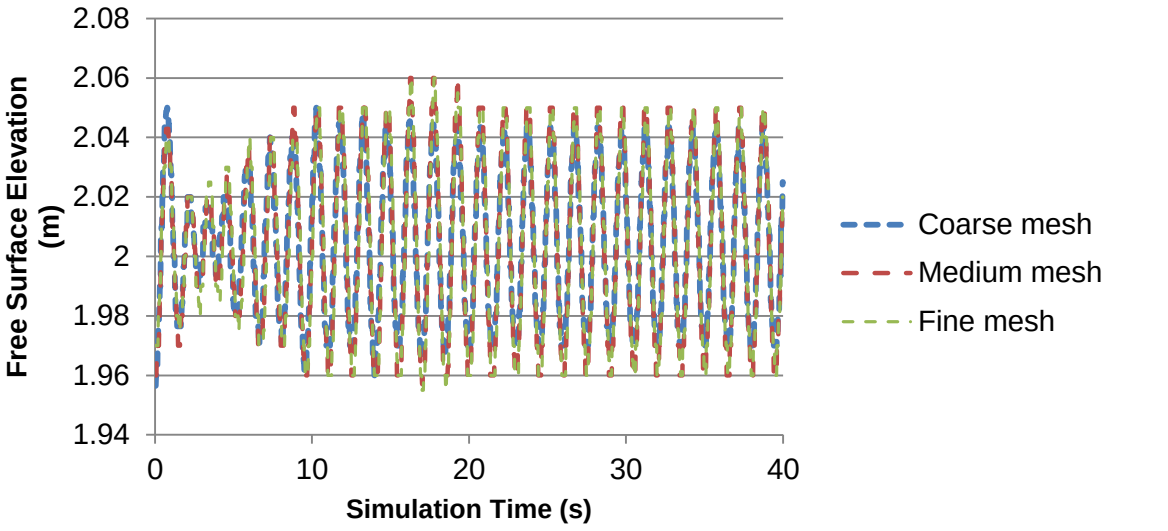

(b)

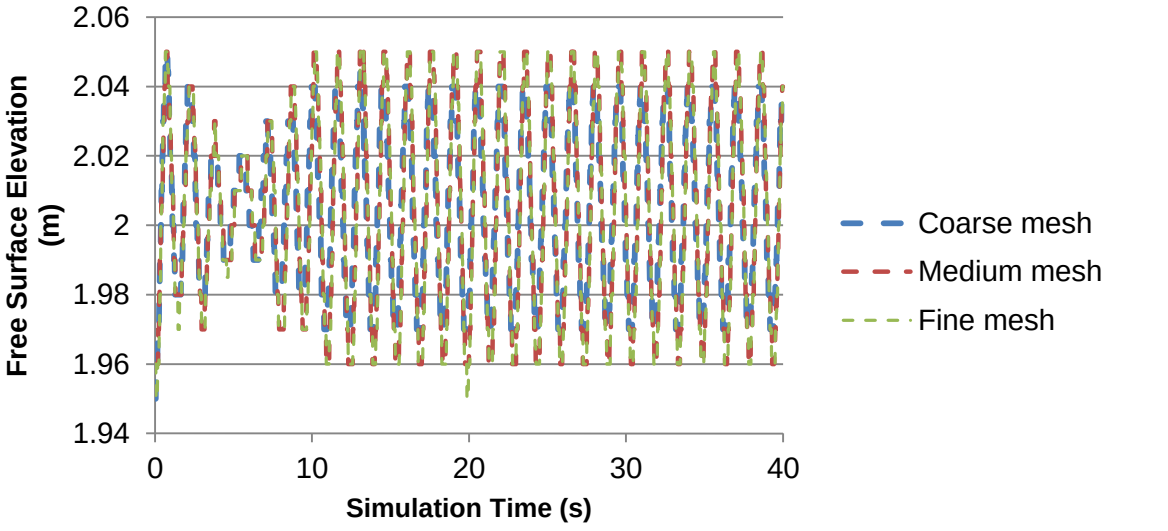

(c)

Figure 74 - Free surface elevation of three meshes at 0.3m (a), 3m (b) and 6m (c) from the inlet (H=0.1m ; T=1.5s)

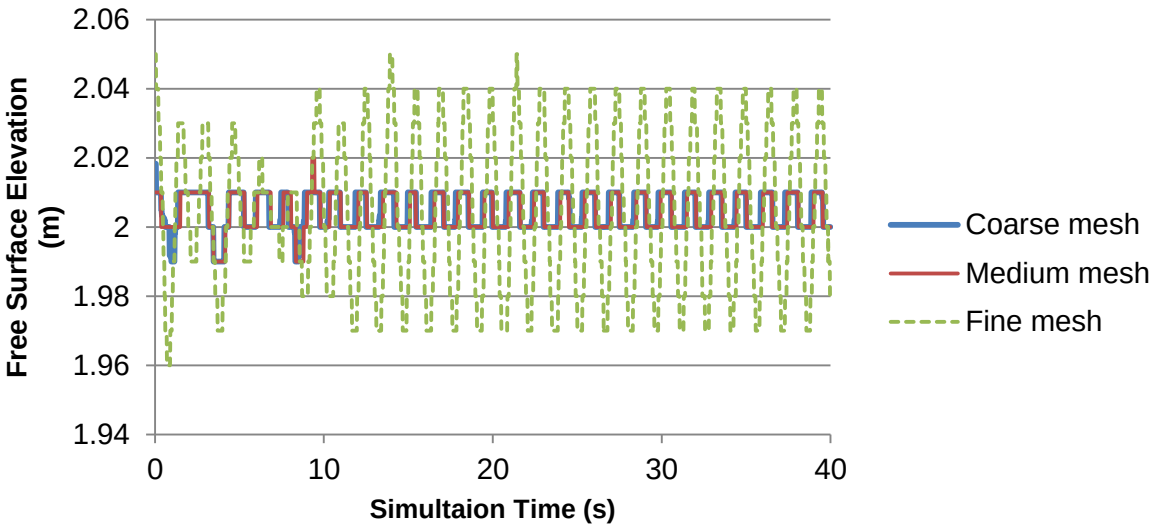

Figure 75 - Free surface elevation of three meshes at 7.2m from the inlet (H=0.1m, T=1.5s)